ISSN 1949-8470 (online)

WJR World Journal of Radiology

World J Radiol 2010 June 28; 2(6): 197-236

A peer-reviewed, online, open-access journal of Radiology

Illustration of enhancement patterns of hepatic tumors in the arterial phase.

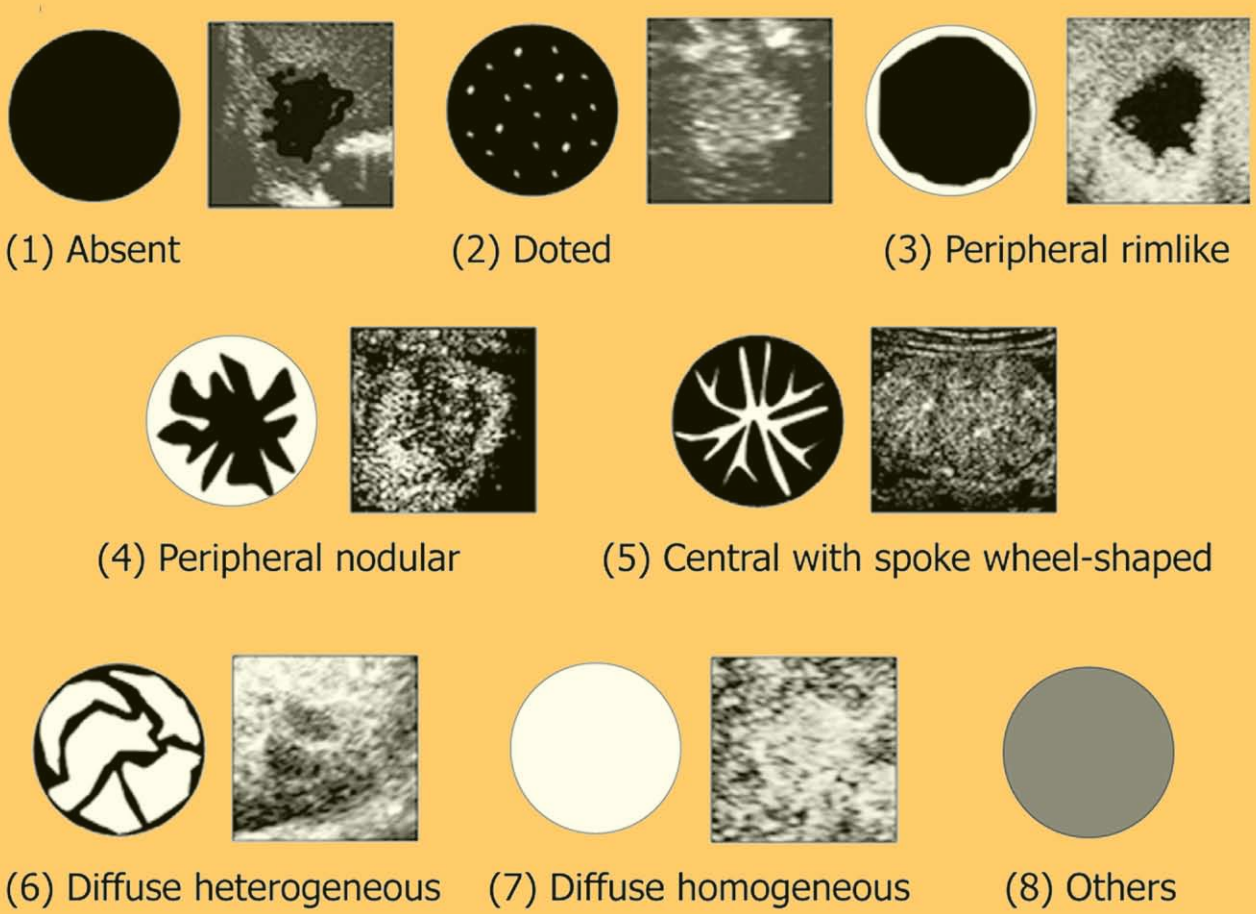

WJR World Journal of Radiology

A peer-reviewed, online, open-access journal of Radiology

Editorial Board

2009-2013

The *World Journal of Radiology* Editorial Board consists of 318 members, representing a team of worldwide experts in radiology. They are from 40 countries, including Australia (3), Austria (4), Belgium (5), Brazil (3), Canada (9), Chile (1), China (24), Czech (1), Denmark (1), Egypt (4), Estonia (1), Finland (1), France (6), Germany (17), Greece (8), Hungary (1), India (9), Iran (5), Ireland (1), Israel (4), Italy (28), Japan (14), Lebanon (1), Libya (1), Malaysia (2), Mexico (1), Netherlands (4), New Zealand (1), Norway (1), Saudi Arabia (3), Serbia (1), Singapore (2), Slovakia (1), South Korea (16), Spain (8), Switzerland (5), Thailand (1), Turkey (20), United Kingdom (16), and United States (82).

France

Alain Chapel, *Fontenay-Aux-Roses*
Nathalie Lassau, *Villejuif*
Youlia M Kirova, *Paris*
Géraldine Le Duc, *Grenoble Cedex*
Laurent Pierot, *Reims*
Frank Pilleul, *Lyon*
Pascal Pommier, *Lyon*

Germany

Ambros J Beer, *München*
Thomas Deserno, *Aachen*
Frederik L Giesel, *Heidelberg*
Ulf Jensen, *Kiel*
Markus Sebastian Juchems, *Ulm*
Kai U Juergens, *Bremen*
Melanie Kettering, *Jena*
Jennifer Linn, *Munich*
Christian Lohrmann, *Freiburg*
David Maintz, *Münster*
Henrik J Michaely, *Mannheim*
Oliver Micke, *Bielefeld*
Thoralf Niendorf, *Berlin-Buch*
Silvia Obenauer, *Duesseldorf*
Steffen Rickes, *Halberstadt*
Lars V Baron von Engelhardt, *Bochum*
Goetz H Welsch, *Erlangen*

Greece

Panagiotis Antoniou, *Alexandroupolis*
George C Kagadis, *Rion*
Dimitris Karacostas, *Thessaloniki*
George Panayiotakis, *Patras*
Alexander D Rapidis, *Athens*
C Triantopoulou, *Athens*
Ioannis Tsalafoutas, *Athens*
Virginia Tsapaki, *Anixi*
Ioannis Valais, *Athens*

Hungary

Peter Laszlo Lakatos, *Budapest*

India

Anil Kumar Anand, *New Delhi*
Surendra Babu, *Tamilnadu*
Sandip Basu, *Bombay*
Kundan Singh Chufal, *New Delhi*
Shivanand Gamanagatti, *New Delhi*
Vimoj J Nair, *Haryana*
R Prabhakar, *New Delhi*
Sanjeeb Kumar Sahoo, *Orissa*

Iran

Vahid Reza Dabbagh Kakhki, *Mashhad*
Mehran Karimi, *Shiraz*
Farideh Nejat, *Tehran*
Alireza Shirazi, *Tehran*
Hadi Rokni Yazdi, *Tehran*

Ireland

Joseph Simon Butler, *Dublin*

Israel

Amit Gefen, *Tel Aviv*
Eyal Sheiner, *Be'er-Sheva*
Jacob Sosna, *Jerusalem*
Simcha Yagel, *Jerusalem*

Italy

Mohssen Ansarin, *Milan*
Stefano Arcangeli, *Rome*
Tommaso Bartalena, *Imola*
Filippo Cademartiri, *Parma*
Sergio Casciaro, *Lecce*
Laura Crocetti, *Pisa*
Alberto Cuocolo, *Napoli*
Mirko D'Onofrio, *Verona*
Massimo Filippi, *Milan*
Claudio Fiorino, *Milano*
Alessandro Franchello, *Turin*
Roberto Grassi, *Naples*
Stefano Guerriero, *Cagliari*
Francesco Lassandro, *Napoli*
Nicola Limbucci, *L'Aquila*
Raffaele Lodi, *Bologna*
Francesca Maccioni, *Rome*
Laura Martincich, *Candiolo*
Mario Mascalchi, *Florence*
Roberto Miraglia, *Palermo*
Eugenio Picano, *Pisa*
Antonio Pinto, *Naples*
Stefania Romano, *Naples*
Luca Saba, *Cagliari*
Sergio Sartori, *Ferrara*
Mariano Scaglione, *Castel Volturno*
Lidia Strigari, *Rome*
Vincenzo Valentini, *Rome*

Japan

Shigeru Ehara, *Morioka*
Nobuyuki Hamada, *Chiba*
Takao Hiraki, *Okayama*
Akio Hiwatashi, *Fukuoka*
Masahiro Jinzaki, *Tokyo*
Hiroshi Matsuda, *Saitama*
Yasunori Minami, *Osaka*
Jun-Ichi Nishizawa, *Tokyo*
Tetsu Niwa, *Yokohama*
Kazushi Numata, *Kanagawa*
Kazuhiko Ogawa, *Okinawa*
Hitoshi Shibuya, *Tokyo*
Akira Uchino, *Saitama*
Haiquan Yang, *Kanagawa*

Lebanon

Aghiad Al-Kutoubi, *Beirut*

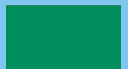

Libya

Anuj Mishra, *Tripoli*

Malaysia

R Logeswaran, *Cyberjaya*
Kwan-Hoong Ng, *Kuala Lumpur*

Mexico

Heriberto Medina-Franco, *Mexico City*

Netherlands

Jurgen J Fütterer, *Nijmegen*
Raffaella Rossin, *Eindhoven*
Paul E Sijens, *Groningen*
Willem Jan van Rooij, *Tilburg*

New Zealand

W Howell Round, *Hamilton*

Norway

Arne Sigmund Borthne, *Lørenskog*

Saudi Arabia

Mohammed Al-Omran, *Riyadh*
Ragab Hani Donkol, *Abha*
Volker Rudat, *Al Khobar*

Serbia

Djordjije Saranovic, *Belgrade*

Singapore

Uei Pua, *Singapore*
Lim CC Tchoyoson, *Singapore*

Slovakia

František Dubecký, *Bratislava*

South Korea

Bo-Young Choe, *Seoul*
Joon Koo Han, *Seoul*
Seung Jae Huh, *Seoul*
Chan Kyo Kim, *Seoul*
Myeong-Jin Kim, *Seoul*
Seung Hyup Kim, *Seoul*
Kyoung Ho Lee, *Gyeonggi-do*
Won-Jin Moon, *Seoul*
Wazir Muhammad, *Daegu*
Jai Soung Park, *Bucheon*
Noh Hyuck Park, *Kyunggi*
Sang-Hyun Park, *Daejeon*
Joon Beom Seo, *Seoul*
Ji-Hoon Shin, *Seoul*
Jin-Suck Suh, *Seoul*
Hong-Gyun Wu, *Seoul*

Spain

Eduardo J Aguilar, *Valencia*
Miguel Alcaraz, *Murcia*
Juan Luis Alcazar, *Pamplona*
Gorka Bastarrika, *Pamplona*
Rafael Martínez-Monge, *Pamplona*
Alberto Muñoz, *Madrid*
Joan C Vilanova, *Girona*

Switzerland

Nicolau Beckmann, *Basel*
Silke Grabherr, *Lausanne*
Karl-Olof Lövblad, *Geneva*
Tilo Niemann, *Basel*
Martin A Walter, *Basel*

Thailand

Sudsriluk Sampatchalit, *Bangkok*

Turkey

Olus Api, *Istanbul*
Kubilay Aydin, *İstanbul*
Işıl Bilgen, *Izmir*
Zulkif Bozgeyik, *Elazig*
Barbaros E Çil, *Ankara*
Gulgun Engin, *Istanbul*
M Fatih Evcimik, *Malatya*
Ahmet Kaan Gündüz, *Ankara*
Tayfun Hakan, *Istanbul*
Adnan Kabaalioglu, *Antalya*
Fehmi Kaçmaz, *Ankara*
Musturay Karcaaltincaba, *Ankara*
Osman Kizilkilic, *Istanbul*
Zafer Koc, *Adana*
Cem Onal, *Adana*
Yahya Paksoy, *Konya*
Bunyamin Sahin, *Samsun*
Ercument Unlu, *Edirne*
Ahmet Tuncay Turgut, *Ankara*
Ender Uysal, *Istanbul*

United Kingdom

K Faulkner, *Wallsend*
Peter Gaines, *Sheffield*
Balaji Ganeshan, *Brighton*
Nagy Habib, *London*
Alan Jackson, *Manchester*
Pradesh Kumar, *Portsmouth*
Tarik F Massoud, *Cambridge*
Igor Meglinski, *Bedfordshire*
Robert Morgan, *London*
Ian Negus, *Bristol*
Georgios A Plataniotis, *Aberdeen*
N J Raine-Fenning, *Nottingham*
Manuchehr Soleimani, *Bath*
MY Tseng, *Nottingham*
Edwin JR van Beek, *Edinburgh*
Feng Wu, *Oxford*

United States

Athanassios Argiris, *Pittsburgh*
Stephen R Baker, *Newark*
Lia Bartella, *New York*
Charles Bellows, *New Orleans*
Walter L Biffl, *Denver*
Homer S Black, *Houston*
Wessam Bou-Assaly, *Ann Arbor*
Owen Carmichael, *Davis*
Shelton D Caruthers, *St Louis*
Yuhchyau Chen, *Rochester*
Melvin E Clouse, *Boston*
Ezra Eddy Wyssam Cohen, *Chicago*
Aaron Cohen-Gadol, *Indianapolis*
Patrick M Colletti, *Los Angeles*
Kassa Darge, *Philadelphia*
Abhijit P Datir, *Miami*
Delia C DeBuc, *Miami*
Russell L Deter, *Houston*
Adam P Dicker, *Phil*
Khaled M Elsayes, *Ann Arbor*
Steven Feigenberg, *Baltimore*
Christopher G Filippi, *Burlington*
Victor Frenkel, *Bethesda*
Thomas J George Jr, *Gainesville*
Patrick K Ha, *Baltimore*
Robert I Haddad, *Boston*
Walter A Hall, *Syracuse*
Mary S Hammes, *Chicago*
John Hart Jr, *Dallas*
Randall T Higashida, *San Francisco*
Juebin Huang, *Jackson*
Andrei Iagaru, *Stanford*
Craig Johnson, *Milwaukee*
Ella F Jones, *San Francisco*
Csaba Juhasz, *Detroit*
Mannudeep K Kalra, *Boston*
Riyad Karmy-Jones, *Vancouver*
Daniel J Kelley, *Madison*
Amir Khan, *Longview*
Euishin Edmund Kim, *Houston*
Vikas Kundra, *Houston*
Kennith F Layton, *Dallas*
Rui Liao, *Princeton*
CM Charlie Ma, *Philadelphia*
Nina A Mayr, *Columbus*
Thomas J Meade, *Evanston*
Steven R Messé, *Philadelphia*
Nathan Olivier Mewton, *Baltimore*
Feroze B Mohamed, *Philadelphia*
Koenraad J Mortele, *Boston*
Mohan Natarajan, *San Antonio*
John L Nosher, *New Brunswick*
Chong-Xian Pan, *Sacramento*
Dipanjan Pan, *St Louis*
Martin R Prince, *New York*
Reza Rahbar, *Boston*
Carlos S Restrepo, *San Antonio*
Veronica Rooks, *Honolulu*
Maythem Saeed, *San Francisco*
Edgar A Samaniego, *Palo Alto*
Kohkan Shamsi, *Doylestown*
Jason P Sheehan, *Charlottesville*
William P Sheehan, *Willmar*
Charles Jeffrey Smith, *Columbia*
Monvadi B Srichai-Parsia, *New York*
Dan Stoianovici, *Baltimore*
Janio Szklaruk, *Houston*
Dian Wang, *Milwaukee*
Jian Z Wang, *Columbus*
Liang Wang, *New York*
Shougang Wang, *Santa Clara*
Wenbao Wang, *New York*
Aaron H Wolfson, *Miami*
Gayle E Woloschak, *Chicago*
Ying Xiao, *Philadelphia*
Juan Xu, *Pittsburgh*
Benjamin M Yeh, *San Francisco*
Terry T Yoshizumi, *Durham*
Jinxing Yu, *Richmond*
Jianhui Zhong, *Rochester*

WJR World Journal of Radiology

Contents

Monthly Volume 2 Number 6 June 28, 2010

World Journal of Radiology
Volume 2 Number 6 June 28, 2010

Contents

NAME OF JOURNAL
World Journal of Radiology

LAUNCH DATE
December 31, 2009

SPONSOR
Beijing Baishideng BioMed Scientific Co., Ltd.,
Room 903, Building D, Ocean International Center,
No. 62 Dongsihuan Zhonglu, Chaoyang District,
Beijing 100025, China
Telephone: 0086-10-8538-1892
Fax: 0086-10-8538-1893
E-mail: baishideng@wjgnet.com
http://www.wjgnet.com

EDITING
Editorial Board of *World Journal of Radiology*,
Room 903, Building D, Ocean International Center,
No. 62 Dongsihuan Zhonglu, Chaoyang District,
Beijing 100025, China
Telephone: 0086-10-5908-0036
Fax: 0086-10-8538-1893
E-mail: wjr@wjgnet.com
http://www.wjgnet.com

PUBLISHING
Beijing Baishideng BioMed Scientific Co., Ltd.,
Room 903, Building D, Ocean International Center,
No. 62 Dongsihuan Zhonglu, Chaoyang District,
Beijing 100025, China
Telephone: 0086-10-8538-1892
Fax: 0086-10-8538-1893
E-mail: baishideng@wjgnet.com
http://www.wjgnet.com

SUBSCRIPTION
Beijing Baishideng BioMed Scientific Co., Ltd.,
Room 903, Building D, Ocean International Center,
No. 62 Dongsihuan Zhonglu, Chaoyang District,
Beijing 100025, China
Telephone: 0086-10-8538-1892
Fax: 0086-10-8538-1893
E-mail: baishideng@wjgnet.com
http://www.wjgnet.com

ONLINE SUBSCRIPTION
One-Year Price 216.00 USD

PUBLICATION DATE
June 28, 2010

CSSN
ISSN 1949-8470 (online)

EDITORIAL OFFICE
Na Ma, Director
World Journal of Radiology
Room 903, Building D, Ocean International Center,
No. 62 Dongsihuan Zhonglu, Chaoyang District,
Beijing 100025, China
Telephone: 0086-10-5908-0036
Fax: 0086-10-8538-1893
E-mail: wjr@wjgnet.com
http://www.wjgnet.com

INSTRUCTIONS TO AUTHORS
Full instructions are available online at http://www.wjgnet.com/1949-8470/g_info_20100316162358.htm. If you do not have web access please contact the editorial office.

ONLINE SUBMISSION
http://www.wjgnet.com/1949-8470office

World Journal of Radiology

Online Submissions: http://www.wjgnet.com/1949-8470office
wjr@wjgnet.com
doi:10.4329/wjr.v2.i6.197

World J Radiol 2010 June 28; 2(6): 197-202
ISSN 1949-8470 (online)

EDITORIAL

Hypofractionated radiotherapy in the treatment of early breast cancer

George Plataniotis

George Plataniotis, Consultant and Senior Lecturer of Clinical Oncology, Department of Oncology, Aberdeen Royal Infirmary Foresterhill, AB25 2ZN, Aberdeen, United Kingdom
Author contributions: Plataniotis G contributed all to the paper.
Correspondence to: George Plataniotis, MD, PhD, Consultant and Senior Lecturer of Clinical Oncology, Department of Oncology, Aberdeen Royal Infirmary Foresterhill, AB25 2ZN, Aberdeen, United Kingdom. george.plataniotis@nhs.net
Telephone: +44-1224-553483 Fax: +44-1224-554183
Received: April 12, 2010 Revised: May 21, 2010
Accepted: May 28, 2010
Published online: June 28, 2010

Abstract

Radiotherapy (RT) after tumorectomy in early breast cancer patients is an established treatment modality which conventionally takes 6-7 wk to complete. Shorter RT schedules have been tested in large multicentre randomized trials and have shown equivalent results to that of standard RT (50 Gy in 25 fractions) in terms of local tumor control, patient survival and late post-radiation effects. Some of those trials have now completed 10 years of follow-up with encouraging results for treatments of 3-4 wk and a total RT dose to the breast of 40-42.5 Gy with or without boost. A reduction of 50% in treatment time makes those RT schedules attractive for both patients and health care providers and would have a significant impact on daily RT practice around the world, as it would accelerate patient turnover and save health care resources. However, in hypofractionated RT, a higher (than the conventional 1.8-2 Gy) dose per fraction is given and should be managed with caution as it could result in a higher rate of late post-radiation effects in breast, heart, lungs and the brachial plexus. It is therefore advisable that both possible dose inhomogeneity and normal tissue protection should be taken into account and the appropriate technology such as three-dimensional/intensity modulated radiation therapy employed in clinical practice, when hypofractionation is used.

Key words: Breast conservation; Early breast cancer; Hypofractionation; Radiotherapy

Peer reviewers: Volker Rudat, Professor, Department of Radiation Oncology, Saad Specialist Hospital, PO Box 30353, Al Khobar 31952, Saudi Arabia; Piyush Kumar, PhD, Associate Clinical Professor, Department of Oncology, University of Alberta, Cross Cancer Institute, 11560 University Avenue, Edmonton, Alberta, T6G 1Z2, Canada

Plataniotis G. Hypofractionated radiotherapy in the treatment of early breast cancer. *World J Radiol* 2010; 2(6): 197-202 Available from: URL: http://www.wjgnet.com/1949-8470/full/v2/i6/197.htm DOI: http://dx.doi.org/10.4329/wjr.v2.i6.197

INTRODUCTION

Breast-conserving therapy is a widely accepted treatment in the management of early breast cancer. It includes wide local excision of the tumor followed by radiotherapy (RT) to the breast (and of course the necessary treatment for lymph-drainage areas). The major benefit of breast-conserving therapy is preservation of the affected breast with all the consequent advantages in terms of patient quality of life. Large randomized trials have demonstrated the equivalence of this therapy, compared to mastectomy, in terms of long-term disease-free and overall survival rates[1,2]. Conventional RT after breast-conserving surgery requires 6-7 wk of daily treatment. The most widely used schedule is 50 Gy in 25 fractions (2 Gy per fraction) over 5 wk plus 3-8 fractions to boost the dose on the tumor bed[1,2]. Such a long treatment schedule has major implications on both patient quality of life and RT departments, as a high number of breast cancer patients receive RT. A shorter breast RT schedule would be more convenient for patients (especially those coming from remote areas to RT facilities) and for

health care providers, as it would increase the turnover in RT departments. The use of a 16-fractions, instead of a 25-fractions regime, for instance (see below), would save 900 treatment sessions per 100 patients (2500 - 1600 = 900). This corresponds to an additional 56 (900:16) patients who could be treated with the same number of fractions. This would result in substantial economic benefit as breast cancer patients represent the majority of patients treated in RT departments.

RADIOBIOLOGY AND FRACTIONATION

A broad variety of RT schedules, hypofractionated or not, have been used in clinical practice, but there is no consensus on the optimum fractionation. A survey of Ontario RT centres alone identified 48 different dose fractionation schedules[3].

However, there are some reservations regarding the shorter RT schedules[4] with a high (> 2 Gy) dose per fraction, which are mainly related to the theoretically expected higher rate of late post-radiotherapy complications. With conventional fractionation, the Early Breast Cancer Trialists' Collaborative Group reported that radiation therapy reduced the annual mortality from breast cancer by 13%, but increased the annual mortality rate from other causes (mainly cardiovascular causes) by 21%[5]. Data from long-term follow-up on late lung and cardiac morbidity and survival rates has yet to emerge for the current hypofractionation schedules, as the cardiac adverse effects may not emerge until 15 years after treatment. However, hypofractionation studies and clinical results reported so far do not suggest a higher risk of late reactions.

Radiation oncologists are generally sceptical about using a RT regime with a higher than the standard (1.8-2 Gy) dose per fraction. One of the main principles of radiobiology is that the late effects of normal tissues are strongly dependent on the size of dose per fraction, so that the higher the dose per fraction the greater the susceptibility of healthy tissues to radiation. This is known as "fractionation sensitivity". Fractionation sensitivity of tissues is quantified, in terms of linear-quadratic (LQ) isoeffect formulation, by the α/β ratio[6,7]; the higher the sensitivity to the size of dose per fraction, the lower the α/β ratio is. Late reacting normal tissues (connective tissue, neural tissue, *etc.*) have an α/β ratio of about 1.5-3 Gy. Late post-radiation effects of breast are fibrosis, oedema, tenderness, telangiectasia and a combination of these effects, in addition to impaired cosmesis and have an α/β = 3 Gy[6,7]. We should mention here that for the assessment of late post-radiation effects on the treated breast, most authors take photographs post-surgery and pre-radiotherapy and then at predetermined times, e.g. 2 and 5 years to assess changes to the breast based on change in size, shrinkage, and shape. Scoring on a 3 or 4 graded scale is carried out in most studies. Changes in breast appearance may be scored by more than one observer usually blind to the treatment arm and year of follow-up.

It has to be mentioned that this discussion on hypofractionation does not apply to treatment of lymphatic pathways due to the very high fractionation sensitivity of the brachial plexus (neural tissue). Acute radiation reactions in normal tissues such as the skin or mucosa and squamous-cell carcinomas have an α/β ratio of 10 Gy[6,7]. It has been shown by radiobiological analysis of clinical data, that breast adenocarcinomas have an α/β ratio of around 4 Gy, i.e. close to late reacting normal tissues[8-11]. Consequently, hypofractionation in breast cancer may have a reasonable radiobiological background as more tumor cells will be killed by a high dose per fraction compared with the conventional 2 Gy per fraction, and would potentially compensate for repopulation of tumor cells during RT.

ESTABLISHMENT OF DOSE-RESPONSE

However, this may be difficult to prove because the local control rates in early breast cancer with radiation therapy are already high, and in breast cancer in particular, there are a number of factors that might influence the results of a RT treatment schedule or a relevant clinical study. Therefore, it is difficult to establish a dose-response relationship in postoperative breast RT, that may be relatively higher than other solid tumors due to the following[12]: (1) An unknown proportion of patients have no residual cancer cells after surgery, whereas others have a subclinical (microscopic) number of residual tumor cells that must be eradicated by radiation[12-14]. This is an inherent problem when analyzing the results of any adjuvant therapy; (2) Dose-escalation studies are usually lacking; information should be taken from randomized controlled studies on RT *vs* no RT which have used a narrow range of RT schedules and doses; and (3) There are a number of factors that may affect the homogeneity of clinical data in existing randomized trials: biologic aggressiveness of the treated tumors (ranging from elderly patients with T1N0, Grade 1 hormone receptor-positive tumors to women with multiple positive nodes, hormone receptor-negative, HER2-positive tumors), variable surgical techniques and skills among centres, variable chemotherapy/endocrine regimes and RT techniques. Additionally, local recurrence could be the result of re-growth of tumor at the initial tumor bed, or of tumor in the same breast but outside the initial tumor bed from cells existing at the time of initial treatment, or the development of a new tumor in the same breast.

In our recent study[12], we attempted to estimate a biologically effective dose (BED)-response for adjuvant breast RT in early-stage breast cancer. Clinical results from nine randomized trials (involving more that 6200 patients) of RT *vs* non-RT were reviewed and the tumor control probability (TCP) after RT was calculated for each. We used the LQ formula and Poisson statistics of cell-kill[15-17] to calculate the average initial number of clonogens per tumor before RT and the average tumor cell radiosensitivity[6,15-17]. An α/β ratio of 4 Gy was assumed[8-11] for these calculations.

A linear regression equation linking BED to TCP was derived {equation: -ln[-ln(TCP)] = -ln(No) + a * BED = -4.08 + 0.07 * BED} and a sigmoid BED-response curve was constructed. We concluded that TCP is essentially maximizing for BED values of about 90 Gy[4]. An example of a BED of 85-90 Gy[4] could be a regimen of 40 Gy in 15 fractions plus a boost of 10-12 Gy in 3-4 fractions.

REVIEW OF CLINICAL STUDIES

Clinical reports from various centres have shown almost equivalent results between short and standard RT schedules[9-11,18-27], and it would be interesting to have an overview of the current situation in this field.

In a well-known randomized trial from Canada, Whelan *et al*[18] reported equivalent results (regarding local control, survival, and post-radiation effects) between the standard fractionation schedule of 50 Gy in 25 fractions and a hypofractionated scheme of 42.5 Gy in 16 fractions over 22 d for women with node-negative early breast cancer. This study has been updated recently and, most importantly, results have not changed after a 10-year follow-up[19]. However, the potential limitations of this study are as follows:

The trial was restricted to women who had node-negative, invasive breast cancer with clear margins of excision after lumpectomy; women with large breasts were not included; few women received adjuvant chemotherapy and we should bear in mind that those patients can be at a higher risk for acute and late post-radiation effects; boost irradiation was not used, as by the time the study was initiated, the efficacy of boost irradiation had not been demonstrated[19] and was later shown in studies from Europe[28,29]. However, boost irradiation was used in both Standardization of Breast Radiotherapy (START) trials (see below), and adjuvant chemotherapy was used more widely than in this trial. In addition, a broader spectrum of tumors and patients (node-positive, larger tumors, no limitation of breast size) were included, but no differences have been noted in tumor control and side-effects between standard and short treatments in those trials so far.

Another short RT schedule, 40 Gy in 15 fractions, has been used traditionally at Christie Hospital in Manchester, UK; the reported results of 2159 treated patients are comparable to those reported from other centres[21,22]. This schedule is now becoming the "standard" in the UK, especially after the publication of the START trials.

The START A trial randomized 2236 patients from 17 centres across the UK and reported that 41.6 Gy/13 fractions or 39 Gy/13 fractions are similar to 50 Gy/25 fractions in terms of local-regional tumor control and late normal tissue effects. The START A trial[9] showed that after a median follow-up of 5.1 years, the rate of local-regional tumor relapse at 5 years was 3.6% [95% confidence interval (CI): 2.2%-5.1%] after 50 Gy, 3.5% (95% CI: 2.1%-4.3%) after 41.6 Gy, and 5.2% (95% CI: 3.5%-6.9%) after 39 Gy. The estimated absolute differences in 5-year local-regional relapse rates compared with 50 Gy were 0.2% (95% CI: -1.3%-2.6%) after 41.6 Gy and 0.9% (95% CI: -0.8%-3.7%) after 39 Gy. Photographic and patient self-assessments suggested lower rates of late adverse effects after 39 Gy than with 50 Gy. The results have shown that breast cancer and late reacting normal tissues respond similarly to change in RT fraction size. 41.6 Gy in 13 fractions was similar to the control regimen of 50 Gy in 25 fractions in terms of local-regional tumor control and late normal tissue effects.

The START B trial[10] randomized 2215 patients from 23 centres across the UK and reported that a RT schedule of 40 Gy/15 fractions offers equivalent results to the standard schedule of 50 Gy/25 fractions. After a median follow-up of 6.0 years, the rate of local-regional tumor relapse at 5 years was 2.2% (95% CI: 1.3%-3.1%) in the 40 Gy group and 3.3% (95% CI: 2.2%-4.5%) in the 50 Gy group. Photographic and patient self-assessments indicated lower rates of late adverse effects after 40 Gy than after 50 Gy. Although the START trials had a relatively limited follow-up time and differences in their design (inclusion criteria) compared with the Canadian trial, their results were similar.

Our early experience from the routine use of the above "Canadian" schedule of hypofractionated breast RT (42.5 Gy in 16 fractions) has been reported recently[30]. We reported on 339 patients treated for 4 years. An electron boost of 9-10 Gy/3-4 fractions was given to 104/339 patients (31%). Median follow-up time was 24 mo (range: 12-48 mo). Radiation Therapy Oncology Group (RTOG) grades 0, 1, 2, 3, and 4 for acute skin toxicity were 9.7%, 68.7%, 17.5%, 4.0%, and 0.3%, respectively. Radiation pneumonitis (promptly resolved by steroids) was suspected/diagnosed in 11/339 patients (3.2%). A total of 8/11 patients had been treated with RT at regional lymph-drainage areas. The only significant correlation was that of radiation pneumonitis and RT of regional lymphatics. Two patients developed metastatic disease and died 14 and 27 mo after RT; another four patients developed metastases; bone metastases developed in two patients, and liver, lung, brain plus regional recurrence (axilla, supraclavicular) in two patients.

Other non-randomized studies have reported similar results. Fujii *et al*[23] reported acceptable results in terms of local control and toxicity (although the median follow-up of this study was 26 mo) with a short fractionation schedule of 42.5-47.8 Gy/16-20 fractions. In another study from the University of Florence, Italy, Livi *et al*[26] reported similar results in 539 patients.

A schedule of 40 Gy in 16 (not 15) fractions in post-lumpectomy invasive breast cancer patients (with clear tumor margins) has shown similar results with a 5-year actuarial breast-relapse rate of 3.5%, while more that 95% of the patients were satisfied with cosmetic results after a median follow-up of 5.5 years[27].

THE LIMITS OF HYPOFRACTIONATION IN BREAST RT

Another study from the UK, investigating the "limits of

hypofractionation in breast RT" is the FAST trial involving 900 patients across the UK (FASTer Radiotherapy for breast cancer patients). This trial is testing 30 Gy in 5 fractions (6 Gy/fraction) over 35 d (5 wk) *vs* 28.5 Gy (5.7 Gy/fraction) over 35 d *vs* 50 Gy in 25 fractions over 35 d (control arm). The trial has ceased recruiting patients and follow-up is ongoing. In the FAST trial, the women being studied are those with completely excised invasive, less than 3 cm, node-negative carcinoma of the breast who underwent breast-preserving surgery and who are older than 49 years[31,32]. In this trial, five fractions of RT are given in 5 wk (one fraction per week), however, this is thought unlikely to represent the "ultimate" hypofractionation. The next step would be to investigate the 30 Gy/5 fractions regime given over a shorter time period.

The same fractionation schedule has also been tested clinically with an overall treatment time of 2 wk[33]. The authors evaluated erythema and moist desquamation in 30 patients receiving 30 Gy in five fractions over 15 d. Grading of skin reactions using RTOG criteria resulted in: 3% grade 0, 67% grade 1, 30% grade 2 and no grade 3 or 4 toxicity. Moist desquamation developed in 4/30 patients (13%). There was some evidence that the risk of acute skin reactions and change in breast appearance (photographically assessed) increased with larger breast size, but the small sample size prevented formal statistical testing. No recurrences were seen after a median follow-up of 3 years. This very short regime showed similar skin toxicity results to the RTOG trial (RTOG 97-13): 7% grade 0, 58% grade 1, 32% grade 2, 3% grade 3 and no grade 4 acute skin toxicity[34]. A correlation between breast size and acute toxicity was reported in the RTOG 97-13 study, with small-breasted women developing 11%-21% grade 2 or higher skin toxicity compared with 43%-50% in large-breasted women.

A further step would be to shorten the RT schedule into 1 wk i.e. to study a 5-fractions RT schedule given over 5 consecutive days. Such a schedule would have significant clinical/practical implications as it would allow RT to be integrated more effectively with surgery and systemic therapies, and it could be used for partial breast RT [see below, Accelerated Partial Breast Radiotherapy (APBI)].

RT EQUIPMENT AND DOSE FRACTIONATION

An important tool in the implementation of hypofractionated RT in early breast cancer is the currently available (in most RT departments in Europe and the US) equipment which obtains a better RT dose distribution i.e. both homogeneous within the planning target volume and sparing neighbouring normal tissues and organs. Three-dimensional treatment planning allows the distribution of the prescribed dose to be evaluated. Dose to the heart and lungs can also be evaluated. This information can be used to optimize the treatment plan accordingly, by the use of techniques such as intensity modulated radiation therapy (IMRT). There is now evidence that such an improvement in dose distribution translates into improved clinical outcome. This improvement in RT planning and delivery would favour hypofractionated RT schedules as it would prevent normal tissues receiving a higher (than the prescribed) dose per fraction and total dose[35,36].

A randomized trial from the Royal Marsden Hospital tested three-dimensional (3D) IMRT against 2D dosimetry using standard wedge compensators, regarding late reactions after whole breast RT. The primary endpoint was change in breast appearance and secondary endpoints were patient self-assessments of breast discomfort, breast hardness, quality of life and physician assessments of breast induration. The 2D-arm patients were 1.7 times more likely to have a change in breast appearance than the IMRT-arm patients (95% CI: 1.2-2.5, $P = 0.008$). Significantly fewer patients in the 3D IMRT group developed palpable breast induration. No significant differences between the treatment groups were found with regard to patient reported breast discomfort, breast hardness or quality of life[36].

Another technique that could make breast RT courses shorter is APBI, which is defined as a radiation technique that employs fractions higher than 1.8-2.0 Gy per day to a partial volume of the breast over a period of less than 5-6 wk[37]. The rationale of this technique is to treat the lumpectomy cavity and an adjacent margin of 1-2 cm as the majority of breast recurrences are diagnosed within this volume. The techniques for APBI include interstitial implantation of radioactive needles, MammoSite (the MammoSite system employs a dual lumen spherical balloon-catheter which is placed in the surgical cavity and filled with water; a high-dose-rate Iridium-192 source in the central lumen delivers the RT in 10 fractions over 5 d), targeted intraoperative therapy, intraoperative electrons and photon beams with 3D conformal/IMRT techniques. Further description of the rationale and techniques of APBI is beyond the scope of the present discussion, however, there are interesting reviews on this method[38,39].

A randomized trial, in progress in the UK, testing intensity modulated RT and partial organ RT following breast-conserving surgery for early breast cancer, is the Intensity Modulated Partial Organ Radiotherapy (IMPORT) trial; the control arm of this trial is: current standard 3-wk RT to the whole breast. Test arm one is: reduced RT to the whole breast (lower-risk areas for recurrence) with standard RT to the partial breast, in the sites of higher risk for recurrence and test arm two: standard RT to the partial breast only (IMPORT Low-risk study). To test dose-escalated IMRT after breast-conserving surgery in women with a higher than average risk of local recurrence, the IMPORT-high trial is also in progress[40,41].

CONCLUSION

In conclusion, hypofractionated RT after breast-conserving surgery for early breast cancer could have a significant

impact in breast oncology and breast cancer patients. Data from randomized trials and the experience from various departments worldwide are encouraging. However, in addition to clinical experience and expertise, appropriate advanced RT equipment and techniques are fundamental in the clinical application of hypofractionated breast RT.

REFERENCES

1 **Fisher B**, Anderson S, Bryant J, Margolese RG, Deutsch M, Fisher ER, Jeong JH, Wolmark N. Twenty-year follow-up of a randomized trial comparing total mastectomy, lumpectomy, and lumpectomy plus irradiation for the treatment of invasive breast cancer. *N Engl J Med* 2002; **347**: 1233-1241

2 **Veronesi U**, Cascinelli N, Mariani L, Greco M, Saccozzi R, Luini A, Aguilar M, Marubini E. Twenty-year follow-up of a randomized study comparing breast-conserving surgery with radical mastectomy for early breast cancer. *N Engl J Med* 2002; **347**: 1227-1232

3 **Whelan T**, Marcellus D, Clark R, Levine M. Adjuvant radiotherapy for early breast cancer: patterns of practice in Ontario. *CMAJ* 1993; **149**: 1273-1277

4 **Goffman TE**, Glatstein E. Hypofractionation redux? *J Clin Oncol* 2004; **22**: 589-591

5 Favourable and unfavourable effects on long-term survival of radiotherapy for early breast cancer: an overview of the randomised trials. Early Breast Cancer Trialists' Collaborative Group. *Lancet* 2000; **355**: 1757-1770

6 **Thames HD**, Bentzen SM, Turesson I, Overgaard M, Van den Bogaert W. Time-dose factors in radiotherapy: a review of the human data. *Radiother Oncol* 1990; **19**: 219-235

7 **Thames HD**, Hendry JH. Fractionation in radiotherapy. London: Taylor and Francis, 1987

8 **Yamada Y**, Ackerman I, Franssen E, MacKenzie RG, Thomas G. Does the dose fractionation schedule influence local control of adjuvant radiotherapy for early stage breast cancer? *Int J Radiat Oncol Biol Phys* 1999; **44**: 99-104

9 **Bentzen SM**, Agrawal RK, Aird EG, Barrett JM, Barrett-Lee PJ, Bliss JM, Brown J, Dewar JA, Dobbs HJ, Haviland JS, Hoskin PJ, Hopwood P, Lawton PA, Magee BJ, Mills J, Morgan DA, Owen JR, Simmons S, Sumo G, Sydenham MA, Venables K, Yarnold JR. The UK Standardisation of Breast Radiotherapy (START) Trial A of radiotherapy hypofractionation for treatment of early breast cancer: a randomised trial. *Lancet Oncol* 2008; **9**: 331-341

10 **Bentzen SM**, Agrawal RK, Aird EG, Barrett JM, Barrett-Lee PJ, Bentzen SM, Bliss JM, Brown J, Dewar JA, Dobbs HJ, Haviland JS, Hoskin PJ, Hopwood P, Lawton PA, Magee BJ, Mills J, Morgan DA, Owen JR, Simmons S, Sumo G, Sydenham MA, Venables K, Yarnold JR. The UK Standardisation of Breast Radiotherapy (START) Trial B of radiotherapy hypofractionation for treatment of early breast cancer: a randomised trial. *Lancet* 2008; **371**: 1098-1107

11 **Yarnold J**, Ashton A, Bliss J, Homewood J, Harper C, Hanson J, Haviland J, Bentzen S, Owen R. Fractionation sensitivity and dose response of late adverse effects in the breast after radiotherapy for early breast cancer: long-term results of a randomised trial. *Radiother Oncol* 2005; **75**: 9-17

12 **Plataniotis GA**, Dale RG. Biologically effective dose-response relationship for breast cancer treated by conservative surgery and postoperative radiotherapy. *Int J Radiat Oncol Biol Phys* 2009; **75**: 512-517

13 **Withers HR**, Peters LJ, Taylor JM. Dose-response relationship for radiation therapy of subclinical disease. *Int J Radiat Oncol Biol Phys* 1995; **31**: 353-359

14 **Kirkpatrick JP**, Marks LB. Modeling killing and repopulation kinetics of subclinical cancer: direct calculations from clinical data. *Int J Radiat Oncol Biol Phys* 2004; **58**: 641-654

15 **Dale RG**. The application of the linear-quadratic dose-effect equation to fractionated and protracted radiotherapy. *Br J Radiol* 1985; **58**: 515-528

16 **Jones B**, Morgan DA. Radiotherapy fractionation. In: Dale RG, Jones B, editors. Radiobiological modelling in radiation oncology. London: The British Institute of Radiology, 2007: 51-78

17 **Fowler JF**. The linear-quadratic formula and progress in fractionated radiotherapy. *Br J Radiol* 1989; **62**: 679-694

18 **Whelan T**, MacKenzie R, Julian J, Levine M, Shelley W, Grimard L, Lada B, Lukka H, Perera F, Fyles A, Laukkanen E, Gulavita S, Benk V, Szechtman B. Randomized trial of breast irradiation schedules after lumpectomy for women with lymph node-negative breast cancer. *J Natl Cancer Inst* 2002; **94**: 1143-1150

19 **Whelan TJ**, Pignol JP, Levine MN, Julian JA, MacKenzie R, Parpia S, Shelley W, Grimard L, Bowen J, Lukka H, Perera F, Fyles A, Schneider K, Gulavita S, Freeman C. Long-term results of hypofractionated radiation therapy for breast cancer. *N Engl J Med* 2010; **362**: 513-520

20 Magee B, Swindell R, Harris M, Banerjee SS. Prognostic factors for breast recurrence after conservative breast surgery and radiotherapy: results from a randomised trial. *Radiother Oncol* 1996; **39**: 223-227

21 **Ribeiro GG**, Magee B, Swindell R, Harris M, Banerjee SS. The Christie Hospital breast conservation trial: an update at 8 years from inception. *Clin Oncol* (R Coll Radiol) 1993; **5**: 278-283

22 **McBain CA**, Young EA, Swindell R, Magee B, Stewart AL. Local recurrence of breast cancer following surgery and radiotherapy: incidence and outcome. *Clin Oncol* (R Coll Radiol) 2003; **15**: 25-31

23 **Fujii O**, Hiratsuka J, Nagase N, Tokiya R, Yoden E, Sonoo H, Murashima N, Iha S, Imajyo Y. Whole-breast radiotherapy with shorter fractionation schedules following breast-conserving surgery: short-term morbidity and preliminary outcomes. *Breast Cancer* 2008; **15**: 86-92

24 **Olivotto IA**, Weir LM, Kim-Sing C, Bajdik CD, Trevisan CH, Doll CM, Lam WY, Basco VE, Jackson SM. Late cosmetic results of short fractionation for breast conservation. *Radiother Oncol* 1996; **41**: 7-13

25 **Ash DV**, Benson EA, Sainsbury JR, Round C, Head C. Seven-year follow-up on 334 patients treated by breast conserving surgery and short course radical postoperative radiotherapy: a report of the Yorkshire Breast Cancer Group. *Clin Oncol* (R Coll Radiol) 1995; **7**: 93-96

26 **Livi L**, Stefanacci M, Scoccianti S, Dicosmo D, Borghesi S, Nosi F, Simontacchi G, Mangoni M, Paiar F, Ponticelli P, Nori J, Chiavacci A, Biti GP. Adjuvant hypofractionated radiation therapy for breast cancer after conserving surgery. *Clin Oncol* (R Coll Radiol) 2007; **19**: 120-124

27 **Shelley W**, Brundage M, Hayter C, Paszat L, Zhou S, Mackillop W. A shorter fractionation schedule for postlumpectomy breast cancer patients. *Int J Radiat Oncol Biol Phys* 2000; **47**: 1219-1228

28 **Bartelink H**, Horiot JC, Poortmans PM, Struikmans H, Van den Bogaert W, Fourquet A, Jager JJ, Hoogenraad WJ, Oei SB, Wárlám-Rodenhuis CC, Pierart M, Collette L. Impact of a higher radiation dose on local control and survival in breast-conserving therapy of early breast cancer: 10-year results of the randomized boost versus no boost EORTC 22881-10882 trial. *J Clin Oncol* 2007; **25**: 3259-3265

29 **Romestaing P**, Lehingue Y, Carrie C, Coquard R, Montbarbon X, Ardiet JM, Mamelle N, Gérard JP. Role of a 10-Gy boost in the conservative treatment of early breast cancer: results of a randomized clinical trial in Lyon, France. *J Clin Oncol* 1997; **15**: 963-968

30 **Plataniotis GA**, Theofanopoulou MA, Sotiriadou K, Kyrgias G. Hypofractionated radiotherapy for breast cancer patients treated by breast-conserving surgery: short-term morbidity and preliminary results. *Breast Cancer* 2010; **17**: 42-47

31 **Yarnold J**, Bloomeld D, LeVay J. Prospective randomized trial testing 5.7Gy and 6.0Gy fractions of whole breast radiotherapy in women with early breastcancer (FAST) trial. *Clin Oncol* 2004; **16**: S30

32 **Brunt AM**, Sydenham M, Bliss J, Coles C, Gothard L, Harnett A, Haviland J, Syndikus I, Wheatley D, Yarnold J. A 5-fraction regimen of adjuvant radiotherapy for women with early breast cancer: first analysis of the randomised UK FAST trial. *Eur J Cancer Suppl* 2009; **7**: 2

33 **Martin S**, Mannino M, Rostom A, Tait D, Donovan E, Eagle S, Haviland J, Yarnold J. Acute toxicity and 2-year adverse effects of 30 Gy in five fractions over 15 days to whole breast after local excision of early breast cancer. *Clin Oncol* (R Coll Radiol) 2008; **20**: 502-505

34 **Fisher J**, Scott C, Stevens R, Marconi B, Champion L, Freedman GM, Asrari F, Pilepich MV, Gagnon JD, Wong G. Randomized phase III study comparing Best Supportive Care to Biafine as a prophylactic agent for radiation-induced skin toxicity for women undergoing breast irradiation: Radiation Therapy Oncology Group (RTOG) 97-13. *Int J Radiat Oncol Biol Phys* 2000; **48**: 1307-1310

35 **Probst H**, Griffiths S. Moving to a high-tech approach to the irradiation of early breast cancer: is it possible to balance efficacy, morbidity and resource use? *Clin Oncol* (R Coll Radiol) 2006; **18**: 268-275

36 **Donovan E**, Bleakley N, Denholm E, Evans P, Gothard L, Hanson J, Peckitt C, Reise S, Ross G, Sharp G, Symonds-Tayler R, Tait D, Yarnold J. Randomised trial of standard 2D radiotherapy (RT) versus intensity modulated radiotherapy (IMRT) in patients prescribed breast radiotherapy. *Radiother Oncol* 2007; **82**: 254-264

37 **Munshi A**. External hypofractionated whole-breast radiotherapy: now where does accelerated partial breast irradiation stand? *J Cancer Res Ther* 2007; **3**: 231-235

38 **Mannino M**, Yarnold J. Accelerated partial breast irradiation trials: diversity in rationale and design. *Radiother Oncol* 2009; **91**: 16-22

39 **Offersen BV**, Overgaard M, Kroman N, Overgaard J. Accelerated partial breast irradiation as part of breast conserving therapy of early breast carcinoma: a systematic review. *Radiother Oncol* 2009; **90**: 1-13

40 Institute of Cancer Research. Visited on September 4, 2010. Available from: URL: http://www.icr.ac.uk/research/research_sections/clinical_trials/clinical_trials_list/10284.shtml

41 **Yarnold J**. Latest developments in local treatment: radiotherapy for early breast cancer. *Ann Oncol* 2005; **16** Suppl 2: ii170-ii173

S- Editor Cheng JX **L- Editor** Webster JR **E- Editor** Zheng XM

World Journal of Radiology

Online Submissions: http://www.wjgnet.com/1949-8470office
wjr@wjgnet.com
doi:10.4329/wjr.v2.i6.203

World J Radiol 2010 June 28; 2(6): 203-214
ISSN 1949-8470 (online)

EDITORIAL

Emerging roles for transthoracic ultrasonography in pulmonary diseases

Sergio Sartori, Paola Tombesi

Sergio Sartori, Paola Tombesi, Section of Interventional Ultrasound, Department of Internal Medicine, St. Anna Hospital, Ferrara 44100, Italy
Author contributions: Sartori S and Tombesi P contributed equally to this work.
Correspondence to: Sergio Sartori, MD, Section of Interventional Ultrasound, Department of Internal Medicine, St. Anna Hospital, Ferrara 44100, Italy. srs@unife.it
Telephone: +39-532-236551 Fax: +39-532-236738
Received: April 28, 2010 Revised: May 21, 2010
Accepted: May 28, 2010
Published online: June 28, 2010

Abstract

As a result of many advantages such as the absence of radiation exposure, non-invasiveness, low cost, safety, and ready availability, transthoracic ultrasonography (TUS) represents an emerging and useful technique in the management of pleural and pulmonary diseases. In this second part of a comprehensive review that deals with the role of TUS in pleuropulmonary pathology, the normal findings, sonographic artifacts and morphology of the most important and frequent pulmonary diseases are described. In particular, the usefulness of TUS in diagnosing or raising suspicion of pneumonia, pulmonary embolism, atelectasis, diffuse parenchymal diseases, adult and newborn respiratory distress syndrome, lung cancer and lung metastases are discussed, as well as its role in guidance for diagnostic and therapeutic interventional procedures. Moreover, the preliminary data about the role of contrast enhanced ultrasonography in the study of pulmonary pleural-based lesions are also reported. Finally, the limits of TUS when compared with chest computed tomography are described, highlighting the inability of TUS to depict lesions that are not in contact with the pleura or are located under bony structures, poor visualization of the mediastinum, and the need for very experienced examiners to obtain reliable results.

Key words: Ultrasonography; Pleural diseases; Lung diseases

Peer reviewers: Jai Soung Park, MD, PhD, Professor, Department of Radiology, Soonchunhyang University Buchen Hospital, 1174 jung-dong, Wonmi-gu, Bucheon, Gyeonggi-do 420-767, South Korea; Ritesh Agarwal, MD, DM, MAMS, FCCP, Assistant Professor, Department of Pulmonary Medicine, Postgraduate Institute of Medical Education and Research, Sector-12, Chandigarh 160012, India

Sartori S, Tombesi P. Emerging roles for transthoracic ultrasonography in pulmonary diseases. *World J Radiol* 2010; 2(6): 203-214 Available from: URL: http://www.wjgnet.com/1949-8470/full/v2/i6/203.htm DOI: http://dx.doi.org/10.4329/wjr.v2.i6.203

INTRODUCTION

In the first part of this review on the role of transthoracic ultrasonography (TUS) in the diagnostic workup of pleuropulmonary pathology, we described the ultrasound equipment, examination technique and limits of TUS, as well as the normal findings and artifacts that originate at the boundary between the pleura and the normally aerated lung pleura (i.e. the pleural line, gliding sign, horizontal reverberation artifacts, and comet-tail artifacts)[1].

In this second part of the review, we deal with the pathological lung. Indeed, as a consequence of its non-invasiveness, TUS can be very useful in lung pathology and can be used for the diagnosis of lung diseases and monitoring progress of sonographically visible processes, thus avoiding radiation exposure. Moreover, the relatively low cost and wide availability of standard conventional ultrasound machines, as well as the increasing use of modern portable devices, allow examination at almost any location and at any time. This makes TUS a valuable tool in many difficult situations, such as in an ambulance, emergency room, or directly at the bedside of critically ill patients.

Pulmonary pathology can be divided into diffuse interstitial (or parenchymal) lung diseases and peripheral or subpleural lung diseases. Peripheral or subpleural diseases commonly appear as pleural-based consolidations, whereas the presence of diffuse interstitial syndromes can be inferred by the detection of different artifacts with respect to normal lung. In particular, multiple comet-tail artifacts departing from the pleural line (much more numerous and diffuse than in the normally aerated lung) and ring-down vertical artifacts (characterized by a series of hyperechoic narrow-based bands spreading from the pleural line into the lung) can be visualized in these cases[2-8]. Interstitial lung diseases include pulmonary edema (due to heart failure, trauma, or inflammation) and interstitial fibrosis. Peripheral diseases with peculiar consolidation aspects are common in pneumonia, atelectasis, and pulmonary infarction. Adult respiratory distress syndrome (ARDS) generally shows mixed TUS features. Finally, neoplastic lesions that abut the pleura (both primary neoplasms and metastases) usually appear as hypoechoic, sometimes inhomogeneous, non-aerated masses.

PULMONARY DISEASES

For the purposes of this article, the main pulmonary diseases are divided into diffuse parenchymal pulmonary diseases, infection diseases, peripheral pulmonary artery embolisms and pulmonary infarction, atelectasis, adult and newborn distress respiratory syndrome, bronchopulmonary tumors and pulmonary metastases.

Diffuse parenchymal lung diseases

Diffuse parenchymal lung diseases (DPLDs) can be divided into those of known cause (e.g. collagen vascular disease), idiopathic interstitial pneumopathy (idiopathic and non-idiopathic pulmonary fibrosis), granulomatous (e.g. sarcoidosis), and other forms[9,10]. High-resolution computed tomography (HRCT) should be considered the gold standard technique to diagnose DPLD, and many other noninvasive and invasive procedures concur in clinical practice to define and characterize DPLD, such as chest radiography, laboratory and serological tests (e.g. angiotensin-converting enzyme and antinuclear antibodies), pulmonary function testing, bronchoscopy with bronchoalveolar lavage, and transbronchial lung biopsy. However, some studies have demonstrated that TUS, as a consequence of its well-known advantages (absence of radiation exposure, ready availability, and cost-effectiveness), can play a complementary role in the diagnosis of DPLD, especially when chest radiography or HRCT are not readily available or undesirable, for instance during pregnancy[9,10]. Moreover, TUS can be useful in monitoring the course of the disease in patients with confirmed DPLD (thus avoiding unnecessary overload of radiation exposure), and confirming the clinical-radiological suspicion of acute pulmonary edema due to heart failure, trauma, or inflammation. Indeed, radiological evidence of ground glass areas that are suggestive of pulmonary edema has often been associated with the presence of sonographic artifacts, such as multiple comet-tail artifacts and vertical ring-down artifacts. Likewise, typical radiological findings and corresponding sonographic findings can be observed in fibrosing pulmonary disease. Fibrosis usually involves the pleural surface as well as the intralobular and interlobular septa, therefore, thickened subpleural intralobular and interlobular septa, and ground glass areas, represent common findings at radiological examination[11]. In the same setting, TUS enables one to document multiple ring-down artifacts (Figure 1) and comet-tail artifacts that depart from a thickened and irregular pleural line (Figure 2). Indeed, in patients with diffuse alveolar-interstitial syndrome, multiple comet-tail artifacts can be observed all over the lung surface, and this finding has been reported to have high sensitivity. In a study of Reissig *et al*[9], almost all the patients with DPLD showed more than six comet-tail artifacts per scan associated with an irregular and fragmented pleural line. Comet-tail artifacts become visible when there is a marked difference in acoustic impedance between an object and its surroundings (as happens at the boundary between the pleural surface and the lung), which demarcates the edge of the normally aerated lung. These artifacts are best visible under real-time conditions, as they might appear less pronounced on frozen sonograms, which makes quantification of the alterations difficult. Lichtenstein *et al*[3] have attributed the origin of the comet-tail artifacts to the thick-

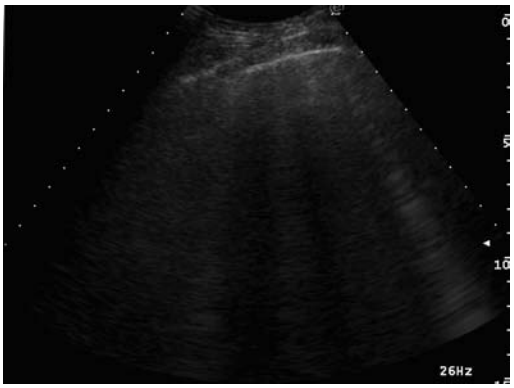

Figure 1 Ring-down artifacts, characterized by a series of hyperechoic, narrow-based bands spreading from the pleural line into the lung.

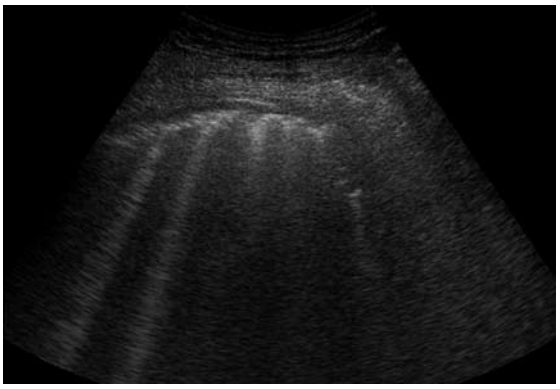

Figure 2 Pulmonary fibrosis. Multiple comet-tail artifacts departing from a thickened and irregular pleural line.

ening of the subpleural interlobular septa, which would cause fragmentation of the pleural reflector at the points of greatest impedance. However, it must be highlighted that pleural alterations and multiple comet-tail artifacts are nonspecific TUS features. They might also occur in patients with chronic obstructive lung disease, bronchiolitis obliterans-organizing pneumonia, and pulmonary alveolar proteinosis, as well as after pneumonia and pulmonary embolism. Some authors have suggested that the number of comet-tail artifacts is smaller and the affected area is more localized in these conditions[8,9,12]. In DPLD, these abnormalities are commonly detected on both sides of the lung, which reflects the diffuse fibrosing process, and corresponds to the findings on HRCT. However, the degree of the pleural involvement can vary within the same patient, and usually a thickened and fragmented pleural line with multiple comet-tail artifacts is better detectable in the lower part of the lung, which reflects the extent of the fibrosis. In conclusion, although diagnosis of DPLD requires chest radiography, HRCT, and often bronchoalveolar lavage and transbronchial biopsy, TUS can play some complementary role in the diagnostic workup. Multiple comet-tail artifacts distributed over the entire lung surface in combination with a thickened, irregular and fragmented pleural line are strongly suggestive of the presence of DPLD.

Infectious diseases

As previously described, peripheral pulmonary lesions in contact with the visceral pleura can easily be visualized by TUS[1,2,13-15]. However, the part of consolidation that can be visualized with TUS is generally smaller than that documented by chest radiography or CT, because just the areas on the level of the pleura can be detected. Indeed, at present pneumonia is mostly diagnosed by X-ray, and CT is considered the gold standard for the diagnosis of infectious lung diseases. However, in the case of a chest X-ray on only one plane, or in the case of a patient in the lying position, the summation image often cannot provide exact information. As concerns CT, its use is limited by the high radiation exposure and cost. TUS shows several advantages, such as its feasibility, low cost, and the possibility of monitoring disease progress, because it can either document resolution or detect complications such as lung abscesses, parapneumonic effusion, empyema, and pleural fibrosis. Moreover, TUS is the method of choice to guide transthoracic aspiration or drainage of pleural effusion, empyema, and pulmonary abscesses in contact with the pleura, playing a very useful role in both diagnosis and treatment of infectious diseases and their complications. In this regard, TUS has recently been reported to be as effective as chest CT in detecting loculated effusion and lung necrosis or abscess that results from complicated pneumonia in children[16]. As a consequence of its efficacy, reliability, and minimal radiation exposure, TUS has been recommended by the British Thoracic Society guidelines for the management of pediatric empyema as the first-line approach for detecting pleural effusion and guiding drain placement in children[17].

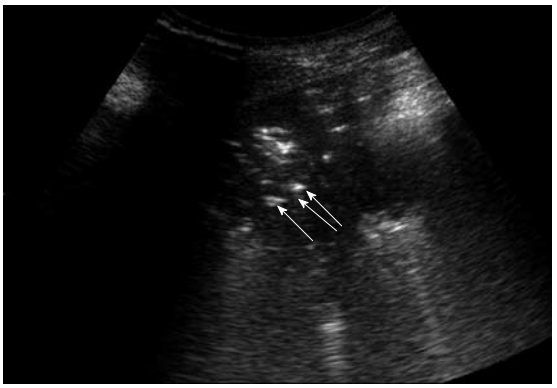

Figure 3 Pneumonia. Posterior intercostal scan shows a hypoechoic consolidated area that contains multiple echogenic lines that represent an air bronchogram (arrows).

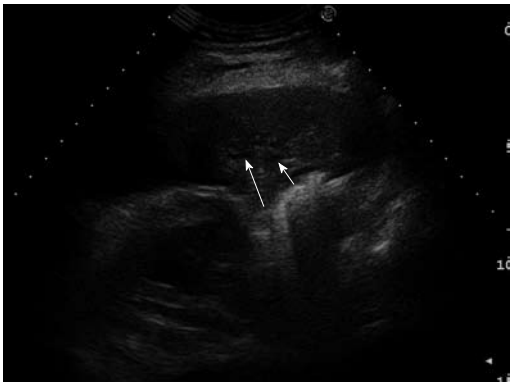

Figure 4 Post-stenotic pneumonia. Posterior intercostal scan shows a hypoechoic consolidated area that contains anechoic, branched tubular structures in the bronchial tree (fluid bronchogram) (arrows).

In this section, TUS findings in pneumonia, lung abscesses, and tuberculosis are described. Pneumonia is commonly visualized by TUS as a hypoechoic consolidated area of varying size and shape, with irregular borders. The echotexture can appear homogeneous or inhomogeneous[14-18]. The most common sonographic feature of pneumonia is the air bronchogram, which is characterized by lens-shape internal echoes within the hypodense area or echogenic lines (Figure 3), and corresponds to air inclusions or air-filled bronchioles and bronchi. Conversely, the fluid bronchogram is characterized by anechoic or hypoechoic tubular structures in the bronchial tree (Figure 4), without perfusion signs inside at color Doppler examination[1,2,13,19-21]. This feature suggests post-stenotic pneumonia that requires further investigation. Besides these common findings, some pleural signs are often present in infectious disease, as well as some vascular features[18]. The pleural line can appear interrupted, fragmented, and hypoechoic where the pneumonic infiltrate is present. A local pleural effusion occurs in about 9% of patients with pneumonia, and a basal pleural effusion appears in about 60% of patients[22]. As concerns vascular criteria, color Doppler sonography can show increased branch-like vessel visualization that corresponds to the segment branches of

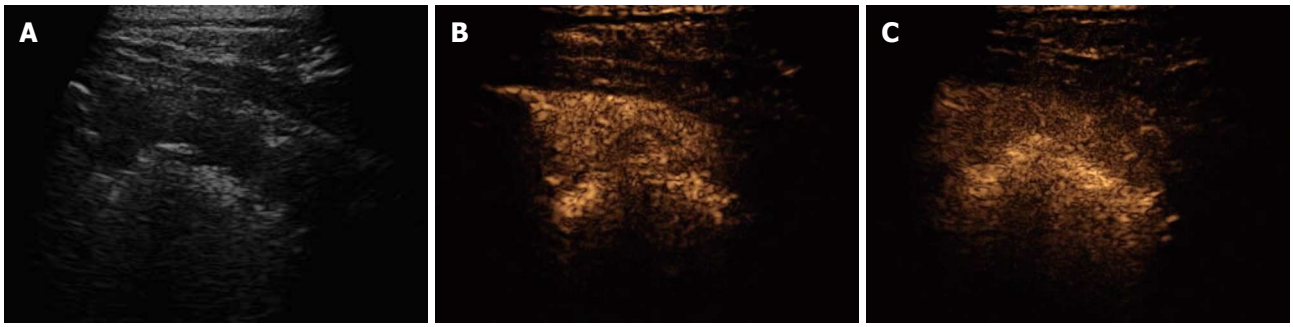

Figure 5 Contrast-enhanced ultrasonography of pneumonia. A: Baseline scan shows a hypoechoic consolidated area; B: Seven seconds after iv bolus of contrast agent, the lesion shows marked and homogeneous enhancement; C: The lesion remains substantially unmodified after 90 s.

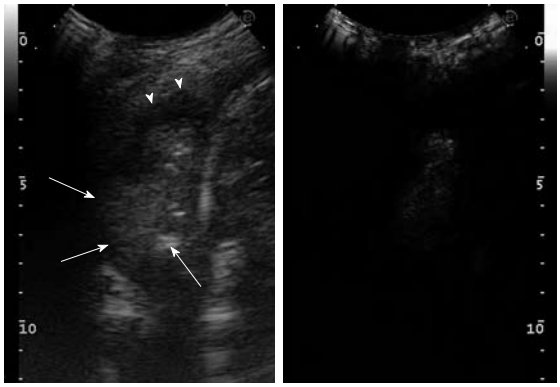

Figure 6 Contrast-enhanced ultrasonography evaluation of pneumonia with pleural effusion. Baseline scan shows parenchymal consolidation with air bronchogram (arrows) and subtle surrounding effusion (arrowheads) (left side of the split-screen). After iv bolus of contrast agent, the consolidation is enhanced and better demarcated from the effusion (right side of the split-screen).

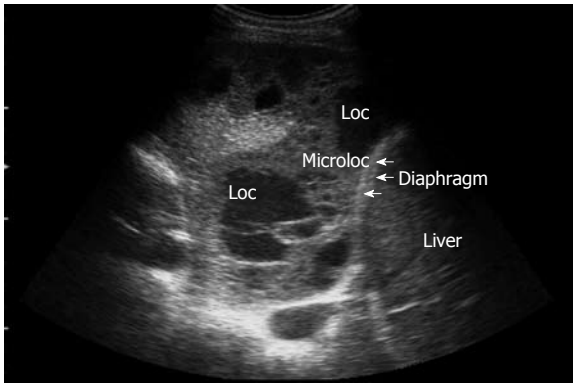

Figure 7 Pneumonia complicated by abscesses. Multiple small collections of fluid are irregularly settled in a consolidated liver-like infiltrate. Loc: Loculation; Microloc: Microloculation.

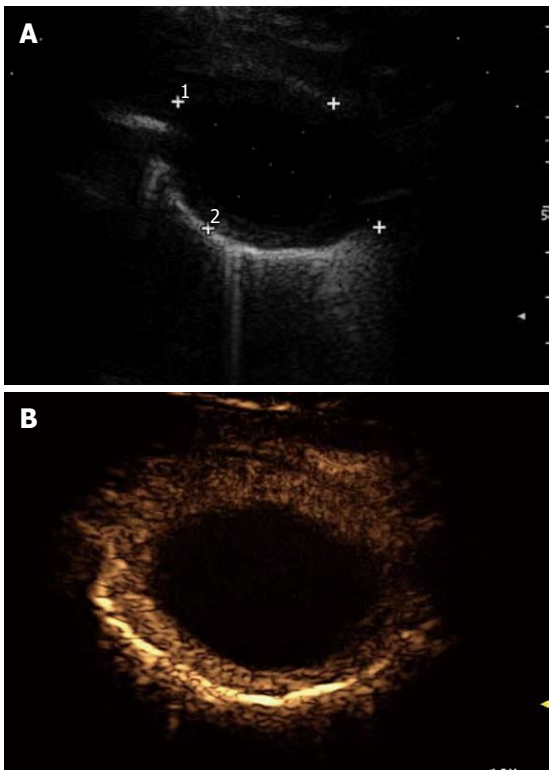

Figure 8 Lung abscess. A: An anechoic oval lesion is surrounded by an echodense capsule; B: After iv bolus of contrast agent, the lesion shows no contrast agent uptake, whereas the capsule is strongly enhanced.

the pulmonary artery. Contrast-enhanced ultrasonography (CEUS) of pneumonia usually shows a short wash-in period during the arterial phase and a prolonged and marked degree of contrast agent accumulation during the parenchymal phase in the case of classic pneumonia (Figure 5)[18]. These findings suggest preferential pulmonary arterial vascularization, as reported by some authors[23-26]. CEUS can also be helpful to detect complications like sequestration, to demarcate surrounding fluid (Figure 6), and to achieve a possible differential diagnosis with respect to pulmonary infarction and malignant lesions, which show different CEUS patterns, as described in the respective sections of this review.

Lung abscesses typically appear as round or oval, largely anechoic lesions[14,18]. In the early stage, small abscesses are visible as a pathological collection of fluid irregularly settled in a consolidated, liver-like infiltrate (Figure 7). Microabscesses are often visible as anechoic areas within the pneumonic consolidation. Commonly, a small pleural effusion is associated with lung abscesses. Depending on the capsule formation, the edge of the abscess can be smooth and echodense (Figure 8A). At CEUS evaluation, lung abscesses show lack of contrast agent uptake (Figure 8B) and this finding can be particularly useful in the detection of microabscesses, and in the differential diagnosis

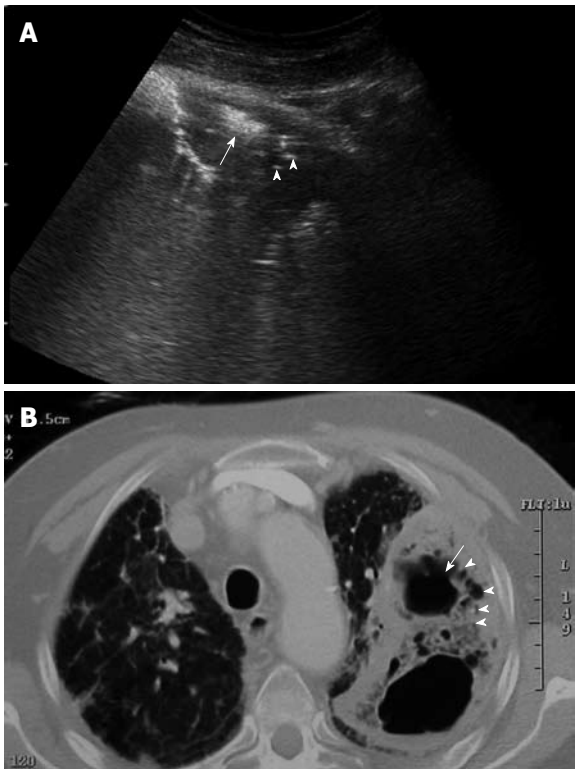

Figure 9 Lung abscess with air inside the lesion. A: High amplitude echoes are clearly visible (arrow), as well as multiple echogenic small air inclusions (arrowheads); B: Corresponding computed tomography scan shows the same findings.

between lung abscesses and malignant lesions[18,23]. The presence of air inside the lesion produces high amplitude echoes, and highly echogenic small air inclusions moving in the fluid with breathing can be observed especially in the case of abscesses due to gas-producing microorganisms, or in the case of connection to the bronchial system (Figure 9). If septa develop inside the lesion, they are visualized as echodense, fluttering threads.

Tubercular lung lesions appear as round or irregularly shaped lesions and show a relatively homogeneous texture. Depending on the size, air inclusions can be visible inside the lesions, but a pronounced air bronchogram, as in the case of pneumonia, is only rarely present. Miliary tuberculosis is characterized by multiple subpleural nodules several millimeters in size. Pleural effusions often occur at the beginning of the disease. Frequently, an initially anechoic pleural effusion shows internal echoes over the course of the disease, and pleural thickening is often associated. However, no specific TUS pattern of pulmonary tuberculosis can be identified, and no definitive CEUS data have been reported in the literature.

Peripheral pulmonary artery embolism and pulmonary infarction

Chest radiography is still considered the first diagnostic step in patients with suspected pulmonary embolism (PE). It can show infiltrates, atelectasis, and effusion, but such features represent just the consequence of PE on the periphery and are nonspecific, because the central embolism cannot be visualized. Consequently, ventilation-perfusion scintigraphy and CT angiography are needed to confirm the diagnosis[27]. However, the Prospective Investigation of Pulmonary Embolism Diagnosis Study has shown that ventilation-perfusion scintigraphy is not sufficiently conclusive. In that study, high-probability scans resulted in detection in only a minority of patients with PE, whereas PE was present in 12% of patients with low-probability scans[28]. In recent years, CT pulmonary angiography (CTPA) has been established as the method of choice for the diagnosis of central PE up to the level of the segmental arteries, because it enables one to show the thromboembolic obstruction directly. Spiral CT scanning shows a sensitivity and specificity of 90% in depicting thrombi within the central pulmonary vessels, and can reveal characteristic consolidations in patients with acute PE[29-31]. Pulmonary angiography has long been considered the gold standard for diagnosing PE, but nowadays, it is rarely used because of its invasive nature and the risk of complications[32], and it has been almost completely replaced by CTPA. However, despite their usefulness, in some circumstances critically ill patients may not tolerate any of these procedures, and occasionally, adequate equipment might not be available. In these cases, TUS can play some useful roles, because it shows the major advantage of bedside availability in the emergency room and in the intensive care unit, and it has been reported to have good accuracy in the diagnosis of PE[33-35]. The sensitivity of TUS for PE has been estimated to range from 80% to 94%, the specificity from 84% and 92%, and the overall accuracy from 82% to 91%[33,36,37]. A recent meta-analysis has reported sensitivity and specificity of 80% and 93%, respectively[38].

Typical sonographic findings in peripheral PE are multiple, hypoechoic lesions that are visible at the level of the pleura, which can usually be well demarcated from the surrounding parenchyma. About two-thirds of PE-based consolidations can be visualized in the dorsal basal position for anatomical and hemodynamic reasons, with a preference for the right lung. Frequently, the lesions show a triangular or wedge shape. In a recent prospective multicenter study of 352 patients, the sonographic morphology was mainly triangular, with the vertex towards the hilum of the lung in 58% of the cases, and rounded or mixed in 42%. In that study, a small pleural effusion was seen in 49%, a basal effusion in 33%, and a focal effusion in 16% of the cases[34]. The lesions are almost always pleural-based, are freely subject to respiratory excursions, and their size usually exceeds 2 cm in diameter. When the lesions are > 3 cm in size, central bronchial echoes can be seen as central hyperechoic structures that indicate the presence of air in the affected bronchioles, which is considered a sign of segmental involvement (Figure 10). Lesions visualized on TUS are smaller than on CT angiography because of the presence of air artifacts at the deeper margins and at the top of the infarct cone, but TUS can depict either a larger number of lesions or smaller lesions than CT scan[34]. Although the specificity of sonographic morphology of the lesions is limited, the detection of two or more

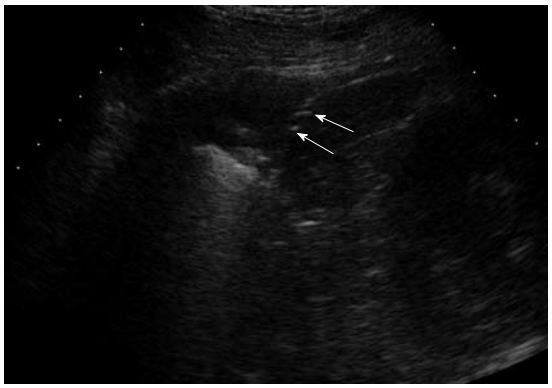

Figure 10 Pulmonary infarction. Posterior intercostal scan shows a triangular-shaped hypoechoic lesion with central hyperechoic structures that indicate the presence of air occupying the affected bronchiole (arrows).

triangular or rounded lesions with a pleural base, 0.5-3 cm in size, can often represent a confirmation of clinically suspected PE, and the contemporary presence of a small pleural effusion makes the diagnosis of PE very likely.

Thromboembolism is often a dynamic event that is associated with recurrent embolization and spontaneous lysis (besides the pharmacologically induced lysis). Moreover, 70%-90% of emboli are associated with peripheral pulmonary hemorrhage, the so-called incomplete or partial infarction, which can be reabsorbed within a few hours or days[34]. Consequently, follow-up imaging techniques can document the disappearance of previously depicted pleural-based pulmonary lesions (Figure 11). On color Doppler sonography, PE-based peripheral lesions do not show flow signals inside, a phenomenon defined as "consolidation with little perfusion"[35]. On the other hand, recanalization of incomplete infarction that results from anticoagulation treatment or intrinsic lysis can be demonstrated by the reappearance of a blood flow signal on follow-up. In addition, a congested thromboembolic vessel (vascular sign) might occasionally be visible, and corresponds to a pulmonary artery with thickened vessel walls around an intraluminal organizing embolus[35]. Corresponding to these findings, initial studies in patients with confirmed PE have reported that the lesions show a lack of contrast agent uptake in the arterial phase at CEUS examination, which suggests the absence of pulmonary arterial blood supply (Figure 12). However, in patients with PE and pleural effusion or in those with chronic PE, mixed enhancement might be observed[18,23,25].

In conclusion, although CTPA is undoubtedly the method of choice to obtain a definitive diagnosis of PE, TUS should be taken into consideration in some circumstances, particularly in critically ill patients who might not tolerate transport for other imaging modalities. Moreover, even though a negative result does not rule out PE, TUS can play a central role in patients with presumed PE in cases of pregnancy, contrast agent allergy, or renal failure.

Atelectasis

Atelectasis is defined as the absence of ventilation in part of the lung or the entire lung, and therefore it can be visualized by sonography. It can be divided into compression atelectasis due to voluminous pleural effusion, and obstructive or resorptive atelectasis caused by bronchial block of air entry[39]. At TUS examination, compression atelectasis appears as a largely apneumatic consolidation with liver-like echotexture. It shows the shape of a jelly bag cap, and can be monoconcave or biconcave (Figure 13). Typically, compression atelectasis can be seen floating in the effusion like a waving hand, and is partially ventilated during breathing. Obstructive atelectasis shows a liver-like and inhomogeneous echotexture with secretion-filled bronchi (fluid bronchogram) and variable shape (Figure 4).

The air content inside the consolidation typically does not change during inspiration. In patients with alveolar consolidations that show air bronchograms, the real-time TUS visualization of bronchograms during breathing movements can often enable one to distinguish between obstructive atelectasis and pneumonia[39]. The presence of the dynamic air bronchogram indicates pneumonia, while a static air bronchogram suggests obstructive atelectasis. In a recent study by Lichtenstein *et al*, the dynamic air bronchogram showed a specificity of 94% and a sensitivity of 61%. In the same study, the authors described early and late signs suggestive for obstructive atelectasis. Early signs included the disappearance of lung sliding associated with the presence of the lung pulse, a cardiac activity visible throughout abolished lung sliding, and the presence of a standstill cupola that demonstrated the absence of lung expansion. The late sign appeared when the air inside the consolidation was progressively absorbed, which yielded a loss of volume of the lesion with the typical static air bronchogram inside[39]. The capability of TUS to detect the air bronchogram represents a major advantage, particularly in critically ill patients, because TUS enables one to visualize this sign also in ventilated newborns, thus reducing the necessity for ionizing radiation exposure. Moreover, TUS is probably more accurate than chest radiography in the detection of air bronchograms[39,40].

Pleural effusion is almost always associated with compression atelectasis and frequently with obstructive atelectasis. In the case of compression atelectasis, the effusion is typically larger compared to that associated with obstructive atelectasis.

At color Doppler evaluation, compression atelectasis shows increased branch-like vessel visualization when compared to the liver. The corresponding findings at CEUS examination include short time to enhancement, which indicates predominant pulmonary arterial vascularization, and marked enhancement during the arterial and parenchymal phase (Figure 14). In patients with compression atelectasis, the contrast agent apparently remains trapped in lung tissue after wash-out of the blood pool, in comparison with splenic enhancement. In the case of obstructive atelectasis, color Doppler sonography almost always shows increased vessel visualization inside the consolidation, and this finding can be useful for distinguishing central space-occupying neoplastic lesions from atelectatic lung parenchyma, because tumor tissue is

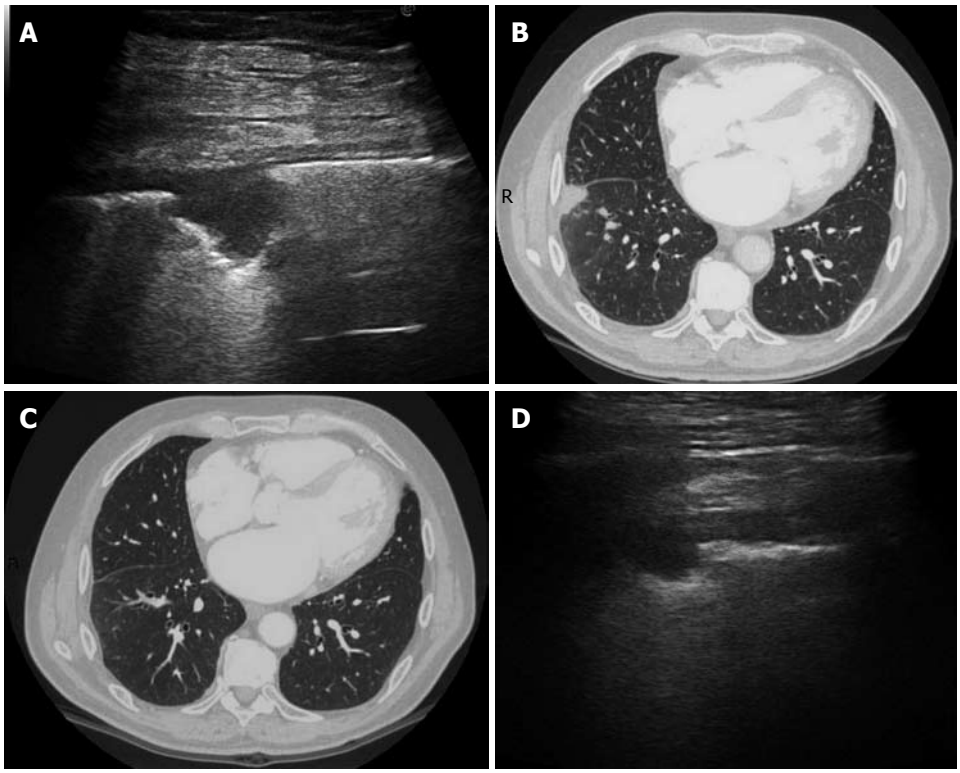

Figure 11 Dynamic course of pulmonary infarction. A: Lateral intercostal scan of the right lung shows a typical triangular-shaped peripheral lesion; B: Likewise, computed tomography scan of the lateral segment of the lower right lobe shows a triangular pleural-based lesion with the vertex towards the hilum; C: After 40 d, the lesion is no longer visible by computed tomography scan; D: The lesion appears reduced in size at transthoracic ultrasonography examination.

Figure 12 Contrast-enhanced ultrasonography of pulmonary infarction. After iv bolus of contrast agent, the lesion (the same one as in Figure 11A) shows no contrast agent uptake in the arterial phase, which suggests the absence of blood supply.

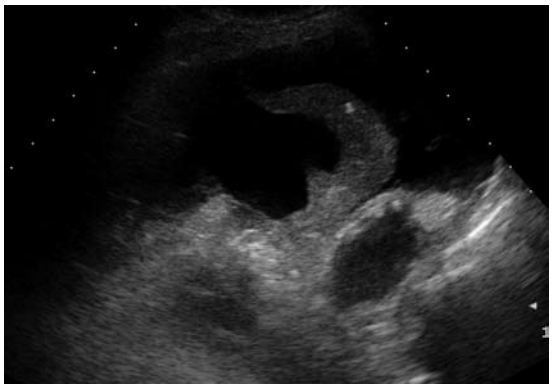

Figure 13 Compression atelectasis. Posterior intercostal scan shows a liver-like consolidation with the typical shape of a jelly bag cap surrounded by pleural effusion.

characterized by minimal representation of flow signals. At CEUS examination, new obstructive atelectasis has been reported to show a short time to enhancement, with accumulation of the contrast agent similar to that in the spleen, which suggests predominant pulmonary arterial vascularization[18,23,25]. However, in a recent study, patients with tumor-associated obstructive atelectasis showed different CEUS patterns, including either a marked extent of enhancement and short time to enhancement, or a delayed time to enhancement and nearly complete absence of extent of enhancement[23]. In the patients with central lung cancer, the delayed time to enhancement could be secondary to transmural tumor growth, with intraluminal cell formation in the pulmonary artery branches, with consequent obliteration and occlusion of pulmonary arteries. The presence of a central tumor can be identified and more clearly distinguished from the atelectatic parenchyma, because it shows a delayed time to enhancement and a reduced extent of enhancement in comparison with the surrounding atelectatic parenchyma.

In both compression and obstructive atelectasis, TUS is able to monitor the course of the disease. In particular, the pleural effusion that causes compression atelectasis can be

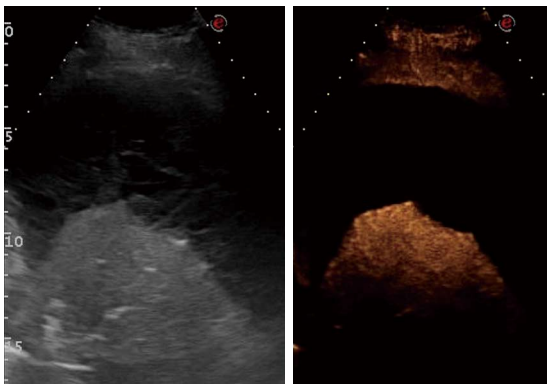

Figure 14 Contrast-enhanced ultrasonography evaluation of compression atelectasis. Baseline scan shows a liver-like consolidation surrounded by multiloculated pleural effusion (left side of the split-screen). Twelve seconds after iv bolus of contrast agent, the consolidation shows marked and homogeneous enhancement, whereas pleural effusion shows no enhancement.

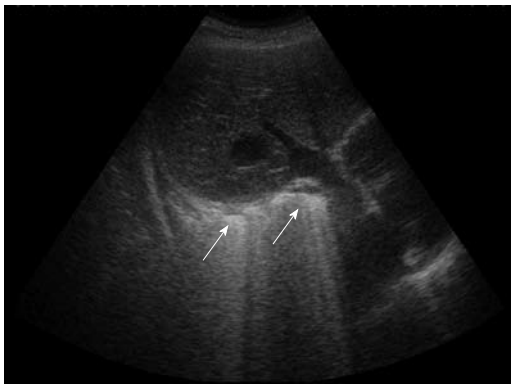

Figure 15 Adult respiratory distress syndrome. Oblique subcostal scan through the right lobe of the liver shows the typical transthoracic ultrasonography pattern of intense retro-phrenic hyperechogenicity due to complete reverberation of the US beam (arrows).

monitored during diuretic treatment, as well as after TUS-guided aspiration. After effusion puncture, compression atelectasis can become smaller or no longer visible, depending on the capability of the lung to re-expand. In the case of obstructive atelectasis, aspiration of pleural effusion can result in formation of a pneumothorax *ex vacuo*, which can be also detected by TUS.

ARDS and newborn respiratory distress syndrome

CT scanning is traditionally considered the gold standard in the evaluation of both ARDS and newborn respiratory distress syndrome (NRDS), and recruitment of atelectatic lung regions after therapy, because it is the only available technique that can directly measure the extension of the affected and healthy lung tissue[41-43]. However, TUS enables a dynamic evaluation of lung recruitment and can be easily performed at the bedside. Such ability feature is particularly useful in patients affected by ARDS/NRDS because they are frequently too instable to be moved to the CT room. Moreover, TUS can be repeated as much as is needed to monitor the course of the disease. Although at present only few preliminary data have been reported, some authors have recently described the important role of TUS in critically ill patients affected by ARDS, as well as in NRDS patients[41-44].

The main features of ARDS/NRDS are diffuse alveolar infiltration and lung consolidation. TUS findings depend on the decreased aeration of the alveoli because of atelectasis, so that the ultrasound beam can be transmitted further beyond the phreno-pulmonary border into the lung parenchyma. Conversely, in normally aerated lungs, the ultrasound beam is completely reflected by the phreno-pulmonary border. The ultrasound beam is then completely reverberated by the dilated and aerated bronchioles and alveolar ducts, which gives rise to the typical TUS pattern of intense retro-phrenic hyperechogenicity that can be observed in patients with ARDS[43,45,46] (Figure 15). In a study of Bober *et al*[43], 131 newborns with clinical signs of respiratory failure underwent ultrasound examination, by application of the transducer in the left and right epigastric regions, and scans were obtained through the right lobe of the liver and the spleen. The pattern of echogenicity above the diaphragm was observed sequentially during numerous respiratory cycles. Alterations in lung aeration suggestive of NRDS were found in 109/131 subjects, and the diagnosis was confirmed in 101 cases by chest X-ray. TUS showed a sensitivity of 100%, and a specificity of 92% in diagnosing NRDS.

Numerous B-lines are typically present in the areas of ventilated parenchyma near the consolidation[41,42]. TUS allows the assessment of lung consolidation adjacent to the visceral pleura, but only parenchymal abnormalities adjacent to the pleura can be evaluated. However, notwithstanding this major limitation, patients with ARDS due to extrapulmonary causes generally show symmetrical consolidations adjacent to the visceral pleura and set behind at the base of the lung[41,44]. Dynamic air bronchogram is often present within the consolidation, which can help in excluding the obstructive origin of the consolidation and in supporting the diagnosis of ARDS.

Primary lung carcinoma

Although differentiating chronic benign lung consolidations from malignant tumors is difficult at TUS examination, and further investigations are always mandatory, TUS enables one to gather a lot of information about malignant peripheral lung lesions. Moreover, the capability of TUS to guide percutaneous biopsy of peripheral lesions, and its feasibility, as well as the interesting preliminary data about CEUS evaluation of lung lesions[18,23-26], make TUS a useful and innovative technique in the study of pulmonary malignancies.

Peripheral bronchial carcinomas usually appear at TUS as round or oval, sometimes polycyclic, hypoechoic consolidated lesions, with relatively well delineated borders[14] (Figure 16). The lesions can appear both homogeneous and inhomogeneous, while air bronchograms typically cannot be detected, because solid carcinomas do not contain aerated lung parenchyma[14,18]. If tumor necrosis occurs, it can be visualized as a particularly hypoechoic to anechoic region within the tumor. CEUS can help to de-

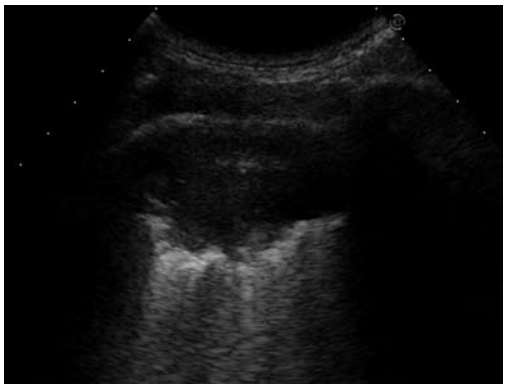

Figure 16 Peripheral bronchial carcinoma. Posterior intercostal scan shows a hypoechoic consolidation with relatively well-delineated borders. The air bronchogram is absent.

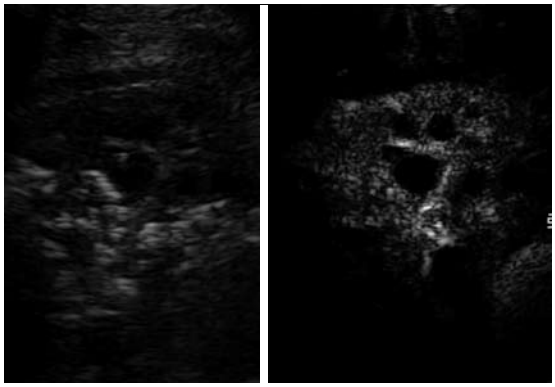

Figure 17 Contrast-enhanced ultrasonography evaluation of bronchial carcinoma. Baseline scan shows consolidation with inhomogeneous echotexture (left side of the split-screen). Twenty seconds after iv bolus of contrast agent, necrotic areas can be depicted as anechoic regions inside the enhanced viable tumor (right side of the split-screen).

fine better necrotic areas that are depicted as anechoic regions inside the enhanced viable tumor[18,23-26] (Figure 17). In some cases, a diffuse or locally infiltrating growth can be observed. The infiltrative growth of solid tissue without regard to anatomical structures is characteristic of malignancy. Indeed, only rare inflammatory diseases, such as actinomycosis or nocardiosis, can also spread in this manner. Typically, malignant consolidations move rigidly and do not change their shape during respiration. Nevertheless, the gliding sign can still be observed if the tumor has not crossed the visceral pleura. Conversely, respiratory excursion can no longer be detected if the tumor infiltrates the thoracic wall. Frequently, the pleural line near the lesion appears fragmented or interrupted. Malignant lesions that abut the pleura commonly form an acute angle with the pleural line, and this finding might be helpful in differentiating malignant from benign lesions, as described in the first part of this review[1]. Bronchial carcinomas are often accompanied by pleural effusion, frequently hemorrhagic, as an expression of pleural carcinomatosis[18]. Pleural metastases from bronchogenic carcinoma are usually too small to be detected by imaging techniques[1]. However, when their size is large enough to

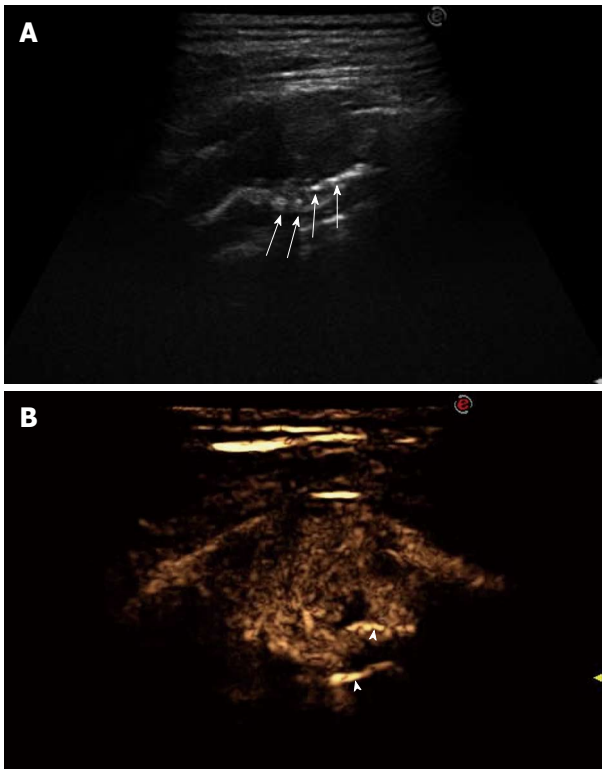

Figure 18 Bronchial carcinoma infiltrating the pleural wall. A: Posterior intercostal scan shows a hypoechoic lesion accompanied by rib destruction (arrows); B: Twenty-four seconds after iv bolus of contrast agent, the lesion appears inhomogeneously enhanced; the disrupted rib appears more echogenic than the tumor (arrowheads), as a consequence of the incomplete tissue suppression due to the strong echogenicity of bone tissue.

allow their visualization by TUS, they appear as hypoechoic nodules attached to the pleura, and are well delimited from the pleural effusion[18]. In the case of central bronchial carcinomas, only the atelectasis due to obstruction can be identified by TUS[14,39]. For long-lasting obstruction, a fluid bronchogram can be observed within the consolidated lung parenchyma. Some preliminary reports have suggested that CEUS can often enable one to demarcate central tumor lesions from the atelectatic parenchyma, as previously described[18,23-26].

A recent review has discussed the role of TUS in diagnosing and staging lung cancer[47]. In particular, the authors have stressed the usefulness of TUS in staging both local tumor spread (T) and distant lymph node invasion (N), as well as in detecting distant metastases (M). Identification of infiltration of the thoracic wall results in a change of the surgical approach because, in such cases, the affected sections of the thoracic wall must be resected together with the primary tumor. In this regard, TUS has been reported to have a significantly higher sensitivity than chest CT in diagnosing thoracic wall infiltration (89%-100% *vs* 42%-68%)[48,49]. Both direct evidence of infiltration of the wall structures and rib destruction can be considered TUS criteria for infiltration of the thoracic wall (Figure 18), whereas an interruption of the pleural line and/or limited respiratory movement of the consolidated lesion provide a suspicion but not a proof of infiltration of the thoracic

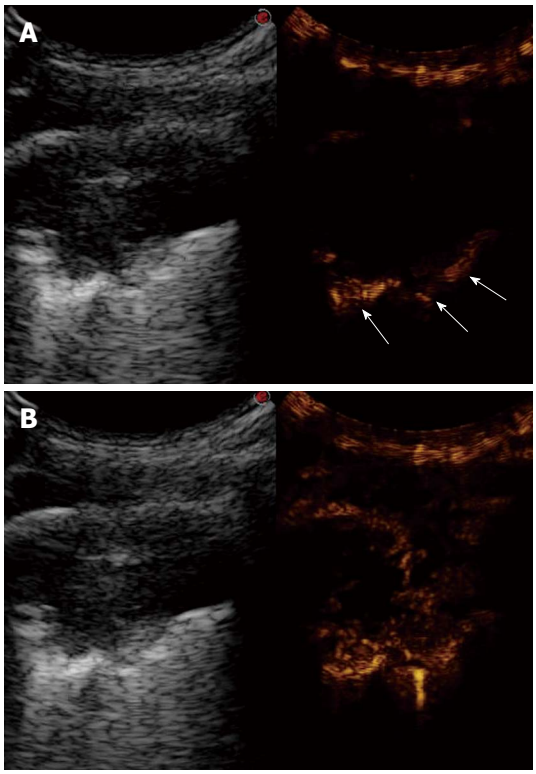

Figure 19 Contrast-enhanced ultrasonography of bronchial carcinoma. A: Baseline scan shows a hypoechoic lesion with irregular borders (left side of the split-screen). Ten seconds after iv bolus of contrast agent, the pulmonary parenchyma near the lesion is already enhanced (arrows), whereas the lesions is still unenhanced (right side of the split-screen); B: Twenty seconds later, the lesion shows delayed inhomogeneous enhancement, which indicates a preferential bronchial arterial supply (right side of the split-screen).

wall[47,48]. The presence of pleural effusion in a patient with bronchial carcinoma usually indicates pleural involvement, and corresponds to a T4 stage tumor[47]. Less frequently, pleural effusion is a para-malignancy that accompanies effusion, due to lymphatic drainage dysfunction, atelectasis, or hypoproteinemia[50]. It follows that correct staging requires differentiation between malignant pleural effusion and reactive accompanying effusion, and TUS is considered the method of choice to identify pleural effusion, as well as to guide aspiration for cytological examination. With respect to N stage, TUS enables one to identify supraclavicular or cervical lymph node involvement, and this finding has a central role in the staging of bronchial carcinoma because lymph node metastases can be identified in 16%-26% of patients[51-53]. Finally, US examination of the abdomen can identify the presence of distant metastases in the liver or adrenal glands, thus contributing to M staging of bronchial carcinoma[47]. However, notwithstanding the usefulness of TUS and the central role played in detecting infiltration of the thoracic wall, CT examination is mandatory for correct and complete staging of lung cancer.

At color Doppler examination, malignant tumors can present with reduced vessel visualization[18]. However, as a rule, color Doppler sonography is not suitable for differentiating benign from malignant peripheral lesions. Based on the dual arterial supply of the lung, CEUS is able to characterize pulmonary arterial and bronchial arterial lung vascularity. Although a definitive differentiation between benign and malignant lesions is not yet possible, preliminary data in the literature support our personal experience in suggesting a possible role of CEUS in the diagnostic workup of patients with pleural-based pulmonary nodules of unknown origin[18,23-26]. Typical CEUS findings in pleural-based lung cancer are a delayed time to enhancement and variable extent of enhancement (Figure 19), which indicates a preferential bronchial arterial supply, which plays a major role in the tumor neoangiogenesis of growing cancer[18,23-26].

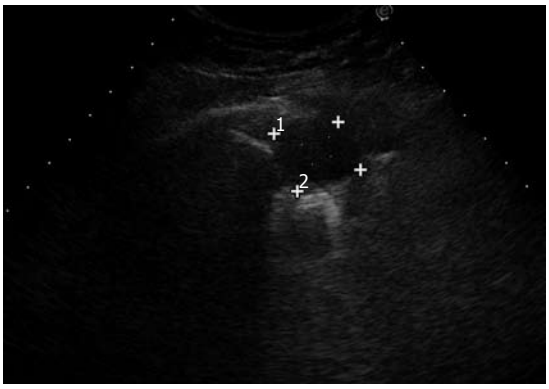

Figure 20 Pulmonary metastasis. Posterior intercostal scan shows a round-shaped, clear-bordered lesion.

Pulmonary metastases

The presence of one or more pulmonary nodules in a patient with a history of underlying malignancy is almost always suggestive of metastatic disease. Spiral CT scanning is the most accurate imaging modality for detecting nodules over the entire lung[14,54-56]. TUS presents the limit of an incomplete view of the lung parenchyma. However, TUS enables one to visualize even small peripheral metastatic lesions, and represents the method of choice to guide the biopsy of peripheral lung lesions that abut the pleura[1].

Pulmonary metastases can appear at TUS with varying echotexture, round shape, and typically clear borders[18] (Figure 20). A reliable differentiation between pulmonary metastases and metastases of the parietal pleura is possible on the basis of the lack of respiratory excursion. However, metastases of the visceral pleura that do not involve the parietal pleura can present respiration-dependent movement, like pulmonary metastases. Peripheral pulmonary metastases are typically small, therefore, it is usually not possible to derive flow signals at color Doppler sonography[18]. Furthermore, respiration-dependent or pulsatile motion artifacts are often present, which makes the value of color Doppler examination hardly useful for the evaluation of peripheral pulmonary metastases. Compared to color Doppler sonography, CEUS can also be performed for small lesions. The arterial supply of lung metastases derives from systemic arterial circulation, therefore, at CEUS examination, they are usually characterized by delayed contrast enhancement and reduced contrast agent extent with respect to the pulmonary parenchyma (Figure 21)[18,23-26].

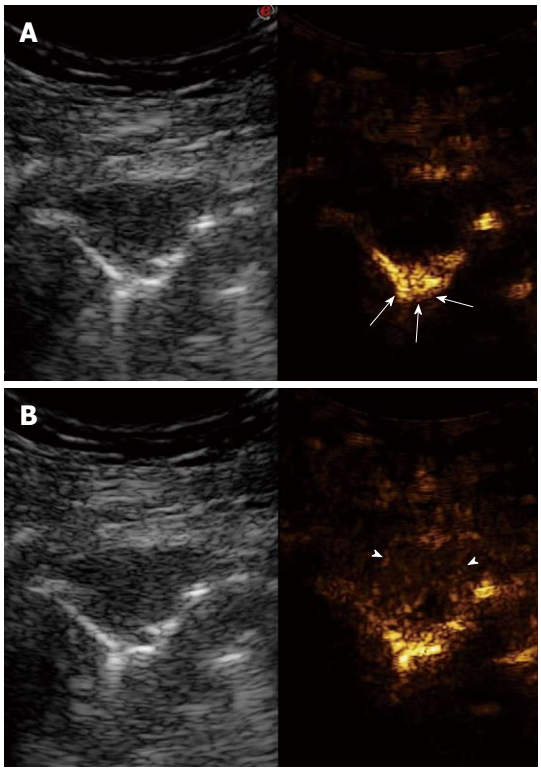

Figure 21 Contrast-enhanced ultrasonography of pulmonary metastasis. A: Baseline scan shows a small hypoechoic lesion (left side of the split-screen). Ten seconds after iv bolus of contrast agent, the lesion appears unenhanced with respect to the early enhancement of the pulmonary parenchyma (arrows) (right side of the split-screen); B: Fifty seconds later, the lesion shows inhomogeneous enhancement with reduced contrast agent extent (arrowhead) with respect to the pulmonary parenchyma (right side of the split-screen).

CONCLUSION

The limits of ultrasonography in the study of the lung are well established. First, the sonographic waves are hindered by air and bony structures, therefore, TUS cannot detect subscapular, paravertebral and retrosternal lesions, nor provide any diagnostic information in the presence of subcutaneous emphysema, and achieves poor visualization of the mediastinum. Second, it can only depict processes at the level of the pleura, thus, centrally located lesions cannot be detected by TUS. Finally, TUS is strictly operator dependent, and a lot of experience is needed to perform a reliable evaluation of pulmonary diseases. It follows that TUS cannot replace chest CT in the study of the lung.

However, certain diseases can be diagnosed with TUS (pneumonia with or without accompanying pleural effusion, PE, and atelectasis), other diseases can be suspected (diffuse parenchymal diseases, ARDS/NRDS, lung cancer and lung metastases that abut the pleura), and some preliminary experiences suggest that the use of second-generation ultrasound contrast agents provides useful information in the differential diagnosis between neoplastic and inflammatory diseases. Moreover, diagnostic and therapeutic interventional procedures can be performed under sonographic guidance. In this regard, TUS is considered the method of choice to guide aspiration and drainage of pleural effusion and empyema, and TUS-guided biopsy has been proved to be as effective as CT-guided biopsy of peripheral pulmonary lesions when they are in contact with the pleura and provide an adequate acoustic window. Finally, the well-known advantages of ultrasonography, such as the lack of radiation exposure, easy availability, and possibility of performing examination at almost any location, make TUS a valuable tool to be used without restriction in pregnant women, newborns, and at the bedside in critically ill patients, as well as to monitor the course of the disease.

In conclusion, TUS of the lung and pleura should be considered a very useful method that is complementary to chest CT in the diagnostic workup of pleuropulmonary pathology, and some effort should be encouraged in clinical and radiological departments to train skilled examiners with wide experience in TUS.

REFERENCES

1 **Sartori S**, Tombesi P. Emerging roles for transthoracic ultrasonography in pleuropulmonary pathology. *World J Radiol* 2010; **2**: 83-90
2 **Soldati G**, Copetti R. Ecografia toracica. Torino: CG Edizioni Medico-Scientifiche, 2006: 12-21
3 **Lichtenstein D**, Mézière G, Biderman P, Gepner A, Barré O. The comet-tail artifact. An ultrasound sign of alveolar-interstitial syndrome. *Am J Respir Crit Care Med* 1997; **156**: 1640-1646
4 **Jambrik Z**, Monti S, Coppola V, Agricola E, Mottola G, Miniati M, Picano E. Usefulness of ultrasound lung comets as a nonradiologic sign of extravascular lung water. *Am J Cardiol* 2004; **93**: 1265-1270
5 **Agricola E**, Bove T, Oppizzi M, Marino G, Zangrillo A, Margonato A, Picano E. "Ultrasound comet-tail images": a marker of pulmonary edema: a comparative study with wedge pressure and extravascular lung water. *Chest* 2005; **127**: 1690-1695
6 **Avruch L**, Cooperberg PL. The ring-down artifact [Abstract]. *J Ultrasound Med* 1985; **4**: 21-28
7 **Soldati G**, Rossi M. Wet and dry lungs: a useful sonographic distinction [abstract]. *Crit Care* 1999; **3** Suppl 1: 61
8 **Kroegel C**, Reissig A, Hengst U. [Diagnosis of parenchymal lung diseases. Possibilities and limits of transthoracic sonography] *Dtsch Med Wochenschr* 1999; **124**: 765-772
9 **Reissig A**, Kroegel C. Transthoracic sonography of diffuse parenchymal lung disease: the role of comet tail artifacts. *J Ultrasound Med* 2003; **22**: 173-180
10 **American Thoracic Society**; European Respiratory Society. American Thoracic Society/European Respiratory Society International Multidisciplinary Consensus Classification of the Idiopathic Interstitial Pneumonias. This joint statement of the American Thoracic Society (ATS), and the European Respiratory Society (ERS) was adopted by the ATS board of directors, June 2001 and by the ERS Executive Committee, June 2001. *Am J Respir Crit Care Med* 2002; **165**: 277-304
11 **Miller WT Jr**, Shah RM. Isolated diffuse ground-glass opacity in thoracic CT: causes and clinical presentations. *AJR Am J Roentgenol* 2005; **184**: 613-622
12 **Soldati G**, Copetti R, Sher S. Sonographic interstitial syndrome: the sound of lung water. *J Ultrasound Med* 2009; **28**: 163-174
13 **Soldati G**. Lung sonography: artifact, movement or echotexture. *J Ultrasound* 2001; **4**: 329-338
14 **Beckh S**, Bölcskei PL, Lessnau KD. Real-time chest ultrasonography: a comprehensive review for the pulmonologist. *Chest* 2002; **122**: 1759-1773
15 **Acunas B**, Celik L, Acunas A. Chest sonography. Differentia-

tion of pulmonary consolidation from pleural disease. *Acta Radiol* 1989; **30**: 273-275
16 **Kurian J**, Levin TL, Han BK, Taragin BH, Weinstein S. Comparison of ultrasound and CT in the evaluation of pneumonia complicated by parapneumonic effusion in children. *AJR Am J Roentgenol* 2009; **193**: 1648-1654
17 **Balfour-Lynn IM**, Abrahamson E, Cohen G, Hartley J, King S, Parikh D, Spencer D, Thomson AH, Urquhart D. BTS guidelines for the management of pleural infection in children. *Thorax* 2005; **60** Suppl 1: i1-i21
18 **Reissig A**, Görg C, Mathis G. Transthoracic sonography in the diagnosis of pulmonary diseases: a systematic approach. *Ultraschall Med* 2009; **30**: 438-454; quiz 455-456
19 **Yang PC**, Luh KT, Chang DB, Yu CJ, Kuo SH, Wu HD. Ultrasonographic evaluation of pulmonary consolidation. *Am Rev Respir Dis* 1992; **146**: 757-762
20 **Targhetta R**, Chavagneux R, Bourgeois JM, Dauzat M, Balmes P, Pourcelot L. Sonographic approach to diagnosing pulmonary consolidation. *J Ultrasound Med* 1992; **11**: 667-672
21 **Weinberg B**, Diakoumakis EE, Kass EG, Seife B, Zvi ZB. The air bronchogram: sonographic demonstration. *AJR Am J Roentgenol* 1986; **147**: 593-595
22 **Reissig A**, Kroegel C. Sonographic diagnosis and follow-up of pneumonia: a prospective study. *Respiration* 2007; **74**: 537-547
23 **Görg C**. Transcutaneous contrast-enhanced sonography of pleural-based pulmonary lesions. *Eur J Radiol* 2007; **64**: 213-221
24 **Sperandeo M**, Sperandeo G, Varriale A, Filabozzi P, Decuzzi M, Dimitri L, Vendemiale G. Contrast-enhanced ultrasound (CEUS) for the study of peripheral lung lesions: a preliminary study. *Ultrasound Med Biol* 2006; **32**: 1467-1472
25 **Görg C**, Kring R, Bert T. Transcutaneous contrast-enhanced sonography of peripheral lung lesions. *AJR Am J Roentgenol* 2006; **187**: W420-W429
26 **Görg C**, Bert T, Kring R, Dempfle A. Transcutaneous contrast enhanced sonography of the chest for evaluation of pleural based pulmonary lesions: experience in 137 patients. *Ultraschall Med* 2006; **27**: 437-444
27 **Alderson PO**, Martin EC. Pulmonary embolism: diagnosis with multiple imaging modalities. *Radiology* 1987; **164**: 297-312
28 Value of the ventilation/perfusion scan in acute pulmonary embolism. Results of the prospective investigation of pulmonary embolism diagnosis (PIOPED). The PIOPED Investigators. *JAMA* 1990; **263**: 2753-2759
29 **Remy-Jardin M**, Remy J, Artaud D, Fribourg M, Beregi JP. Spiral CT of pulmonary embolism: diagnostic approach, interpretive pitfalls and current indications. *Eur Radiol* 1998; **8**: 1376-1390
30 **Kim KI**, Müller NL, Mayo JR. Clinically suspected pulmonary embolism: utility of spiral CT. *Radiology* 1999; **210**: 693-697
31 **Garg K**, Sieler H, Welsh CH, Johnston RJ, Russ PD. Clinical validity of helical CT being interpreted as negative for pulmonary embolism: implications for patient treatment. *AJR Am J Roentgenol* 1999; **172**: 1627-1631
32 **Goldhaber SZ**. Pulmonary embolism. *N Engl J Med* 1998; **339**: 93-104
33 **Mathis G**, Bitschnau R, Gehmacher O, Scheier M, Kopf A, Schwärzler B, Amann T, Doringer W, Hergan K. Chest ultrasound in diagnosis of pulmonary embolism in comparison to helical CT. *Ultraschall Med* 1999; **20**: 54-59
34 **Mathis G**, Blank W, Reissig A, Lechleitner P, Reuss J, Schuler A, Beckh S. Thoracic ultrasound for diagnosing pulmonary embolism: a prospective multicenter study of 352 patients. *Chest* 2005; **128**: 1531-1538
35 **Reissig A**, Kroegel C. Transthoracic ultrasound of lung and pleura in the diagnosis of pulmonary embolism: a novel non-invasive bedside approach. *Respiration* 2003; **70**: 441-452
36 **Reissig A**, Heyne JP, Kroegel C. Sonography of lung and pleura in pulmonary embolism: sonomorphologic characterization and comparison with spiral CT scanning. *Chest* 2001; **120**: 1977-1983
37 **Lechleitner P**, Riedl B, Raneburger W, Gamper G, Theurl A, Lederer A. Chest sonography in the diagnosis of pulmonary embolism: a comparison with MRI angiography and ventilation perfusion scintigraphy. *Ultraschall Med* 2002; **23**: 373-378
38 **Niemann T**, Egelhof T, Bongartz G. Transthoracic sonography for the detection of pulmonary embolism--a meta-analysis. *Ultraschall Med* 2009; **30**: 150-156
39 **Lichtenstein D**, Mezière G, Seitz J. The dynamic air bronchogram. A lung ultrasound sign of alveolar consolidation ruling out atelectasis. *Chest* 2009; **135**: 1421-1425
40 **Lichtenstein D**, Goldstein I, Mourgeon E, Cluzel P, Grenier P, Rouby JJ. Comparative diagnostic performances of auscultation, chest radiography, and lung ultrasonography in acute respiratory distress syndrome. *Anesthesiology* 2004; **100**: 9-15
41 **Gardelli G**, Feletti F, Gamberini E, Bonarelli S, Nanni A, Mughetti M. Using sonography to assess lung recruitment in patients with acute respiratory distress syndrome. *Emerg Radiol* 2009; **16**: 219-221
42 **Caironi P**, Gattinoni L. How to monitor lung recruitment in patients with acute lung injury. *Curr Opin Crit Care* 2007; **13**: 338-343
43 **Bober K**, Swietliński J. Diagnostic utility of ultrasonography for respiratory distress syndrome in neonates. *Med Sci Monit* 2006; **12**: CR440-CR446
44 **Copetti R**, Soldati G, Copetti P. Chest sonography: a useful tool to differentiate acute cardiogenic pulmonary edema from acute respiratory distress syndrome. *Cardiovasc Ultrasound* 2008; **6**: 16
45 **Cosgrove DO**, Garbutt P, Hill CR. Echoes across the diaphragm. *Ultrasound Med Biol* 1978; **3**: 385-392
46 **Avni EF**, Braude P, Pardou A, Matos C. Hyaline membrane disease in the newborn: diagnosis by ultrasound. *Pediatr Radiol* 1990; **20**: 143-146
47 **Prosch H**, Mathis G, Mostbeck GH. Percutaneous ultrasound in diagnosis and staging of lung cancer. *Ultraschall Med* 2008; **29**: 466-478; quiz 479-484
48 **Bandi V**, Lunn W, Ernst A, Eberhardt R, Hoffmann H, Herth FJ. Ultrasound vs. CT in detecting chest wall invasion by tumor: a prospective study. *Chest* 2008; **133**: 881-886
49 **Suzuki N**, Saitoh T, Kitamura S. Tumor invasion of the chest wall in lung cancer: diagnosis with US. *Radiology* 1993; **187**: 39-42
50 **Rivera MP**, Mehta AC. Initial diagnosis of lung cancer: ACCP evidence-based clinical practice guidelines (2nd edition). *Chest* 2007; **132**: 131S-148S
51 **van Overhagen H**, Brakel K, Heijenbrok MW, van Kasteren JH, van de Moosdijk CN, Roldaan AC, van Gils AP, Hansen BE. Metastases in supraclavicular lymph nodes in lung cancer: assessment with palpation, US, and CT. *Radiology* 2004; **232**: 75-80
52 **Fultz PJ**, Feins RH, Strang JG, Wandtke JC, Johnstone DW, Watson TJ, Gottlieb RH, Voci SL, Rubens DJ. Detection and diagnosis of nonpalpable supraclavicular lymph nodes in lung cancer at CT and US. *Radiology* 2002; **222**: 245-251
53 **Prosch H**, Strasser G, Sonka C, Oschatz E, Mashaal S, Mohn-Staudner A, Mostbeck GH. Cervical ultrasound (US) and US-guided lymph node biopsy as a routine procedure for staging of lung cancer. *Ultraschall Med* 2007; **28**: 598-603
54 **Munden RF**, Pugatch RD, Liptay MJ, Sugarbaker DJ, Le LU. Small pulmonary lesions detected at CT: clinical importance. *Radiology* 1997; **202**: 105-110
55 **Remy-Jardin M**, Remy J, Giraud F, Marquette CH. Pulmonary nodules: detection with thick-section spiral CT versus conventional CT. *Radiology* 1993; **187**: 513-5200
56 **Webb WR**. Radiologic evaluation of the solitary pulmonary nodule. A*JR Am J Roentgenol* 1990; **154**: 701-708

S- Editor Cheng JX **L- Editor** Kerr C **E- Editor** Zheng XM

World Journal of Radiology

Online Submissions: http://www.wjgnet.com/1949-8470office
wjr@wjgnet.com
doi:10.4329/wjr.v2.i6.215

World J Radiol 2010 June 28; 2(6): 215-223
ISSN 1949-8470 (online)

TOPIC HIGHLIGHT

Hui-Xiong Xu, MD, PhD, *Series Editor*

Computer-aided diagnosis for contrast-enhanced ultrasound in the liver

Katsutoshi Sugimoto, Junji Shiraishi, Fuminori Moriyasu, Kunio Doi

Katsutoshi Sugimoto, Junji Shiraishi, Kunio Doi, Kurt Rossmann Laboratories for Radiologic Imaging Research, Department of Radiology, The University of Chicago, Chicago, IL 60637, United States
Katsutoshi Sugimoto, Fuminori Moriyasu, Department of Gastroenterology and Hepatology, Tokyo Medical University, Tokyo 160-0023, Japan
Junji Shiraishi, School of Health Sciences, Kumamoto University, Kumamoto 862-0976, Japan
Author contributions: All authors analyzed and interpreted the data; Sugimoto K drafted the manuscript; Sugimoto K and Doi K researched the literature; Shiraishi J and Doi K edited the manuscript.
Correspondence to: Katsutoshi Sugimoto, MD, Department of Gastroenterology and Hepatology, Tokyo Medical University, Japan 6-7-1 Nishishinjuku, Shinjuku-ku, Tokyo 160-0023, Japan. sugimoto@tokyo-med.ac.jp
Telephone: +81-3-33426111 Fax: +81-3-53816654
Received: February 21, 2010 Revised: May 6, 2010
Accepted: May 13, 2010
Published online: June 28, 2010

Abstract

Computer-aided diagnosis (CAD) has become one of the major research subjects in medical imaging and diagnostic radiology. The basic concept of CAD is to provide computer output as a second opinion to assist radiologists' image interpretations by improving the accuracy and consistency of radiologic diagnosis and also by reducing the image-reading time. To date, research on CAD in ultrasound (US)-based diagnosis has been carried out mostly for breast lesions and has been limited in the fields of gastroenterology and hepatology, with most studies being conducted using B-mode US images. Two CAD schemes with contrast-enhanced US (CEUS) that are used in classifying focal liver lesions (FLLs) as liver metastasis, hemangioma, or three histologically differentiated types of hepatocellular carcinoma (HCC) are introduced in this article: one is based on physicians' subjective pattern classifications (subjective analysis) and the other is a computerized scheme for classification of FLLs (quantitative analysis). Classification accuracies for FLLs for each CAD scheme were 84.8% and 88.5% for metastasis, 93.3% and 93.8% for hemangioma, and 98.6% and 86.9% for all HCCs, respectively. In addition, the classification accuracies for histologic differentiation of HCCs were 65.2% and 79.2% for well-differentiated HCCs, 41.7% and 50.0% for moderately differentiated HCCs, and 80.0% and 77.8% for poorly differentiated HCCs, respectively. There are a number of issues concerning the clinical application of CAD for CEUS, however, it is likely that CAD for CEUS of the liver will make great progress in the future.

Key words: Computer-aided diagnosis; Focal liver lesion; Ultrasonography; Contrast agent; Micro-flow imaging

Peer reviewer: Juan Xu, PhD, University of Pittsburgh School of Medicine, UPMC Eye Center, 203 Lothrop St EEI- 835, Pittsburgh, PA 15213, United States

Sugimoto K, Shiraishi J, Moriyasu F, Doi K. Computer-aided diagnosis for contrast-enhanced ultrasound in the liver. *World J Radiol* 2010; 2(6): 215-223 Available from: URL: http://www.wjgnet.com/1949-8470/full/v2/i6/215.htm DOI: http://dx.doi.org/10.4329/wjr.v2.i6.215

INTRODUCTION

Ultrasound (US) is an easy-to-use and minimally invasive imaging modality that is useful for detection and qualitative diagnosis of focal liver lesions (FLLs). In addition, the detection and qualitative diagnosis of FLLs have been markedly improved by the development of US contrast agents consisting of microbubbles[1-5] and by harmonic imaging that can visualize nonlinear scattering of microbubbles[6-12].

It is well known that a major problem with US examinations is their operator-dependent nature, as compared with computed tomography (CT) and magnetic resonance (MR) imaging[13]. It is therefore necessary to reduce the operator-dependent limitations of US examinations. Computer-aided diagnosis (CAD) may be an approach that overcomes this problem.

To date, research on CAD in US-based diagnosis has been carried out mostly on breast lesions[14-19] and has been limited in the fields of gastroenterology and hepatology. In this article, we introduce CAD aimed at differential diagnosis of FLLs by use of contrast-enhanced US (CEUS), in addition to reviewing CAD on US in liver research.

WHAT IS CAD?

Recently, CAD has become a major research subject in medical imaging and diagnostic radiology[20-24]. Many different types of CAD schemes are being developed for the detection and/or characterization of lesions in various tissues using medical imaging, including conventional projection radiography, CT, MR imaging, and US. CAD research is being carried out on detecting lesions in breast, chest, colon, brain, liver and kidney, as well as the vascular and skeletal systems.

CAD is defined as a diagnosis made by a physician who takes into account the computer output based on quantitative analysis of radiologic images. This definition is clearly distinct from automated computerized diagnosis[25-27], which was attempted in the 1960s and 1970s and included replacing radiologists by computers. Subsequently, Doi *et al*[20-22] began their investigations on CAD at the University of Chicago in the 1980s with a clear goal of assisting radiologists with computerized information. The goal of CAD research is to improve the quality and productivity of radiologists' tasks by improving the accuracy and consistency of radiologic diagnoses and also by reducing the image-reading time.

CURRENT STATUS OF RESEARCH ON CAD BASED ON US OF THE LIVER

To date, CAD based on US of the liver has been frequently used in diffuse liver disease for quantifying the degree of liver fibrosis and fat deposition[28-30]. In addition, CAD for FLLs has been reported[31-34]; however, the number of such reports is small compared with the reports on CAD for diffuse liver disease. This is somewhat surprising because computers are, in general, superior to humans in quantitative measurements and in differential diagnosis, but inferior in lesion detection because of a large number of false positives. However, CAD has been used for quantitative evaluation of liver volume for support treatment, which included liver resection and radiofrequency ablation therapy applied to hepatocellular carcinoma (HCC) by application of volume measurements in 3D-US images[35,36]. All such applications have been developed based on B-mode US images.

Second-generation US contrast agents have been developed recently. Definity (Lantheus Inc., MA, USA) and SonoVue (Bracco, Milan, Italy) became available commercially in Canada and Europe, respectively, in 2001, whereas SonoVue became available in China in 2006, followed by Sonazoid (Daiichi Sankyo, Tokyo, Japan) in Japan in 2007 and SonoVue in Korea in 2008. Their utility for the diagnosis of FLLs has been reported[1-5]. In parallel, CAD with CEUS images for differentiating FLLs has been reported[33,34]. In these studies, FLLs were diagnosed by analysis of relatively simple blood flow parameters obtained from measurements of the time-intensity curve (TIC), which reflects tumor hemodynamics. Thus, research on CAD with CEUS images of the liver has just begun worldwide. In the next section, we introduce two different types of CAD schemes aimed at the differential diagnosis of FLLs, which were developed in collaboration with colleagues at the University of Chicago as examples of CAD[31,32].

SUBJECTIVE CLASSIFICATION OF FLLs USING PHYSICIANS' SUBJECTIVE PATTERN CLASSIFICATIONS (SUBJECTIVE ANALYSIS)

In this study, a total of 137 nodules in 137 cases were used for the development of CAD; specifically, there were 74 HCCs [23 well-differentiated (w-HCC), 36 moderately differentiated (m-HCC) and 15 poorly differentiated (p-HCC)], 33 liver metastases and 30 liver hemangiomas. HCC and liver metastasis were diagnosed based on histology after liver resection or liver biopsy in all cases. Liver hemangioma was diagnosed by contrast-enhanced CT and/or MR imaging. The US equipment used in this study was an SSA-790A (Aplio™XG; Toshiba Medical Systems Co., Otawara, Japan). The imaging mode was wideband harmonic imaging (commercially called Pulse subtraction) with transmission and reception frequencies of 3.75 MHz and 7.5 MHz, respectively. The contrast agent used was Sonazoid, which consists of perflubutane-based microbubbles surrounded by phospholipids with a median diameter of 2-3 μm.

From the baseline US features of an FLL, three experienced physicians were requested to classify the echogenic patterns of the FLL into one of the following eight patterns: (1) hyperechoic; (2) hypoechoic; (3) anechoic; (4) thin hypoechoic rim; (5) thick hypoechoic rim (bull's eye); (6) hyperechoic rim; (7) mosaic; and (8) others (Figure 1A). These patterns were proposed by Itai *et al*[37] for describing the characteristics of FLLs from baseline US.

After rating the echogenic patterns of FLLs from baseline US, the physicians were asked to classify the contrast-enhancement patterns of FLLs into one of the following eight patterns: (1) absent; (2) dotted; (3) peripheral rimlike; (4) peripheral nodular; (5) central with spoke wheel-shape; (6) diffuse heterogeneous; (7) diffuse homogeneous; and (8) others (Figure 1B). These patterns were proposed by

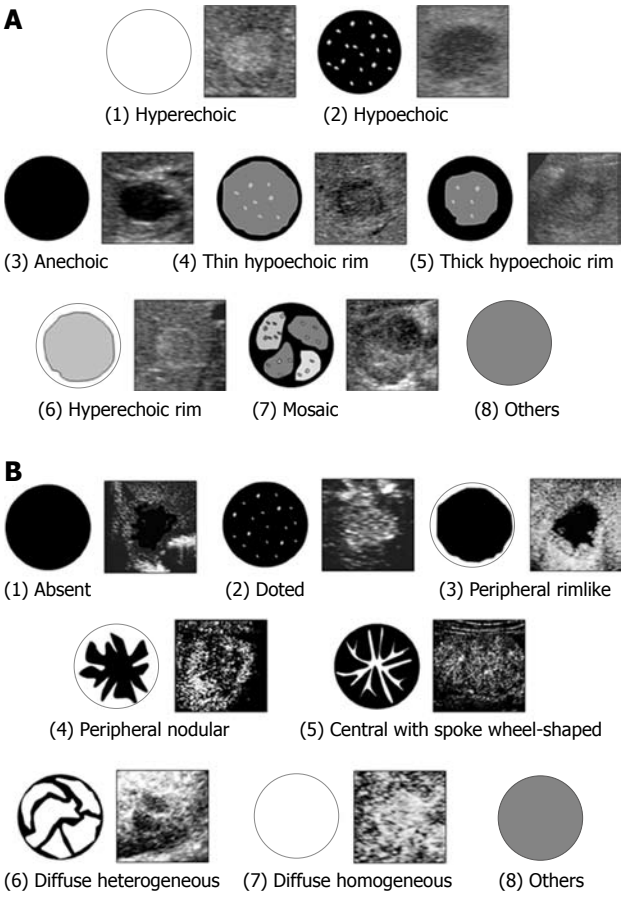

Figure 1 Hepatic tumors. A: Illustration of morphologic patterns of hepatic tumors in the B-mode ultrasonography; B: Illustration of enhancement patterns of hepatic tumors in the arterial phase.

Quaia *et al*[38]. The physicians were not asked to provide a diagnosis in this study.

For analysis of the subjective ratings obtained by the three physicians, we created a matrix of 137 FLLs and 16 patterns, which indicated the total number of physicians who rated lesions in each pattern.

To classify the five types of FLLs (i.e. w-HCCs, m-HCCs, p-HCCs, metastases and hemangiomas) in this CAD scheme, we employed four artificial neural networks (ANNs), as shown in Figure 2. ANNs are mathematical models based on biologic neural networks, which consist of an interconnected group of artificial neurons that can process information by using a connectionist approach to computation. The order of the four decisions (labeled D1-D4) in each ANN was determined by considering the diagnostic difficulty, which was based on the physicians' knowledge levels. The four decisions used in this study were the following: (1) D1: Is this lesion an HCC (yes) or other (no)? (2) D2: Is this lesion a hemangioma (yes) or metastasis (no)? (3)D3: Is this lesion a p-HCC (yes) or other HCC (no)? and (4) D4: Is this lesion a w-HCC (yes) or a m-HCC (no)?

All decisions were determined using each of the ANNs with a two-alternative choice method. In the learning and testing process of the ANNs, a leave-one-out test was employed in individual ANNs. In this method, one

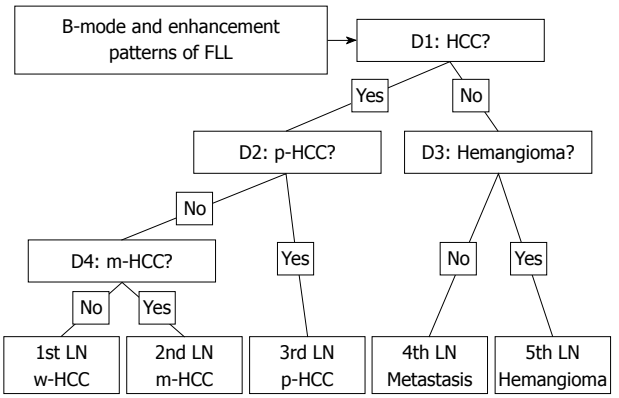

Figure 2 Illustration of the decision tree model used in this study. Four decision nodes in which alternative choice was determined by all five FLLs, leading to a final diagnostic decision for five liver lesions. D: Decision node; FLL: Focal liver lesion; HCC: Hepatocellular carcinoma; LN: Leaf node; m-HCC: Moderately differentiated HCC; p-HCC: Poorly differentiated HCC; w-HCC: Well-differentiated HCC.

case is left out for a test, and the ANN is trained to learn using the remaining cases. The one case that was left out is used for testing the trained ANN. The same procedure was then repeated until all cases were tested.

In the four ANNs, we did not use one of the subjective classifications (i.e. others), because we assumed that uncertain data might have a detrimental effect on the training of the ANNs. Thus, we used 14 input units corresponding to seven patterns of subjective classification data in the matrix as described previously.

The correct classification of the CAD scheme for the five types of FLLs was determined when the final outcome from the four ANNs agreed with the "gold standard". The classification accuracies for each type of FLL and also for all 137 FLLs were determined with the percentages of correctly classified cases among the total number of cases.

Table 1 shows the performance of the computerized scheme for the classification of the five types of FLLs. The classification accuracies for the 137 FLLs were 84.8% for metastasis, 93.3% for hemangioma, 65.2% for w-HCC, 41.7% for m-HCC, and 80.0% for p-HCC. When the classification was conducted only for three types of FLLs (i.e. HCCs, metastasis, and hemangioma), the classification accuracy for all HCCs was 98.6%, as shown in Table 2. The average classification accuracies for the three and five types of FLLs were 94.2% and 71.5%, respectively.

COMPUTERIZED SCHEME FOR CLASSIFICATION OF FLLs

Micro-flow imaging with contrast-enhanced ultrasonography

Micro-flow imaging (MFI; Toshiba Medical Systems Co., Otawara, Japan) is a novel image-processing technique that is accompanied by high-mechanical-index (MI > 1.0) disruptive flash frames and the maximum intensity projection (MIP) technique[32,39]. MIP processing is initi-

Table 1 Performance of CAD scheme for classification in five categories using physicians' pattern classification *n* (%)

Lesion	*n*	Classification with CAD				
		HCC			Metastasis	Hemangioma
		w-HCC	m-HCC	p-HCC		
HCC	74					
w-HCC	23	15 (65.2)	4 (17.4)	4 (17.4)	0 (0.0)	0 (0.0)
m-HCC	36	16 (44.4)	15 (41.7)	5 (13.9)	0 (0.0)	1 (2.7)
p-HCC	15	1 (6.7)	1 (6.7)	12 (80.0)	1 (6.7)	0 (0.0)
Metastasis	33	1 (3.0)	0 (0.0)	1 (3.0)	28 (84.8)	3 (9.1)
Hemangioma	30	0 (0.0)	0 (0.0)	1 (3.3)	1 (3.3)	28 (93.3)

Overall diagnostic accuracy: 98/137 (71.5%). CAD performance was evaluated by a leave-one-case-out methods. Reproduced, with modification, form Sugimoto *et al*[31], *Acad Radiol* 2009; 16: 401-411. CAD: Computer-aided diagnosis; HCC: Hepatocellular carcinoma; w-HCC: Well-differentiated HCC; m-HCC: Moderately differentiated HCC; p-HCC: Poorly differentiated HCC.

Table 2 Performance of CAD scheme for classification in three categories using physicians' subjective pattern classification *n* (%)

Lesion	*n*	Classification with CAD		
		HCC	Metastasis	Hemangioma
HCC	74	73 (98.6)	1 (1.4)	0 (0.0)
Metastasis	33	2 (6.1)	28 (84.8)	3 (9.1)
Hemangioma	30	1 (3.3)	1 (3.3)	28 (93.3)

Overall diagnostic accuracy: 129/137 (94.2%). CAD performance was evaluated by a leave-one-case out method. Reproduced, with modification, form Sugimoto *et al*[31], *Acad Radiol* 2009; 16: 401-411.

ated after a sonographic flash frame disrupts bubbles in the field of view. Using this technique, we could obtain information about the microbubble pathway between frames and observe exquisite detail of lesional vessels, with the potential to show both their morphology and their direction of filling[32,39,40].

To date, some investigators[39,41] have reported that the intratumoral vasculature of HCCs was clearly visualized using this technique and pattern classification was possible; these results suggested the possibility of differential diagnosis of the degree of HCCs[39,41]. CEUS with MFI could be useful for diagnosis of HCCs, and other FLLs, because MFI can depict the minute intratumoral vasculature of the tumor better than harmonic imaging. In this study, we therefore used various kinds of image features that can be derived from MFI findings as input data for the CAD.

Image database

A total of 103 nodules in 97 cases were used for the development of CAD. In more detail, there were 61 HCCs (24 w-HCC, 28 m-HCC and nine p-HCC), 26 liver metastases and 16 liver hemangiomas. HCCs and liver metastases were diagnosed based on histology after liver resection or liver biopsy in all cases. Liver hemangioma was diagnosed by contrast-enhanced CT and/or MR imaging. The US equipment used in this study was SSA-770A (Aplio™XV; Toshiba Medical Systems Co., Otawara, Japan). The imaging mode was wideband harmonic imaging (commercially called Pulse subtraction) with transmission and reception frequencies of 3.75 MHz and 7.5 MHz, respectively. The contrast agent we used was SonoVue, which consists of sulfur hexafluoride microbubbles surrounded by phospholipids with a median diameter of 2.5 μm.

Computerized scheme for classification of FLLs

A series of image-processing steps in CAD, which basically consisted of three major parts, were as follows: (1) image data input and construction of processed images; (2) extraction of image feature values; and (3) application of ANNs and output for differential diagnosis. Please note that we simplified into three major steps (although six major steps were described in the referenced paper[32]).

Image data input and construction of processed images: After irrelevant information, such as patient names, IDs, and other symbols, was removed from the cine clips in the audio-video interleaving format as the input data, only continuous MFI images were reconstructed, and then four kinds of processed images were constructed. Figure 3A-H shows examples of the processed images. Image feature values were determined by use of the MFI image and the four processed images, and were used as input data for the CAD.

Extraction of image feature values: The image feature value is defined as the objective value by computer analysis of the subjective criteria that are used for diagnosing an FLL accurately in clinical practice, such as quick (slow) contrast-enhancement of an FLL, stronger (weaker) contrast enhancement of an FLL compared with liver parenchyma, and homogeneous (heterogeneous) contrast-enhancement of an FLL. For example, with regard to the speed of contrast enhancement, changes in average pixel values in an FLL are plotted against the time axis, and the slope (β value) is calculated. The steeper the slope, the faster the speed of contrast enhancement would be. Similarly, the maximum level of the average pixel value is compared between an FLL and a liver parenchyma for determining which region showed stronger contrast enhancement.

In this study, four kinds of major image feature values were used as CAD input data. Their image characteristics were as follows: (1) temporal feature; (2) morpho-

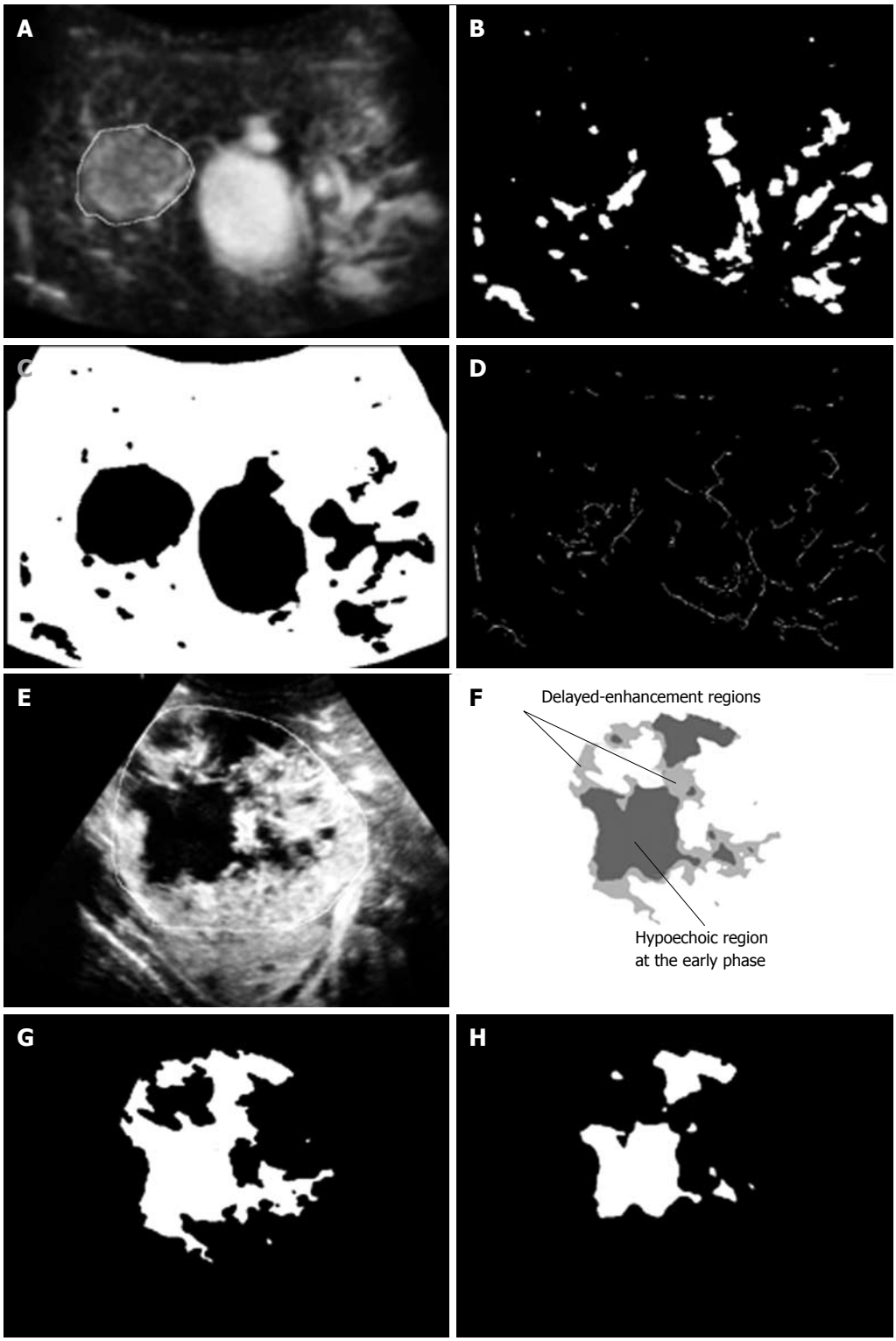

Figure 3 Extraction of morphologic and gray-level image features. A: Original MFI image at the early phase including one FLL (shown as the contour) and a portal vein; B: Vessel-like pattern enhanced image; C: Segmented adjacent liver parenchyma regions obtained from the original MFI image; D: Skeleton of vessel-like pattern enhanced image for estimating the average size of vessel-like patterns on the MFI image; Example of original MFI image at the delayed phase (E) and its segmented images for hyperechoic regions at the early (G) and delayed phase (H). The difference in the regions between two images at two phases was defined as delayed-enhancement region (F). Please note that we defined an "early phase" and a "delayed phase" in the MFI as a replenishment time for reaching 50% and 98% of the maximum average pixel value within a FLL, respectively. MFI: Micro-flow imaging. Reproduced, with modification, from Shiraishi *et al*[32], *Med Phys* 2008; 35: 1734-1746.

logic feature; (3) gray-level feature; and (4) features for a hypoechoic region. The details are shown in Table 3.

Feature 1 is an image feature value obtained from TIC, such as replenishment time, the peak pixel value, and the slope factor (β). In CEUS, for example, a hemangioma is characterized by a typical pattern, namely, a

Table 3 Image feature values used for CAD input data

Image feature values
Temporal features
Replenishment time (s)
Peak pixel value
Slope factor (β)
Morphologic features
Effective diameter of focal liver lesion
Average size of vessel-like patterns
Area ratio of vessel-like patterns
Gray-level features
Average pixel value with vessel-like patterns
Average pixel value without vessel-like patterns
Standard deviation of pixel value with vessel-like patterns
Standard deviation of pixel value without vessel-like patterns
Average pixel value ratio (focal liver lesion/adjacent liver parenchyma)
Average pixel value ratio (central/peripheral)
Features for hypoechoic region
Average pixel value
No. of hypoechoic regions
Area ratio of hypoechoic region
Difference in pixel value (delay-early)
Change in pixel value (delay-early)/s

Reproduced, with modification, from Shiraishi *et al*[32], *Med Phys* 2008; 35: 1734-1746.

peripheral globular enhancement with centripetal filling, whereas HCC and metastatic liver tumor are characterized by rapid contrast enhancement in an arterial phase. Use of the temporal feature as an image feature value, therefore, may be useful for differentiation of FLLs with different speeds of blood flow.

Feature 2 is an image feature value representing the morphologic characteristics of FLLs and intratumoral blood vessels, such as the effective diameter of an FLL, the average size of vessel-like patterns and the area ratio of vessel-like patterns. It has been reported that HCC with a larger tumor diameter exhibits poorer histological differentiation (i.e. higher percentages of p-HCC)[42], and thus the effective diameter of an FLL may be useful for diagnosis of histological grades of HCC. In addition, previous reports showed that the intratumoral vasculature visualized by MFI was dependent on the histological grade of HCC[39,41]. Thus, use of the morphologic image feature values obtained from the vessel-like pattern and the skeleton of a vessel-like pattern image may be useful for diagnosis of the histologic grade of HCC.

Feature 3 is an image feature value that represents tumor enhancement patterns, such as stronger contrast enhancement at the periphery of the tumor than at the center and at the tumor compared to the liver parenchyma. It has been reported that metastatic liver tumors often exhibit ring-like enhancement, and thus use of this image feature value may be useful for diagnosis of tumors with different contrast enhancement patterns.

Feature 4 is an image feature value that represents intratumoral heterogeneity in contrast enhancement. For example, spatial and temporal heterogeneity of a tumor in contrast enhancement can be evaluated by comparison

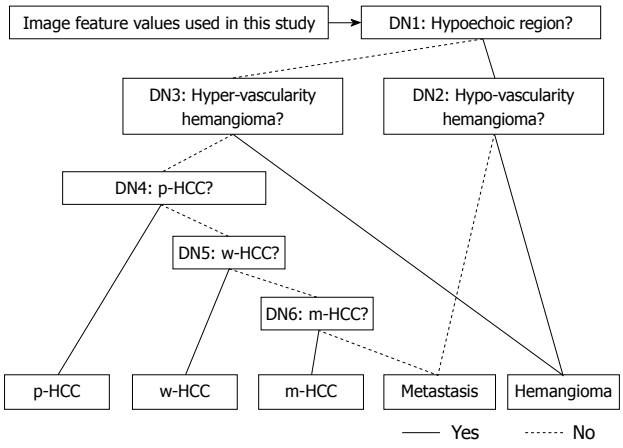

Figure 4 Illustration of the cascade of six artificial neural networks used in this. Six decisions in which alternative choices for specific groups of FLLs were determined by single ANN, leading a final diagnostic decision for five liver diseases.

of hypoechoic areas (no enhanced areas) between the MFI early-phase image and the MFI delayed-phase image. It has been reported that metastatic liver tumors and p-HCC often exhibit heterogeneous enhancement when compared with other liver tumors[38,43], and thus these image features may be useful for the differentiation of these tumors.

In order to select appropriate combinations of temporal and morphologic image features for each of the six ANNs, we used a stepwise method[44]. We thereby selected 16 temporal and morphologic image features, which were selected from 43 initial extracted features, and used them as input data for the six different ANNs for making decisions at each decision step in the cascade.

Application of ANNs and output for differential diagnosis: In the CAD, image feature values extracted from MFI images were used for input data for ANNs. We used parameters in the ANNs to learn the relationship between the repeated presentation of input data in random order and their corresponding output "teacher" data. Our ANNs were constructed with the stratified six different ANNs in order to classify "unknown" FLL input into one of five types of liver diseases (e.g. w-HCC, m-HCC, p-HCC, liver metastasis and liver hemangioma).

All decisions in each of the stratified six different ANNs, shown in Figure 4, were determined using a two-alternative choice. The six decisions used in the six ANNs were determined as follows: (1) D1: Does this lesion have hypoechoic regions (yes) or not (no)? (2) D2: Is this lesion a hypovascular hemangioma (yes) or a hypovascularity metastasis (no)? (3) D3: Is this lesion a hypervascular hemangioma (yes) or other (no)? (4) D4: Is this lesion a p-HCC (yes) or other (no)? (5) D5: Is this lesion a w-HCC (yes) or other (no)? and (6) D6: Is this lesion a m-HCC (yes) or a hypervascular metastasis (no)?

A set of image feature values was selected for each ANN, and learning processes and tests were carried out independently. In learning and testing tasks with ANNs,

Table 4 Performance of CAD scheme for classification in five categories using computerized scheme *n* (%)

Lesion	*n*	Classification with CAD				
		HCC			Metastasis	Hemangioma
		w-HCC	m-HCC	p-HCC		
Total	103					
w-HCC	24	19 (79.2)	1 (4.2)	2 (8.3)	2 (8.3)	0 (0.0)
m-HCC	28	5 (17.9)	14 (50.0)	4 (14.3)	3 (10.7)	2 (7.1)
P-HCC	9	1 (11.1)	0 (0.0)	7 (77.8)	1 (11.1)	0 (0.0)
Metastasis	26	2 (7.7)	1 (3.8)	0 (0.0)	23 (88.5)	0 (0.0)
Hemangioma	16	0 (0.0)	0 (0.0)	0 (0.0)	1 (6.3)	15 (93.8)

Overall diagnostic accuracy: 78/103 (75.7%). CAD performance was evaluated by a leave-one-case-out methods.Reproduced, with modification, from Shiraishi *et al*[32], *Med Phys* 2008; 35: 1734-1746.

the leave-one-out test method was employed in individual ANNs.

The classification accuracies for each type of FLL and also for all 103 FLLs were determined with percentages (%) of correctly classified cases among the total number of cases.

CAD results

Table 4 shows the performance of the computerized scheme for the classification of five types of FLLs (w-HCCs, m-HCCs, p-HCCs, metastases and hemangiomas). The classification accuracies for the 103 FLLs were 88.5% for metastasis, 93.8% for hemangioma, 79.2% for w-HCC, 50.0% for m-HCC and 77.8% for p-HCC. When the classification was done for three types of FLLs (HCCs, metastasis and hemangioma), the classification accuracies for all HCCs was 86.9%. The average classification accuracies for three and five types of FLLs were 88.3% and 75.7%, respectively.

PRACTICAL ISSUES IN CAD AND PERSPECTIVES FOR THE FUTURE

In general, a reliable image database is indispensable for research and development of CAD. In particular, an appropriate number of clinical cases should be used, and attention must be paid to the detection and/or characterization of lesions contained in the images and to the degrees of diagnostic difficulty. For development of a CAD scheme that will become available for clinical application, cases in the database should include various degrees of difficulty in diagnosis, from relatively easy to markedly difficult. Furthermore, the liver is the largest organ in the human body and part of the liver is protected by ribs. Unlike CT and MR imaging, it is therefore difficult to scan the whole liver by US[45]. In addition, US scanning can be difficult in cases of severe obesity. These factors seem to interfere with US on the liver, and also CAD for US on the liver.

One of the most critical components for research on CAD is software development. To this end, programming technology, image processing and knowledge of information processing are required. In general, however, physicians have insufficient knowledge of these skills, and thus close collaboration with physicists is required. On the other hand, it is difficult for software to be developed by physicists alone, because they have insufficient medical knowledge about diagnosis and detection. Therefore, close collaboration with physicians is also necessary.

As a characteristic of CAD, it would be useful if CAD could detect and/or characterize lesions that physicians are likely to overlook and/or misdiagnose, even if the performance of CAD is not highly accurate; and conversely, CAD would not be useful if physicians do not believe the results even when correct. Thus, once the algorithm of CAD is developed, its objective evaluation is necessary. To date, however, no paper on CAD in the liver has included an objective evaluation of the performance of CAD. An observer performance study is a representative evaluation method; observers are required to carry out evaluations under two conditions, with and without the results of computer analysis. Receiver operating characteristic curves can then be obtained based on the results for evaluation of the performance of CAD.

In addition, when the results of evaluation are satisfactory, based on the database in the laboratory, it is necessary to carry out practical tests on a number of unexplored clinical cases as the next step. It is also necessary to develop a practical CAD prototype system and to install it in the workplace in the hospital for a prospective clinical trial. To this end, cooperation by the hospital and physicians would be required for reliable evaluation.

Eventually, to reap the advantages of CAD, commercialization by companies is required. When equipment, systems and software applicable for clinical practice become available commercially, they can be used in hospitals worldwide.

CONCLUSION

In this article, we provided an overview of CAD based on US in the liver. Moreover, we introduced two different types of CAD schemes with CEUS images aimed at the differential diagnosis of FLLs.

The performance of our CAD system for the classification of FLLs could be considered as comparable to those reported by Wilson *et al*[9]. Although their report

was not on results of CAD, their algorithm used subjective assessment of physicians for information on portal venous enhancement for the distinction between benign and malignant FLLs, and their results indicated a high classification accuracy (i.e. 92% for benign and 93% for malignant FLLs).

As shown in this article, the diagnostic accuracies of CAD based on the results of physicians' subjective pattern classification could be considered as comparable to those of CAD based on a computerized scheme. Interestingly, the former CAD was, however, superior to the latter in the diagnosis of three types of FLLs (i.e. HCCs, metastasis, and hemangioma; 94.2% *vs* 88.3%). In contrast, the latter was superior to the former in the diagnosis of five types of FLLs (w-HCCs, m-HCCs, p-HCCs, metastases and hemangiomas; 75.7% *vs* 71.5%). These results suggest that human observers might differ in determining feature values from a computer in the diagnosis of FLLs. Thus, if we take advantage of computer outputs, diagnostic accuracy could be greatly improved.

In our present studies, to establish CAD for FLLs, we used temporal and morphologic features, including physicians' subjective pattern classifications, as image features of FLLs on the contrast-enhancement patterns in the arterial phase of CEUS. However, we did not use findings from portal and late phases (i.e. the presence or absence of washout) as image features of our CADs. That is because, as it is now, it is difficult to recognize automatically all of the data in a dynamic-imaging series for input data because of the problem of the timing of patient breath holding.

Our CAD results showed that the accuracy of m-HCC in both CADs was quite low (subjective analysis: 41.7% and quantitative analysis: 50.0%). This can be related to the fact that we did not use portal and late phase images as input data of CADs, because both w-HCC and m-HCC frequently show arterial enhancement in the same fashion. It is a principal limitation of our CADs. Thus, if our CAD schemes would have portal and late phase information, the performance of our CADs would be much more improved. Our future work should be to recognize hole ultrasonographic image data (i.e. wash-in and wash-out information) automatically as input data to the CAD system.

The other limitation is that focal nodular hyperplasia (FNH) and hepatocellular adenoma were not included in these studies. Both FNH and hepatic adenoma tend to have FLLs presenting a hypervascular pattern in the arterial phase, and it can be difficult to distinguish from HCC, liver metastasis, and hemangioma. However, Kim *et al*[46] reported that monitoring the direction of early arterial filling or the vascular morphology continuously by CEUS enable one to differentiate, to some extent, among FLLs with hypervascularity, including FNH, hemangioma, HCCs, or metastases. However, hepatic adenoma lacks characteristic features even with CEUS, and differentiation of hepatic adenoma from other plethoric FLLs has been reported to be difficult. Hepatocellular adenoma is rare tumor, and therefore it seems extremely rare for this tumor to become a subject of differential diagnosis.

ACKNOWLEDGMENTS

The authors are grateful to Mrs. Elisabeth Lanzl for improving the manuscript.

REFERENCES

1 **Kitzman DW**, Goldman ME, Gillam LD, Cohen JL, Aurigemma GP, Gottdiener JS. Efficacy and safety of the novel ultrasound contrast agent perflutren (definity) in patients with suboptimal baseline left ventricular echocardiographic images. *Am J Cardiol* 2000; **86**: 669-674
2 **Leen E**, Angerson WJ, Yarmenitis S, Bongartz G, Blomley M, Del Maschio A, Summaria V, Maresca G, Pezzoli C, Llull JB. Multi-centre clinical study evaluating the efficacy of SonoVue (BR1), a new ultrasound contrast agent in Doppler investigation of focal hepatic lesions. *Eur J Radiol* 2002; **41**: 200-206
3 **Krix M**, Kiessling F, Essig M, Herth F, Karcher A, Le-Huu M, Kauczor HU, Delorme S. Low mechanical index contrast-enhanced ultrasound better reflects high arterial perfusion of liver metastases than arterial phase computed tomography. *Invest Radiol* 2004; **39**: 216-222
4 **Maruyama H**, Matsutani S, Saisho H, Mine Y, Yuki H, Miyata K. Different behaviors of microbubbles in the liver: time-related quantitative analysis of two ultrasound contrast agents, Levovist and Definity. *Ultrasound Med Biol* 2004; **30**: 1035-1040
5 **Gaiani S**, Celli N, Piscaglia F, Cecilioni L, Losinno F, Giangregorio F, Mancini M, Pini P, Fornari F, Bolondi L. Usefulness of contrast-enhanced perfusional sonography in the assessment of hepatocellular carcinoma hypervascular at spiral computed tomography. *J Hepatol* 2004; **41**: 421-426
6 **Burns PN**, Wilson SR, Simpson DH. Pulse inversion imaging of liver blood flow: improved method for characterizing focal masses with microbubble contrast. *Invest Radiol* 2000; **35**: 58-71
7 **Albrecht T**, Hoffmann CW, Schettler S, Overberg A, Ilg M, von Behren PL, Bauer A, Wolf KJ. B-mode enhancement at phase-inversion US with air-based microbubble contrast agent: initial experience in humans. *Radiology* 2000; **216**: 273-278
8 **Kim AY**, Choi BI, Kim TK, Kim KW, Lee JY, Han JK. Comparison of contrast-enhanced fundamental imaging, second-harmonic imaging, and pulse-inversion harmonic imaging. *Invest Radiol* 2001; **36**: 582-588
9 **Wilson SR**, Burns PN. An algorithm for the diagnosis of focal liver masses using microbubble contrast-enhanced pulse-inversion sonography. *AJR Am J Roentgenol* 2006; **186**: 1401-1412
10 **Wilson SR**, Burns PN. Liver mass evaluation with ultrasound: the impact of microbubble contrast agents and pulse inversion imaging. *Semin Liver Dis* 2001; **21**: 147-159
11 **Eckersley RJ**, Chin CT, Burns PN. Optimising phase and amplitude modulation schemes for imaging microbubble contrast agents at low acoustic power. *Ultrasound Med Biol* 2005; **31**: 213-219
12 **Leavens C**, Williams R, Foster FS, Burns PN, Sherar MD. Golay pulse encoding for microbubble contrast imaging in ultrasound. *IEEE Trans Ultrason Ferroelectr Freq Control* 2007; **54**: 2082-2090
13 **Harvey CJ**, Blomley MJ, Eckersley RJ, Cosgrove DO, Patel N, Heckemann RA, Butler-Barnes J. Hepatic malignancies: improved detection with pulse-inversion US in late phase of enhancement with SH U 508A-early experience. *Radiology* 2000; **216**: 903-908
14 **Gruszauskas NP**, Drukker K, Giger ML, Chang RF, Sennett CA, Moon WK, Pesce LL. Breast US computer-aided diagnosis system: robustness across urban populations in South Korea and the United States. *Radiology* 2009; **253**: 661-671
15 **Drukker K**, Gruszauskas NP, Sennett CA, Giger ML. Breast US computer-aided diagnosis workstation: performance with a large clinical diagnostic population. *Radiology* 2008; **248**: 392-397
16 **Wu WJ**, Moon WK. Ultrasound breast tumor image comput-

er-aided diagnosis with texture and morphological features. *Acad Radiol* 2008; **15**: 873-880
17 **Shen WC**, Chang RF, Moon WK. Computer aided classification system for breast ultrasound based on Breast Imaging Reporting and Data System (BI-RADS). *Ultrasound Med Biol* 2007; **33**: 1688-1698
18 **Sahiner B**, Chan HP, Roubidoux MA, Hadjiiski LM, Helvie MA, Paramagul C, Bailey J, Nees AV, Blane C. Malignant and benign breast masses on 3D US volumetric images: effect of computer-aided diagnosis on radiologist accuracy. *Radiology* 2007; **242**: 716-724
19 **Chen CM**, Chou YH, Han KC, Hung GS, Tiu CM, Chiou HJ, Chiou SY. Breast lesions on sonograms: computer-aided diagnosis with nearly setting-independent features and artificial neural networks. *Radiology* 2003; **226**: 504-514
20 **Doi K**, Giger ML, Nishikawa RM, Hoffmann KR, MacMahon H, Schmidt RA, Chua KG. Digital radiography. A useful clinical tool for computer-aided diagnosis by quantitative analysis of radiographic images. *Acta Radiol* 1993; **34**: 426-439
21 **Doi K**, MacMahon H, Katsuragawa S, Nishikawa RM, Jiang Y. Computer-aided diagnosis in radiology: potential and pitfalls. *Eur J Radiol* 1999; **31**: 97-109
22 **Doi K**. Current status and future potential of computer-aided diagnosis in medical imaging. *Br J Radiol* 2005; **78** Spec No 1: S3-S19
23 **Abe H**, MacMahon H, Engelmann R, Li Q, Shiraishi J, Katsuragawa S, Aoyama M, Ishida T, Ashizawa K, Metz CE, Doi K. Computer-aided diagnosis in chest radiography: results of large-scale observer tests at the 1996-2001 RSNA scientific assemblies. *Radiographics* 2003; **23**: 255-265
24 **Gur D**, Zheng B, Fuhrman CR, Hardesty L. On the testing and reporting of computer-aided detection results for lung cancer detection. *Radiology* 2004; **232**: 5-6
25 **Lodwick GS**, Haun CL, Smith WE, Keller RF, Robertson ED. Computer diagnosis of primary bone tumors: a preliminary report. *Radiology* 1963; **80**: 273-275
26 **Meyers PH**, Nice CM Jr, Becker HC, Nettleton WJ JR, Sweeney JW, Meckstroth GR. Automated computer analysis of radiographic images. *Radiology* 1964; **83**: 1029-1034
27 **Winsberg F**, Elkin M, Macy J, Bordaz V, Weymouth W. Detection of radiographic abnormalities in mammograms by means of optical scanning and computer analysis. *Radiology* 1967; **89**: 211-215
28 **Li G**, Luo Y, Deng W, Xu X, Liu A, Song E. Computer aided diagnosis of fatty liver ultrasonic images based on support vector machine. *Conf Proc IEEE Eng Med Biol Soc* 2008; **2008**: 4768-4771
29 **Thijssen JM**, Starke A, Weijers G, Haudum A, Herzog K, Wohlsein P, Rehage J, De Korte CL. Computer-aided B-mode ultrasound diagnosis of hepatic steatosis: a feasibility study. *IEEE Trans Ultrason Ferroelectr Freq Control* 2008; **55**: 1343-1354
30 **Jeong JW**, Lee S, Lee JW, Yoo DS, Kim S. The echotextural characteristics for the diagnosis of the liver cirrhosis using the sonographic images. *Conf Proc IEEE Eng Med Biol Soc* 2007; **2007**: 1343-1345
31 **Sugimoto K**, Shiraishi J, Moriyasu F, Doi K. Computer-aided diagnosis of focal liver lesions by use of physicians' subjective classification of echogenic patterns in baseline and contrast-enhanced ultrasonography. *Acad Radiol* 2009; **16**: 401-411
32 **Shiraishi J**, Sugimoto K, Moriyasu F, Kamiyama N, Doi K. Computer-aided diagnosis for the classification of focal liver lesions by use of contrast-enhanced ultrasonography. *Med Phys* 2008; **35**: 1734-1746
33 **Huang-Wei C**, Bleuzen A, Olar M, Portalez D, Roumy J, Trillaud H, Tranquart F. Role of parametric imaging in contrast-enhanced sonography of hepatic focal nodular hyperplasia. *J Clin Ultrasound* 2006; **34**: 367-373
34 **Huang-Wei C**, Bleuzen A, Bourlier P, Roumy J, Bouakaz A, Pourcelot L, Tranquart F. Differential diagnosis of focal nodular hyperplasia with quantitative parametric analysis in contrast-enhanced sonography. *Invest Radiol* 2006; **41**: 363-368
35 **Ishizawa T**, Yamamoto T, Sekikawa T. The diagnostic values of measuring the liver volume in detecting occult hepatic metastases from colorectal cancer. *Hepatogastroenterology* 2007; **54**: 514-517
36 **Gilja OH**, Hausken T, Berstad A, Odegaard S. Measurements of organ volume by ultrasonography. *Proc Inst Mech Eng H* 1999; **213**: 247-259
37 **Itai Y**, Ohtomo K, Ohnishi S, Atomi Y, Itoh T, Fukuhisa K, Iinuma T. Ultrasonography of small hepatic tumors. *Radiat Med* 1987; **5**: 14-19
38 **Quaia E**, Calliada F, Bertolotto M, Rossi S, Garioni L, Rosa L, Pozzi-Mucelli R. Characterization of focal liver lesions with contrast-specific US modes and a sulfur hexafluoride-filled microbubble contrast agent: diagnostic performance and confidence. *Radiology* 2004; **232**: 420-430
39 **Sugimoto K**, Moriyasu F, Kamiyama N, Metoki R, Yamada M, Imai Y, Iijima H. Analysis of morphological vascular changes of hepatocellular carcinoma by microflow imaging using contrast-enhanced sonography. *Hepatol Res* 2008; **38**: 790-799
40 **Wilson SR**, Jang HJ, Kim TK, Iijima H, Kamiyama N, Burns PN. Real-time temporal maximum-intensity-projection imaging of hepatic lesions with contrast-enhanced sonography. *AJR Am J Roentgenol* 2008; **190**: 691-5
41 **Yang H**, Liu GJ, Lu MD, Xu HX, Xie XY. Evaluation of the vascular architecture of hepatocellular carcinoma by micro flow imaging: pathologic correlation. *J Ultrasound Med* 2007; **26**: 461-467
42 **Fan ZH**, Chen MH, Dai Y, Wang YB, Yan K, Wu W, Yang W, Yin SS. Evaluation of primary malignancies of the liver using contrast-enhanced sonography: correlation with pathology. *AJR Am J Roentgenol* 2006; **186**: 1512-1519
43 **Jang HJ**, Kim TK, Burns PN, Wilson SR. Enhancement patterns of hepatocellular carcinoma at contrast-enhanced US: comparison with histologic differentiation. *Radiology* 2007; **244**: 898-906
44 **Hocking RR**. The analysis and selection of variables in linear regression. *Biometrics* 1976; **32**: 1-49
45 **Sugimoto K**, Shiraishi J, Moriyasu F, Saito K, Doi K. Improved detection of hepatic metastases with contrast-enhanced low mechanical-index pulse inversion ultrasonography during the liver-specific phase of sonazoid: observer performance study with JAFROC analysis. *Acad Radiol* 2009; **16**: 798-809
46 **Kim TK**, Jang HJ, Burns PN, Murphy-Lavallee J, Wilson SR. Focal nodular hyperplasia and hepatic adenoma: differentiation with low-mechanical-index contrast-enhanced sonography. *AJR Am J Roentgenol* 2008; **190**: 58-66

S- Editor Cheng JX **L- Editor** Lutze M **E- Editor** Zheng XM

World Journal of Radiology

Online Submissions: http://www.wjgnet.com/1949-8470office
wjr@wjgnet.com
doi:10.4329/wjr.v2.i6.224

World J Radiol 2010 June 28; 2(6): 224-229
ISSN 1949-8470 (online)

REVIEW

Different imaging techniques in the head and neck: Assets and drawbacks

Thomas J Vogl, Marc Harth, Petra Siebenhandl

Thomas J Vogl, Marc Harth, Petra Siebenhandl, Department of Diagnostic and Interventional Radiology, Clinic of Johann Wolfgang Goethe-University, 60590 Frankfurt/Main, Germany
Author contributions: Vogl TJ and Siebenhandl P contributed equally to this article; Harth M assisted in preparing the manuscript.
Correspondence to: Thomas J Vogl, Professor, Department of Diagnostic and Interventional Radiology, Clinic of Johann Wolfgang Goethe-University, Theodor-Stern-Kai 7, 60590 Frankfurt/Main, Germany. t.vogl@em.uni-frankfurt.de
Telephone: +49-69-63017277 Fax: +49-69-63017258
Received: March 27, 2010 Revised: May 15, 2010
Accepted: May 22, 2010
Published online: June 28, 2010

Abstract

In this review, the gold standard imaging techniques for the head and neck and the latest upcoming techniques are presented, by comparing computed tomography (CT), magnetic resonance imaging and positron emission tomography-CT, as well as ultrasound, depending on the examined area. The advantages and disadvantages of each examination protocol are presented. This article illustrates the connection between the imaging technique and the examined area. Therefore, the head and neck area is divided into different sections such as bony structures, nervous system, mucous membranes and squamous epithelium, glandular tissue, and lymphatic tissue and vessels. Finally, the latest techniques in the field of head and neck imaging such as multidetector CT, dual-energy CT, flash CT, magnetic resonance angiography, spectroscopy, and diffusion tensor tractography using 3 tesla magnetic resonance are discussed.

Key words: Magnetic resonance imaging; Computed tomography; Positron emission tomography; Head and neck; Tumors; Bones

Peer reviewers: Patrick K Ha, MD, Assistant Professor, Johns Hopkins Department of Otolaryngology, Johns Hopkins Head and Neck Surgery at GBMC, 1550 Orleans Street, David H Koch Cancer Research Building, Room 5M06, Baltimore, MD 21231, United States; Alexander D Rapidis, MD, DDS, PhD, FACS, Professor, Chairman, Department of Head and Neck/Maxillofacial Surgery, Greek Anticancer Institute, Saint Savvas Hospital, 171 Alexandras Avenue, 115 22 Athens, Greece

Vogl TJ, Harth M, Siebenhandl P. Different imaging techniques in the head and neck: Assets and drawbacks. *World J Radiol* 2010; 2(6): 224-229 Available from: URL: http://www.wjgnet.com/1949-8470/full/v2/i6/224.htm DOI: http://dx.doi.org/10.4329/wjr.v2.i6.224

BONY STRUCTURES IN THE HEAD AND NECK

Most bony lesions of the skull are benign tumors. They are mainly bone tumors and tumor-like lesions. With the exception of osteomas of the paranasal sinuses and exostosis of the external auditory canal, these lesions occur rarely. Osteomas and exostosis of the external auditory canal are mostly incidental findings with computed tomography (CT). Due to its location close to the tympanic membrane, exostosis can be easily differentiated from osteoma, which is located more laterally. If only magnetic resonance imaging (MRI) is performed, a compact osteoma in an air-filled cavity, as well as exostosis, cannot be proven due to the absence of a signal[1].

Fibrous dysplasia with bony lesions can be documented by MRI with low signal intensity in the T2-weighted sequences. Therefore, CT should be performed afterwards. Due to its high uptake of contrast medium, fibrous dysplasia is often falsely diagnosed as a malignant tumor[2].

Chordomas are the most common primary malignant tumors of the skull base[3]. They are mostly located at the clivus[4]. CT shows lobulated, sharply restricted osteolysis. In T2-weighted sequences, they appear with a high intensity and high contrast enhancement[5]. In numerous cases, chordomas can be mistaken for chondrosarcomas, which are cartilage-producing tumors. Chondrosarcomas most

commonly appear in the petro-occipital fissure and clivus, and rare cases of chondrosarcoma are found in the temporomandibular joint[6]. Chondrosarcomas show the same T2-weighted images as chondromas. In these cases, biopsy is necessary[7].

Solitary and multiple metastases at the skull base are more common than primary malignant tumors. Thus, CT or a whole body scan with 18-fluoro-2-deoxy-D-glucose (FDG) positron emission tomography (PET) is performed regarding tumor staging, especially in breast cancer[8], renal cell carcinoma, and lung cancer[9].

Traumatic lesions offer a wide range of injuries. Emergency examinations allow a very short time frame to start the treatment before causing permanent damage or death. For that reason, the first choice of examination should be CT, with its short examination time.

The advantage of three-dimensional reconstruction in emergency patients with skull-base fractures using solid and transparent volume-rendering techniques and maximum intensity projection (MIP) has been examined by Ringl *et al*[10]. They have ascertained that MIP with regard to sensitivity ($P = 0.9$) visualizes fractures slightly better than high resolution multiplanar reformation (HR-MPR). Due to the relatively low detection rate using HR-MPR alone, it has been recommended to read MIP reconstructions in addition to the obligatory HR-MPRs to improve fracture detection[11].

NERVOUS SYSTEM

The differentiation between benign and malignant tumors is one of the most important challenges. For that reason, it is necessary to evaluate infiltration of bony structures, especially in neurovascular tumors.

Multidetector CT (MDCT), with its soft tissue and bone window setting, is a good option. The application of non-ionic, iodine-based contrast medium enhances the sensitivity of the image of the lesion[12].

MRI is useful for imaging the nervous system. Therefore axial and coronal sequences with an array of 512 or 1024 pixels are performed. The slices should not be thicker than 3 mm. It is important that the MRI images the whole pathology[13].

Basically, axial T2-weighted sequences are performed to get an overview. Afterwards coronal and axial high-resolution T1-weighted sequences are performed before and after contrast application. In order to increase the outline of the lesion, fat-suppressed sequences can be added[14].

Diffusion tensor tractography (DTT) using 3 tesla (3T) MRI is an upcoming innovation. DTT facilitates the imagination of neural fibers with 3T MRI. Akter *et al*[15] have compared the results of DTT with surgery and have found agreement.

MUCOUS MEMBRANES AND SQUAMOUS EPITHELIUM

Due to its availability MDCT is a frequently used method[16]. The view of the nasopharynx and oropharynx should be parallel to the hard palate, and the view of the hypopharynx and larynx parallel to the vocal cords. The examined area reaches from the skull base to the height of the manubrium of the sternum[17]. Furthermore, the application of non-ionic, iodine-based contrast medium is mandatory in order to differentiate the pathology more clearly. Axial MDCT is performed in a soft tissue window setting (minimal slice thickness 2-3 mm) and in a bone window setting (minimal slice thickness 1-2 mm)[18]. Moreover, sagittal and coronary reconstructions provide a clearer depiction of the pathology. Finally, MDCT provides accurate imaging of the spreading of tumor masses due to higher contrast uptake, as well as infiltration of the muscle or fat tissue[19].

In comparison to MDCT, MRI is the preferable method in soft tissue imaging and provides a good topographic relationship to the anatomical structures. The drawbacks are long examination times (30-40 min) and the necessity for patient compliance.

The most common inflammations in the head and neck are sinusitis and inflammation of the inner ear. Unenhanced CT is the gold standard to examine the sinuses or the inner ear. The advantage of CT is the possibility of three-dimensional reconstructions[20]. To verify chronic sinusitis, CT of the paranasal sinuses should be performed[21]. The images illustrate mucosal swelling, whereas acute sinusitis additionally shows air-fluid level[21].

A new upcoming technique in the CT area is Flash CT. It could gain importance in the near future, for example, for imaging the sinuses, because the radiation dose for patients is reduced and the examination time is shortened. However, the patients should be slim in order to obtain proper images (Figure 1).

Examinations of the middle ear are usually performed with spiral CT of the petrous portion of the temporal bone. Features that are revealed by CT are thickening of the tympanic membrane and fluid in the middle ear[22].

In the case of recurrent cholesteatoma, diffusion-weighted MRI shows a positive predictive value; however, CT still remains the gold standard[23]. Plouin-Gaudon *et al*[24] have concluded that, in cases of doubtful CT, diffusion-weighted MRI can confirm recurrence or avoid second-look surgery.

Several sequences should be performed as: (1) axial T2-weighted fat-suppressed sequences; (2) axial T1-weighted spin-echo-sequences before and after contrast application with a slice thickness of 2-3 mm; and (3) coronary and sagittal T1-weighted spin-echo sequences after contrast application with fat suppression in 256 × 256 pixels[18,19] (Figure 2).

In the case of recurrent tumors, FDG-PET can be performed. This technique has a high sensitivity for detection of recurrent tumors, which depends on FDG uptake[25,26]. The higher metabolism of glucose in malignant cells and inflammatory tissues can be documented. A disadvantage of this method is that inflammatory tissue, for example, after radiotherapy, and malignant tissue have a higher FDG uptake. For that reason, a PET scan should be performed 2-4 mo after therapy, at the earliest[27] (Figure 3).

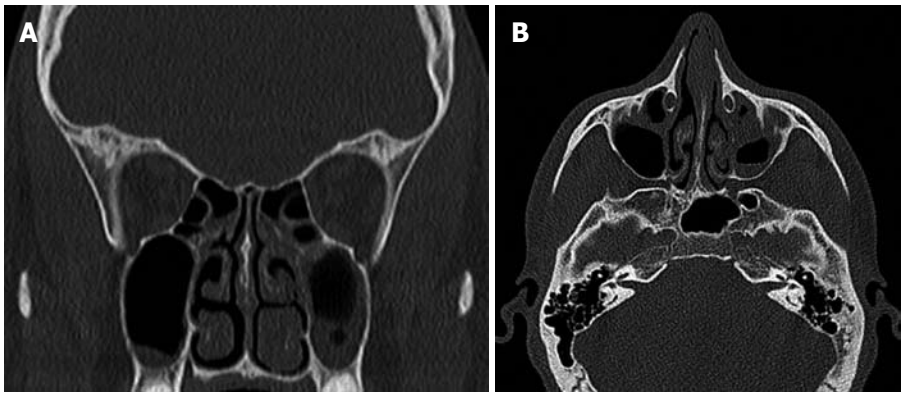

Figure 1 Chronic sinusitis, especially in the left maxillary sinus. A: SOMATOM Definition Flash coronal reconstruction; B: SOMATOM Definition Flash computed tomography axial layer.

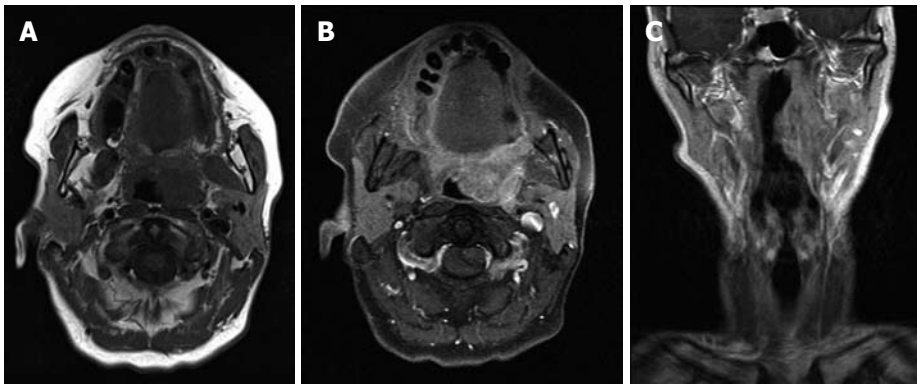

Figure 2 Palatine tonsil carcinoma on the left side. A: MRT T2-weighted axial layer; B: MRT T1-weighted axial layer; C: MRT T1-weighted coronal layer.

GLANDULAR TISSUE

Salivary glands

The most common malignancy of the parotid gland is mucoepidermoid carcinoma[28,29]. In the submandibular gland, pleomorphic adenomas remain the most common benign tumor[30]. The same diagnoses prevail in the sublingual and minor salivary glands, where malignancies outnumber benign tumors[31].

Some would advocate the use of MRI as the best technique to evaluate a neoplasm of the major salivary glands. Implicit in such a decision is that the clinicians are highly confident that the process in the gland is neoplastic and not obstructive or inflammatory. If the mass is considered to be related to sialolithiasis, CT should be recommended first, because MRI is not as reliable in detecting small calculi. If the lesion is suspected to be neoplastic, MRI should be preferred over other modalities, as nearly all parotid lesions are well visualized on T1-weighted MRI because of the hyperintense background of the gland[32]. The T1-weighted image provides an excellent assessment of the tumor margin, its extent, and its pattern of infiltration. This sequence, coupled with fat suppression and contrast-enhanced T1-weighted imaging, which is primarily used to address perineural spread, bone invasion, or meningeal infiltration, is the best means for documenting tumor spread[33,34]. On fat-suppressed images, the bony structures and the skull base are hypointense. Enhancing tissue extending into this hypointense background is indicative of bone invasion. If it is likely to be a nervous infiltration, MRI is usually the method of choice. In cases of meningeal symptoms, MRI is preferred because the leptomeninges are better illustrated with MRI than with CT[35]. T2-weighted MRI has been shown to be a reasonably reliable predictor regarding malignancy or benignity of a salivary gland tumor[36]. In general, however, the most common benign tumor of the salivary glands, pleomorphic adenoma, has very high signal intensity on T2-weighted images[37]. The value of contrast enhancement also applies to CT, as the attenuation of the cyst is not comparable to that of pure fluid. Berg *et al*[38] have reckoned that CT attenuation of masses, other than for differentiating benign cysts from solid masses, and lipomas from other neoplasms, does not replace histological diagnosis, because most malignant and non-malignant solid masses have similar CT attenuation. Malignancies tend to have irregular infiltration into the glandular parenchyma, which can be detected with MRI and CT, therefore, there are some exceptions that CT has sufficient accuracy to predict the histological diagnosis of a lesion. CT is less precise than MRI for determining the extent of disease, therefore, there is little reason to perform CT rather than MRI for suspected salivary gland masses[39].

Nakamura *et al*[40] have evaluated various physiological FDG accumulations in the head and neck, and have

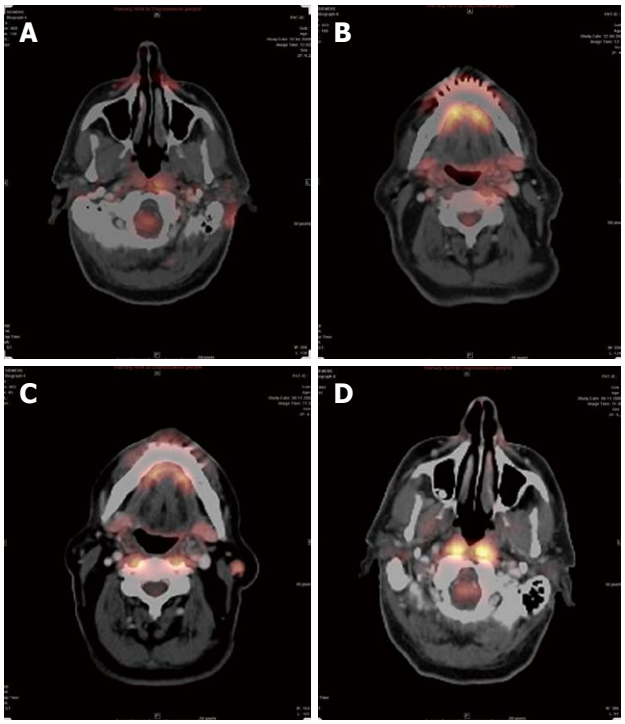

Figure 3 Positron emission tomography-CT after resection of a melanocytic tumor of uncertain malignant origin. A: The resection area still showed a higher glucose metabolism than normal healthy tissue at 2 mo after therapy; B: A small lymph node (LN), but no sign of higher metabolism; C: A malignant LN with higher metabolism; D: There was no higher glucose metabolism noticeable at 6 mo after therapy.

compared them with tumor FDG accumulation, and have come to the conclusion that tonsil, extraocular muscle, and sublingual glands show a relatively high FDG accumulation, which is sometimes similar to tumor accumulation. The right-to-left ratio of standardized uptake value (SUVmax) is useful in differentiating tumor from physiological accumulation, and the presence of tumor might be highly suspected in cases with a ratio of $\geqslant 1.5$.

Ultrasound is also mentioned in the literature as one of the first choices in imaging the salivary glands[41,42]. The advantage of this examination mode is the combination of fine needle aspiration cytology with its ability to differentiate between benign and malignant lesions[43].

Thyroid gland

Thyroid nodules irrespective of their malignancy or benignity are sometimes found incidentally during other examinations such as thoracic CT. The gold standard in the literature is doubtless ultrasound; mostly due to its availability and low costs[44].

As already mentioned above, ultrasound can be used to guide invasive procedures such as biopsy, and to visualize moving features such as blood vessels, the esophagus, and blood flow. Another advantage is that there is no radiation like in a CT.

In patients, who suffer from hyperthyrosis CT with contrast medium is only possible if the patient has been prepared with sodium perchlorate, because the contrast medium contains iodine, which might result in a thyrotoxic crisis. MRI of the thyroid gland is possible and shows nodular non-homogeneity as well as contrast enhancement, but is rarely performed in daily routine; mostly due to its high costs and long examination times.

Lymphatic tissue

Increased lymph node (LN) size is usually palpated by patients themselves. The gold standard for suspicious LNs is ultrasound. If there are more pathologically increased LNs or a primary tumor is noted, CT is the better choice to detect all increased LNs and follow-up is easier, in comparison with ultrasound, because the latter is highly dependent on the examiner.

Blood vessels

MDCT, dynamic CT angiography (CTA), high-field MRI, four-dimensional MR angiography (MRA) are recent improvements in imaging arteries. These techniques form the basis for planning further investigations[45].

In emergency examination, CTA is a state-of-the-art technique, whereas contrast-enhanced MRA is the technique that is recommended in the literature. In cases of acute stroke, diagnosis has to be made as quickly as possible. Damage detection at 24-48 h after onset of symptoms is not always possible. Therefore, Totaro *et al*[45] have concluded that diffusion-weighted imaging in the post-acute phase of cerebral ischemia in patients in whom CT did not yield a definite diagnosis could be the solution[10].

MRA, with its improvements in parallel imaging at high-field strength, with resultant high-spatial-resolution data acquisition over large fields of view has become an interesting alternative to the traditional catheter-directed selective angiography[46]. This technique allows preoperative noninvasive identification of stenosis and restenosis and detection of intracranial aneurysms[47].

A further new topic is the role of selective intra-arterial, catheter-directed chemotherapy for head and neck cancer. In these cases, pre-interventional MRA is profitable for imaging tumor-feeding vessels, anatomical structures[48] and the caliber of the vessels[49].

MRA is the best way to avoid a primary surgical operation. Moreover, the anatomical structures, as well as the vascularization, can be illustrated. The vascularization is important in embolizing head and neck tumors before starting the intervention. One of the most promising upcoming innovations is dual-energy CTA (DE-CTA). The possibility of suppressing the bones and providing three-dimensional vascular models for the attending doctor makes DE-CTA of the carotid arteries an attractive alternative to MRA[50]. The bone removal speeds up the imaging analysis, although, due to the slightly limited specificity and segmentation error, each case should be double checked on the original images[51] (Figures 4 and 5). In emergency patients with suspected arterial injury in the head and neck, MDCT angiography should be performed as standard[52].

A new upcoming technique is dual-energy CT, with

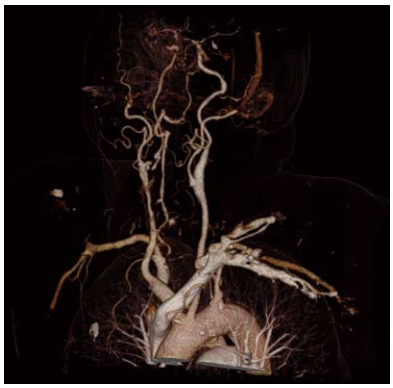

Figure 4 Flash CT dual-energy bone removal head collection showing the carotid arteries.

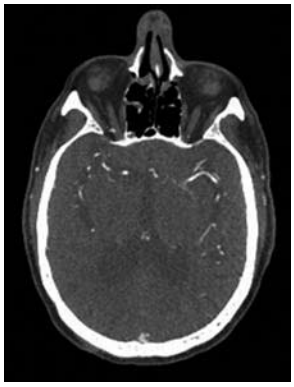

Figure 5 Definition Flash-CT showing the cerebral arteries.

its possibility of bone removal and three-dimensional reconstructions, which provides excellent images. Nevertheless there are disadvantages such as material artifacts of metal and segmentation errors.

CONCLUSION

Currently, various options are available for head and neck imaging. To decide on the best method in each case, the examination method has to be illuminated more precisely, because CT, MRI, PET-CT and ultrasound each have their advantages and disadvantages. It is important to decide which structure in the examined area is affected in order to find the most suitable method. The advantages of CT compared to MRI are its availability, short examination time, and its detailed imaging of bony structures, inflammatory lesions and acute vascular lesions. The disadvantages are the worse soft tissue imaging, although contrast application improves the quality. MRI is the better choice for imaging soft tissue but its disadvantages are long examination times and the necessity for patient compliance. For imaging the nervous system and salivary glands, MRI is more useful than CT unless infiltration of the bone or calcification in the gland is assumed. In such cases, CT should be performed afterwards. PET-CT in diagnosing recurrent tumors utilizes the high glucose uptake of tumors to visualize the tumor. The negative aspect is the high metabolism of inflammatory tissue in comparison to healthy tissue, which can lead to incorrect diagnosis of malignancy. Ultrasound benefits from its availability and low costs, as well as from the short examination time but it is considerably dependent on the examiner. Finally, there are many new upcoming techniques in the CT field, such as dual-energy CT and Flash CT, and in the MRI field, such as MRA, spectroscopy and tractography. Each new technique has its particular advantages. Flash CT could gain importance in the near future because the radiation dose for patients is reduced and the examination time is shortened in comparison to standard CT scanning. Dual-energy CT, with its possibility of bone removal and three-dimensional reconstruction, provides excellent images. Nevertheless there are disadvantages such as material artifacts of metal and segmentation errors. DTT using 3T MRI is one of the most recent techniques in imaging neural fibers. In conclusion, new techniques are increasingly becoming available, and it is important to choose the right examination procedure for each medical question.

REFERENCES

1 **Kösling S**, Neumann K, Brandt S. [CT and MRI of intrinsic space-occupying lesions of the bony skull base] *Radiologe* 2009; **49**: 598-607

2 **Chong VF**, Khoo JB, Fan YF. Fibrous dysplasia involving the base of the skull. *AJR Am J Roentgenol* 2002; **178**: 717-20

3 **Oikawa S**, Kyoshima K, Goto T, Iwashita T, Takizawa T, Kobayashi S, Ito M. Histological study on local invasiveness of clival chordoma. Case report of autopsy. *Acta Neurochir* (Wien) 2001; **143**: 1065-1069

4 **Pallini R**, Sabatino G, Doglietto F, Lauretti L, Fernandez E, Maira G. Clivus metastases: report of seven patients and literature review. *Acta Neurochir* (Wien) 2009; **151**: 291-296; discussion 296

5 **Tsuboi Y**, Hayashi N, Kurimoto M, Nagai S, Sasahara M, Endo S. Malignant transformation of clival chordoma after gamma knife surgery - case report -. *Neurol Med Chir* (Tokyo) 2007; **47**: 479-482

6 **Oliveira RC**, Marques KDS, Mendonça AR, Mendonça EF, Silva MRB, Batista AC, Ribeiro-Rotta RF. Chondrosarcoma of the temporomandibular joint: a case report in a child. *J Orofac Pain* 2009; **23**: 275-281

7 **Neff B**, Sataloff RT, Storey L, Hawkshaw M, Spiegel JR. Chondrosarcoma of the skull base. *Laryngoscope* 2002; **112**: 134-139

8 **Jager JJ**, Keymeulen K, Beets-Tan RG, Hupperets P, van Kroonenburgh M, Houben R, de Ruysscher D, Lambin P, Boersma LJ. FDG-PET-CT for staging of high-risk breast cancer patients reduces the number of further examinations: A pilot study. *Acta Oncol* 2010; **49**: 185-191

9 **Takenaka D**, Ohno Y, Matsumoto K, Aoyama N, Onishi Y, Koyama H, Nogami M, Yoshikawa T, Matsumoto S, Sugimura K. Detection of bone metastases in non-small cell lung cancer patients: comparison of whole-body diffusion-weighted imaging (DWI), whole-body MR imaging without and with DWI, whole-body FDG-PET/CT, and bone scintigraphy. *J Magn Reson Imaging* 2009; **30**: 298-308

10 **Ringl H**, Schernthaner R, Philipp MO, Metz-Schimmerl S, Czerny C, Weber M, Gäbler C, Steiner-Ringl A, Peloschek P, Herold CJ, Schima W. Three-dimensional fracture visualisation of multidetector CT of the skull base in trauma patients: comparison of three reconstruction algorithms. *Eur Radiol* 2009; **19**: 2416-2424

11 **Delgado Almandoz JE**, Schaefer PW, Kelly HR, Lev MH, Gonzalez RG, Romero JM. Multidetector CT angiography in the evaluation of acute blunt head and neck trauma: a proposed acute craniocervical trauma scoring system. *Radiology*

2010; **254**: 236-244
12 **Nemec SF**, Kasprian G, Nemec U, Czerny C. [Cranial nerves - spectrum of inflammatory and tumorous changes] *Radiologe* 2009; **49**: 608-613
13 **Laine FJ**, Nadel L, Braun IF. CT and MR imaging of the central skull base. Part 1: Techniques, embryologic development, and anatomy. *Radiographics* 1990; **10**: 591-602
14 **Casselman JW**. The skull base: tumoral lesions. *Eur Radiol* 2005; **15**: 534-542
15 **Akter M**, Hirai T, Minoda R, Murakami R, Saiki S, Okuaki T, Kitajima M, Fukuoka H, Sasao A, Nishimura S, Yumoto E, Awai K, Yamashita Y. Diffusion tensor tractography in the head-and-neck region using a clinical 3-T MR scanner. *Acad Radiol* 2009; **16**: 858-865
16 **Becker M**, Burkhardt K, Dulguerov P, Allal A. Imaging of the larynx and hypopharynx. *Eur J Radiol* 2008; **66**: 460-479
17 **Czerny C**, Formanek M. [Malignant tumors of the pharynx] *Radiologe* 2000; **40**: 625-631
18 **Ruffing S**, Struffert T, Grgic A, Reith W. [Imaging diagnostics of the pharynx and larynx] *Radiologe* 2005; **45**: 828-836
19 **Wycliffe ND**, Grover RS, Kim PD, Simental A Jr. Hypopharyngeal cancer. *Top Magn Reson Imaging* 2007; **18**: 243-258
20 **Kim J**, Song SW, Cho JH, Chang KH, Jun BC. Comparative study of the pneumatization of the mastoid air cells and paranasal sinuses using three-dimensional reconstruction of computed tomography scans. *Surg Radiol Anat* 2010; Epub ahead of print
21 **Marple BF**, Stankiewicz JA, Baroody FM, Chow JM, Conley DB, Corey JP, Ferguson BJ, Kern RC, Lusk RP, Naclerio RM, Orlandi RR, Parker MJ. Diagnosis and management of chronic rhinosinusitis in adults. *Postgrad Med* 2009; **121**: 121-139
22 **Zhiqi L**, Kun Y, Zhiwu H. Tympanometry in infants with middle ear effusion having been identified using spiral computerized tomography. *Am J Otolaryngol* 2010; **31**: 96-103
23 **Lemmerling MM**, De Foer B, Verbist BM, VandeVyver V. Imaging of inflammatory and infectious diseases in the temporal bone. *Neuroimaging Clin N Am* 2009; **19**: 321-337
24 **Plouin-Gaudon I**, Bossard D, Fuchsmann C, Ayari-Khalfallah S, Froehlich P. Diffusion-weighted MR imaging for evaluation of pediatric recurrent cholesteatomas. *Int J Pediatr Otorhinolaryngol* 2010; **74**: 22-26
25 **Anzai Y**, Carroll WR, Quint DJ, Bradford CR, Minoshima S, Wolf GT, Wahl RL. Recurrence of head and neck cancer after surgery or irradiation: prospective comparison of 2-deoxy-2-[F-18]fluoro-D-glucose PET and MR imaging diagnoses. *Radiology* 1996; **200**: 135-141
26 **Lonneux M**, Lawson G, Ide C, Bausart R, Remacle M, Pauwels S. Positron emission tomography with fluorodeoxyglucose for suspected head and neck tumor recurrence in the symptomatic patient. *Laryngoscope* 2000; **110**: 1493-1497
27 **Isles MG**, McConkey C, Mehanna HM. A systematic review and meta-analysis of the role of positron emission tomography in the follow up of head and neck squamous cell carcinoma following radiotherapy or chemoradiotherapy. *Clin Otolaryngol* 2008; **33**: 210-222
28 **Kane WJ**, McCaffrey TV, Olsen KD, Lewis JE. Primary parotid malignancies. A clinical and pathologic review. *Arch Otolaryngol Head Neck Surg* 1991; **117**: 307-315
29 **Batsakis JG**. Tumors of the head and neck: clinical and pathological considerations. 2nd ed. Baltimore: Williams & Wilkins, 1979
30 **Weber RS**, Byers RM, Petit B, Wolf P, Ang K, Luna M. Submandibular gland tumors. Adverse histologic factors and therapeutic implications. *Arch Otolaryngol Head Neck Surg* 1990; **116**: 1055-1060
31 **Weber RS**, Palmer JM, el-Naggar A, McNeese MD, Guillamondegui OM, Byers RM. Minor salivary gland tumors of the lip and buccal mucosa. *Laryngoscope* 1989; **99**: 6-9
32 **Schlakman BN**, Yousem DM. MR of intraparotid masses. *AJNR Am J Neuroradiol* 1993; **14**: 1173-1180
33 **Parker GD**, Harnsberger HR. Clinical-radiologic issues in perineural tumor spread of malignant diseases of the extracranial head and neck. *Radiographics* 1991; **11**: 383-399
34 **Barakos JA**, Dillon WP, Chew WM. Orbit, skull base, and pharynx: contrast-enhanced fat suppression MR imaging. *Radiology* 1991; **179**: 191-198
35 **Dillon WP**. Imaging of central nervous system tumors. *Curr Opin Radiol* 1991; **3**: 46-50
36 **Som PM**, Biller HF. High-grade malignancies of the parotid gland: identification with MR imaging. *Radiology* 1989; **173**: 823-826
37 **Swartz JD**, Rothman MI, Marlowe FI, Berger AS. MR imaging of parotid mass lesions: attempts at histopathologic differentiation. *J Comput Assist Tomogr* 1989; **13**: 789-796
38 **Berg HM**, Jacobs JB, Kaufman D, Reede DL. Correlation of fine needle aspiration biopsy and CT scanning of parotid masses. *Laryngoscope* 1986; **96**: 1357-1362
39 **Kaneda T**, Minami M, Ozawa K, Akimoto Y, Okada M, Yamamoto H, Suzuki H, Sasaki Y. Imaging tumors of the minor salivary glands. *Oral Surg Oral Med Oral Pathol* 1994; **78**: 385-390
40 **Nakamura S**, Okochi K, Murata Y, Shibuya H, Kurabayashi T. [18F]Fluorodeoxyglucose-PET/CT differentiation between physiological and pathological accumulations in head and neck. *Nucl Med Commun* 2009; **30**: 498-503
41 **Yang WT**, Ahuja AT, Metreweli C. Role of ultrasound in the imaging of parotid swellings. *S Afr J Radiol* 1996; 18-22
42 **Bradley MJ**. Salivary glands. In: Ahuja AT, Evans RM, editors. Practical head and neck ultrasound. London: Greenwich Medical Media Ltd., 2000: 19-33
43 **Wong KT**, Ahuja AT, Yuen HY, King AD. Ultrasound of salivary glands. *ASUM Bulletin* 2003; **6**: 18-22
44 **Sipos JA**. Advances in ultrasound for the diagnosis and management of thyroid cancer. *Thyroid* 2009; **19**: 1363-1372
45 **Totaro P**, Toni D, Durastanti L, Bozzao L, Gualdi GF, Raz E, Kouleridou A, Pantano P. Diffusion-weighted MRI in patients with non-diagnostic CT in the post-acute phase of cerebral ischemia. *Eur Neurol* 2010; **63**: 94-100
46 **Gandhi D**, Kathuria S, Ansari SA, Shah G, Gemmete JJ. State of the art head and neck imaging for the endovascular specialist. *Neuroimaging Clin N Am* 2009; **19**: 133-147, Table of Contents
47 **Lohan DG**, Barkhordarian F, Saleh R, Krishnam M, Salamon N, Ruehm SG, Finn JP. MR angiography at 3 T for assessment of the external carotid artery system. *AJR Am J Roentgenol* 2007; **189**: 1088-1094
48 **Tomandl BF**, Köstner NC, Schempershofe M, Huk WJ, Strauss C, Anker L, Hastreiter P. CT angiography of intracranial aneurysms: a focus on postprocessing. *Radiographics* 2004; **24**: 637-655
49 **Ferré JC**, Brunet JF, Carsin-Nicol B, Larralde A, Godey B, Gauvrit JY. Optimized time-resolved 3D contrast-enhanced MRA at 3T: appreciating the feasibility of assessing cervical paragangliomas. *J Neuroradiol* 2010; **37**: 104-108
50 **Lell MM**, Hinkmann F, Nkenke E, Schmidt B, Seidensticker P, Kalender WA, Uder M, Achenbach S. Dual energy CTA of the supraaortic arteries: Technical improvements with a novel dual source CT system. *Eur J Radiol* 2009; Epub ahead of print
51 **Thomas C**, Korn A, Krauss B, Ketelsen D, Tsiflikas I, Reimann A, Brodoefel H, Claussen CD, Kopp AF, Ernemann U, Heuschmid M. Automatic bone and plaque removal using dual energy CT for head and neck angiography: Feasibility and initial performance evaluation. *Eur J Radiol* 2009; Epub ahead of print
52 **Filter ER**, Fernandes JR. Fatal traumatic subarachnoid hemorrhage due to assault-related tear of the basilar artery. *J Forensic Leg Med* 2009; **16**: 414-416

S- Editor Cheng JX **L- Editor** Kerr C **E- Editor** Zheng XM

World Journal of Radiology

Online Submissions: http://www.wjgnet.com/1949-8470office
wjr@wjgnet.com
doi:10.4329/wjr.v2.i6.230

World J Radiol 2010 June 28; 2(6): 230-232
ISSN 1949-8470 (online)

CASE REPORT

Revisiting normal perfusion pressure breakthrough in light of hemorrhage-induced vasospasm

Matthew D Alexander, E Sander Connolly, Philip M Meyers

Matthew D Alexander, Department of Diagnostic Imaging, Santa Clara Valley Medical Center, San Jose, CA 95128, United States
E Sander Connolly, Department of Neurological Surgery, Columbia University, College of Physicians and Surgeons, New York, NY 10032, United States
Philip M Meyers, Department of Radiology, Columbia University, College of Physicians and Surgeons, New York, NY 10032, United States
Author contributions: Alexander MD performed the literature and chart reviews and wrote the manuscript; Connolly ES participated in patient care and edited the manuscript; Meyers PM was the primary clinician caring for the patient throughout her course and edited the manuscript.
Correspondence to: Matthew D Alexander, MD, Department of Diagnostic Imaging, Santa Clara Valley Medical Center, San Jose, CA, United States. matthew.alexander@caa.columbia.edu
Telephone: +1-408-8856370 Fax: +1-408-8856360
Received: April 19, 2010 Revised: June 2, 2010
Accepted: June 28, 2010
Published online: June 28, 2010

Abstract

Cerebral arteriovenous malformations (AVMs) have abnormally enlarged arteries and veins prone to spontaneous hemorrhage. Immediately following surgical excision of a cerebral AVM, even normal brain tissue surrounding the lesion is subject to hemorrhage, a phenomenon termed normal perfusion pressure breakthrough (NPPB) syndrome. According to this theory, arteries supplying cerebral AVMs become dilated and lose their capacity to dilate or constrict to autoregulate pressure. Acutely after removal of a cerebral AVM, excessive blood pressure in these arterial feeders can cause normal brain tissue to bleed. However, this theory remains controversial. We present a patient with a cerebral AVM that demonstrated cerebrovascular reactivity and argues against an assumption underlying the theory of NPPB syndrome.

Key words: Arteriovenous malformation; Autoregulation; Normal perfusion pressure breakthrough; Subarachnoid hemorrhage; Vasospasm

Peer reviewer: Panagiotis Antoniou, PhD, MSc, Medical Physics, Certified Medical Physicist, School of Medicine Democritus University of Thrace, 31 Irinis Str. Alexandroupolis 68100, Greece

Alexander MD, Connolly ES, Meyers PM. Revisiting normal perfusion pressure breakthrough in light of hemorrhage-induced vasospasm. *World J Radiol* 2010; 2(6): 230-232 Available from: URL: http://www.wjgnet.com/1949-8470/full/v2/i6/230.htm DOI: http://dx.doi.org/10.4329/wjr.v2.i6.230

INTRODUCTION

Cerebral arteriovenous malformations (AVMs) have abnormally enlarged arteries and veins prone to spontaneous hemorrhage. Immediately following surgical excision of a cerebral AVM, the remaining normal brain tissue surrounding the lesion is subject to hemorrhage, a phenomenon termed normal perfusion pressure breakthrough (NPPB) syndrome[1]. The theory proposed to explain this phenomenon remains controversial. We present a patient with cerebral AVM that demonstrated cerebrovascular reactivity and argues against an assumption underlying the theory of NPPB syndrome.

CASE REPORT

A 47 year-old woman with chronic headaches and a previously diagnosed right occipital cerebral AVM developed a severe headache followed 5 d later by left-sided weakness and neglect. Computed tomography and magnetic resonance imaging brain scans showed subacute subarachnoid hemorrhage and ischemic changes in the right middle cerebral artery distribution (Figure 1A and B).

Catheter arteriography demonstrated a 12 mm an-

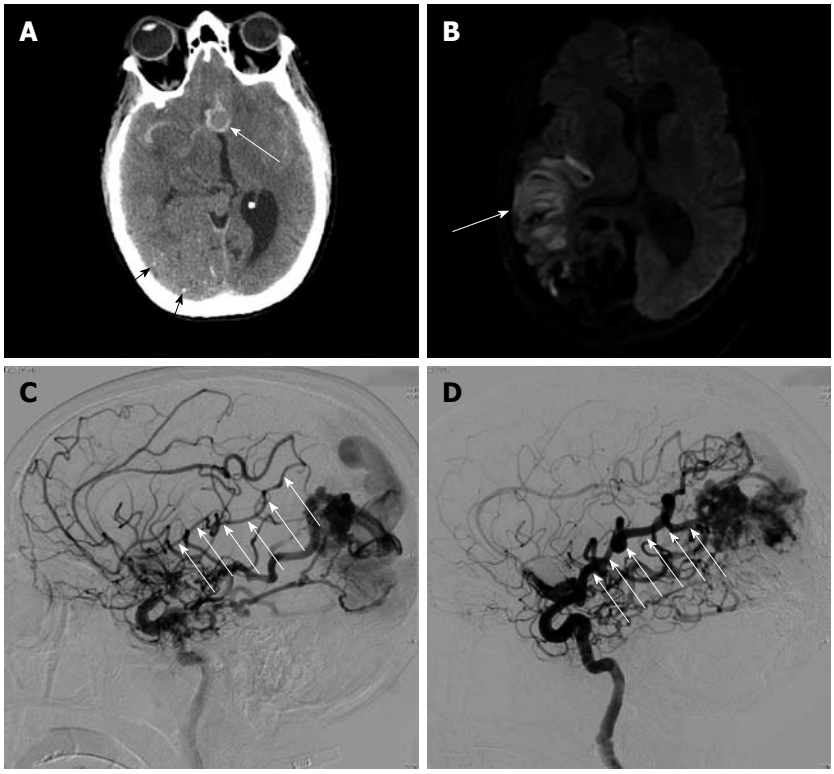

Figure 1 A 47-year-old woman with ruptured anterior communicating artery aneurysm associated with a large arteriovenous malformation. A: Computed tomography brain scan shows the 12 mm anterior communicating artery aneurysm in relief surrounded by high-density subarachnoid hemorrhage (white arrow). Also note small stippled calcifications in the large parietal-occipital arteriovenous malformation (black arrows); B: Diffusion-weighted magnetic resonance imaging shows area of restricted diffusion in the posterior right frontal lobe (white arrow) corresponding with the patient's left-sided weakness and hemineglect; C: Catheter arteriography of the right internal carotid artery in the lateral projection at the time of initial presentation approximately 1 wk following subarachnoid hemorrhage shows significant narrowing in the angular and Rolandic branches of the right middle cerebral artery, both of which supply the arteriovenous malformation (white arrows); D: Catheter arteriography of the right internal carotid artery in the lateral projection 4 mo after initial presentation and following complete neurological recovery shows resolution of vasospasm in the angular and parietal branches of the right middle cerebral artery supplying the arteriovenous malformation (white arrows).

terior communicating artery aneurysm, a 5 cm right occipital cerebral AVM, and relatively slow flow through small caliber arteries to the cerebral AVM representing vasospasm (Figure 1C). Endovascular coil occlusion of the aneurysm was immediately performed, and the vasospasm was treated with verapamil. Subsequent arteriography for treatment of the cerebral AVM showed interval resolution of the narrowed arteries in the distribution of the stroke (Figure 1D). Despite her deficits at the time of original presentation with stroke, the patient made a full neurological recovery, even after embolization and resection of the cerebral AVM.

DISCUSSION

Cerebral AVMs can cause pathological states including hemorrhage, vascular steal, chronic hypoperfusion, and low-grade ischemia, all of which were demonstrated by the patient reported here. In 1978, Spetzler *et al*[1] published the theory of NPPB, positing that chronic hypoperfusion causes branches of the AVM feeding arteries, that supply normal tissue, to become markedly dilated, remaining paralyzed due to lost autoregulatory capacity. After AVM extirpation, these branches in the remaining normal tissue experience increased perfusion but lack ability to constrict and autoregulate cerebral blood flow. They argued that, in some cases, this vascular dysfunction leads to hyperemia and compromise of capillary beds, resulting in massive edema and hemorrhage.

Several studies using various methodologies have supported the claims of NPPB[2-9]. However, more recent investigations contradict many aspects of the theory, casting doubt on the link between impaired vasoreactivity and postoperative complications. NPPB theory rests on the assumption that lost autoregulatory capacity persists following resection of a cerebral AVM. Nevertheless, several studies demonstrate a postoperative return to normal CO_2 reactivity in vessels with previously diminished reactivity[3,10-16]. Young *et al*[12,13] showed intact CO_2 reactivity both before and after resection. Similarly, Ogasawara demonstrated postoperative hyperperfusion in areas with normal response to acetazolamide in the preoperative period[17].

Young *et al*[18] reported that cerebral AVM removal improved perfusion in the hemisphere ipsilateral to the lesion, but increasing mean arterial pressure pharmacologically did not increase CBF, suggesting intact cerebral autoregulation. This was true for uncomplicated cases, as well as patients with NPPB-like complications. Demonstrating intact vasoreactivity both before and after resection, Young *et al*[13,18,19] suggested the true problem is a leftward shift of the autoregulatory curve such that normal pressure exceeds the upper limit of autoregulation.

Batjer demonstrated the ability of arteries to vasodilate but an inability to vasoconstrict in response to increased pressure, a finding confirmed in a rat model[11,20,21]. We suggest that the vasoconstriction in response to SAH in our patient demonstrated that the impairment of vasoconstriction in response to elevated pressure, which has been argued to underlie NPPB syndrome, is not due to some global inability of the vasculature to constrict. This agrees with both Batjer's findings and Young's proposal of a leftward shift of the autoregulation curve. However, we must maintain the possibility that vasospasm in response to SAH and the vessel properties underlying autoregulation, which have been argued are impaired in NPPB-like states, might result from two distinct mechanisms.

Another condition of Spetzler's theory that has come under scrutiny is that NPPB-like complications occur in areas adjacent to the malformation that formerly shared the arterial blood supply with it, and that such former feeders are prone to complications because of the chronic stress placed upon them by the cerebral AVM. Barnett *et al*[3] showed the worst steal effect exists in tissue 2-4 cm from the malformation, and higher flow occurred in tissue distal to the location of the cerebral AVM. To the contrary, Young *et al*[22] showed that increased cerebral blood flow following cerebral AVM resection occurs throughout the entire brain, not just in regions that shared vascular supply with the cerebral AVM. This suggests that mechanisms implicating preoperative focal hypoperfusion due to vascular steal are not the sole cause of postoperative complications. Indeed, our patient demonstrated vasospasm, infarction, and edema both ipsilateral and contralateral to her AVM, consistent with such findings.

The findings in this case illustrate that arteries surrounding cerebral AVMs can maintain vasoconstrictive capacity, although the contractile activity in response to subarachnoid hemorrhage and autoregulation might be different processes. Future studies should compare microvascular changes between procedures with uneventful cerebral AVM resection and those with these complications. However, comparison will prove difficult given the relative rarity of these complications and the resultant difficulty designing adequately powered investigations. Furthermore, better diagnostic definitions for these complications must be standardized. Differing interpretations of what constitutes an NPPB-like state have undoubtedly made studies difficult to compare. Better characterization of blood flow parameters surrounding cerebral AVMs will lead to improved prevention, prompt identification, and treatment.

REFERENCES

1 **Spetzler RF**, Wilson CB, Weinstein P, Mehdorn M, Townsend J, Telles D. Normal perfusion pressure breakthrough theory. *Clin Neurosurg* 1978; **25**: 651-672
2 **Nornes H**, Grip A. Hemodynamic aspects of cerebral arteriovenous malformations. *J Neurosurg* 1980; **53**: 456-464
3 **Barnett GH**, Little JR, Ebrahim ZY, Jones SC, Friel HT. Cerebral circulation during arteriovenous malformation operation. *Neurosurgery* 1987; **20**: 836-842
4 **Muraszko K**, Wang HH, Pelton G, Stein BM. A study of the reactivity of feeding vessels to arteriovenous malformations: correlation with clinical outcome. *Neurosurgery* 1990; **26**: 190-199; discussion 199-200
5 **Pennings FA**, Ince C, Bouma GJ. Continuous real-time visualization of the human cerebral microcirculation during arteriovenous malformation surgery using orthogonal polarization spectral imaging. *Neurosurgery* 2006; **59**: 167-171; discussion 167-171
6 **Chyatte D**. Normal pressure perfusion breakthrough after resection of arteriovenous malformation. *J Stroke Cerebrovasc Dis* 1997; **6**: 130-136
7 **Luessenhop AJ**, Ferraz FM, Rosa L. Estimate of the incidence and importance of circulatory breakthrough in the surgery of cerebral arteriovenous malformations. *Neurol Res* 1982; **4**: 177-190
8 **Asgari S**, Röhrborn HJ, Engelhorn T, Fauser B, Stolke D. Intraoperative measurement of cortical oxygen saturation and blood volume adjacent to cerebral arteriovenous malformations using near-infrared spectroscopy. *Neurosurgery* 2003; **52**: 1298-1304; discussion 1304-1306
9 **Spetzler RF**, Martin NA, Carter LP, Flom RA, Raudzens PA, Wilkinson E. Surgical management of large AVM's by staged embolization and operative excision. *J Neurosurg* 1987; **67**: 17-28
10 **Hassler W**, Steinmetz H. Cerebral hemodynamics in angioma patients: an intraoperative study. *J Neurosurg* 1987; **67**: 822-831
11 **Batjer HH**, Devous MD Sr, Meyer YJ, Purdy PD, Samson DS. Cerebrovascular hemodynamics in arteriovenous malformation complicated by normal perfusion pressure breakthrough. *Neurosurgery* 1988; **22**: 503-509
12 **Young WL**, Prohovnik I, Ornstein E, Ostapkovich N, Sisti MB, Solomon RA, Stein BM. The effect of arteriovenous malformation resection on cerebrovascular reactivity to carbon dioxide. *Neurosurgery* 1990; **27**: 257-266; discussion 266-267
13 **Young WL**, Solomon RA, Prohovnik I, Ornstein E, Weinstein J, Stein BM. 133Xe blood flow monitoring during arteriovenous malformation resection: a case of intraoperative hyperperfusion with subsequent brain swelling. *Neurosurgery* 1988; **22**: 765-769
14 **De Salles AA**, Manchola I. CO2 reactivity in arteriovenous malformations of the brain: a transcranial Doppler ultrasound study. *J Neurosurg* 1994; **80**: 624-630
15 **Diehl RR**, Henkes H, Nahser HC, Kühne D, Berlit P. Blood flow velocity and vasomotor reactivity in patients with arteriovenous malformations. A transcranial Doppler study. *Stroke* 1994; **25**: 1574-1580
16 **Massaro AR**, Young WL, Kader A, Ostapkovich N, Tatemichi TK, Stein BM, Mohr JP. Characterization of arteriovenous malformation feeding vessels by carbon dioxide reactivity. *AJNR Am J Neuroradiol* 1994; **15**: 55-61
17 **Ogasawara K**, Yoshida K, Otawara Y, Kobayashi M, Yasuda S, Doi M, Ogawa A. Cerebral blood flow imaging in arteriovenous malformation complicated by normal perfusion pressure breakthrough. *Surg Neurol* 2001; **56**: 380-384
18 **Young WL**, Kader A, Prohovnik I, Ornstein E, Fleischer LH, Ostapkovich N, Jackson LD, Stein BM. Pressure autoregulation is intact after arteriovenous malformation resection. *Neurosurgery* 1993; **32**: 491-496; discussion 496-497
19 **Young WL**, Pile-Spellman J, Prohovnik I, Kader A, Stein BM. Evidence for adaptive autoregulatory displacement in hypotensive cortical territories adjacent to arteriovenous malformations. Columbia University AVM Study Project. *Neurosurgery* 1994; **34**: 601-610; discussion 610-611
20 **Batjer HH**, Devous MD Sr. The use of acetazolamide-enhanced regional cerebral blood flow measurement to predict risk to arteriovenous malformation patients. *Neurosurgery* 1992; **31**: 213-217; discussion 217-218
21 **Irikura K**, Morii S, Miyasaka Y, Yamada M, Tokiwa K, Yada K. Impaired autoregulation in an experimental model of chronic cerebral hypoperfusion in rats. *Stroke* 1996; **27**: 1399-1404
22 **Young WL**, Kader A, Ornstein E, Baker KZ, Ostapkovich N, Pile-Spellman J, Fogarty-Mack P, Stein BM. Cerebral hyperemia after arteriovenous malformation resection is related to "breakthrough" complications but not to feeding artery pressure. The Columbia University Arteriovenous Malformation Study Project. *Neurosurgery* 1996; **38**: 1085-093; discussion 1093-1095

S- Editor Cheng JX **L- Editor** Webster JR **E- Editor** Zheng XM

World Journal of Radiology

Online Submissions: http://www.wjgnet.com/1949-8470office
wjr@wjgnet.com
doi:10.4329/wjr.v2.i6.233

World J Radiol 2010 June 28; 2(6): 233-236
ISSN 1949-8470 (online)

CASE REPORT

Unusual radiological finding of lethal pneumatosis intestinalis and portomesenteric vein gas

Ioannis D Kyriazanos, Theodoros A Bazinas, Grigorios G Tsoukalos, Christos N Stoidis

Ioannis D Kyriazanos, Christos N Stoidis, Department of Surgery, Athens Navy Hospital, 70 Deinokratous Street, 11521, Athens, Greece
Theodoros A Bazinas, Department of Radiology, 251 Hellenic Airforce General Hospital, 3 P. Kanellopoulou Street, 11525, Athens, Greece
Grigorios G Tsoukalos, Department of Radiology, Athens Navy Hospital, 70 Deinokratous Street, 11521, Athens, Greece
Author contributions: Kyriazanos ID was the patients' surgeon and was involved in drafting the manuscript and revising it critically for important intellectual content; Stoidis CN, Tsoukalos GG and Bazinas TA contributed to the study conception and design; Stoidis CN contributed to the analysis and interpretation of data and wrote the manuscript; all authors contributed equally to the final draft of the manuscript. all authors read and approved the final manuscript; Kyriazanos ID has given the final approval of the version to be published.
Correspondence to: Christos N Stoidis, MD, Department of Surgery, Athens Navy Hospital, 70 Deinokratous Street, 11521, Athens, Greece. aris.80@hotmail.com
Telephone: +30-210-9235157 Fax: +30-2310-643149
Received: May 18, 2010 Revised: June 1, 2010
Accepted: June 8, 2010
Published online: June 28, 2010

Abstract

Pneumatosis intestinalis and portomesenteric vein gas are rare and potentially severe radiological findings that occur both in pediatric and adult populations. They actually are radiographic signs of underlying intra-abdominal pathology, abnormality or diagnostic medical interference. If combined with other radiological or clinical signs of intestinal ischemia or sepsis, the prognosis is dismal and urgent laparotomy is mandatory. We report two cases of surgical treatment with ominous outcome in an effort to characterize this finding correctly as an absolute surgical indication or as an additional diagnostic criterion that simply marks a further breakdown of the systems in patients with a long list of severe medical conditions.

Key words: Pneumatosis intestinalis; Portomesenteric vein gas; Intestinal obstruction; Intestinal ischemia; Surgery

Peer reviewers: Dr. Stéphane Supiot, MD, PhD, Department of Radiation Oncology, Centre René Gauducheau, St-Herblain, Nantes, 44800, France; Dr. Dinesh Vyas, Department of Minimally and Endosopic Surgery, St John Mercy Hospital, 851 E Fifth Street, Washington, DC 63090, United States

Kyriazanos ID, Bazinas TA, Tsoukalos GG, Stoidis CN. Unusual radiological finding of lethal pneumatosis intestinalis and portomesenteric vein gas. *World J Radiol* 2010; 2(6): 233-236 Available from: URL: http://www.wjgnet.com/1949-8470/full/v2/i6/233.htm DOI: http://dx.doi.org/10.4329/wjr.v2.i6.233

INTRODUCTION

Pneumatosis is characterized by collections of gas within the wall of the bowel, which might involve the esophagus, stomach, small intestine, and colon[1]. When localized in the small intestine or the portomesenteric vein system, it is characterized as pneumatosis intestinalis (PI) or portomesenteric vein gas (PVG), respectively. PVG can be seen in conjunction with or in isolation from PI, and represents a different phase of the same fundamental pathophysiology. In PVG, branching lucencies are seen within the mesenteric venous tributaries or in the liver, which often drain sites of PI[2].

There are two main theories that explain the pathophysiology of PI/PVG: mechanical and bacterial[3]. The mechanical theory supports the hypothesis that PI develops when defects in the mucosa, in combination with increased intraluminal pressure, allow gas to infiltrate the gastrointestinal (GI) tract wall. The bacterial theory postulates that PI develops when gas-producing bacteria gain entry to the GI tract wall and produce pockets of gas. Much of the

evidence for these two theories is derived from observational studies and one could argue that the mechanical and bacterial mechanisms could occur simultaneously[4].

The underlying pathological mechanism is most often associated with intestinal obstruction (e.g. diverticulitis, adhesions, feeding tubes, tumor, or radiation enteritis), mesenteric ischemia due to thrombosis or emboli (e.g. mesenteric infarction, or necrotizing enterocolitis in infants), or volvulus[5], but also with benign or idiopathic conditions (e.g. endoscopic examination, or liver cirrhosis)[6].

Diagnostically, computed tomography (CT) can identify PI/PVG in such patients. With the added sensitivity and increased utilization of modern CT, PI and PVG are being identified more frequently. This poses a difficult clinical question because the clinical significance of PI and PVG, identified by modern CT, ranges from benign to catastrophic[7]. Historically, their presence has mandated laparotomy due to the high mortality rate associated with mesenteric ischemia, but practically, surgical treatment should always be considered in symptomatic patients[8].

We report herein the surgical treatment of obstructive and ischemic abdominal pathology, accompanied by this unusual radiological finding, with a lethal outcome. The progression of the patients' histories according to our experience and the study of the limited number of case series in the international literature led us to useful conclusions on the appropriate treatment of such patients.

CASE REPORT

A 70-year-old woman with amyotrophic lateral sclerosis (Lou Ghering's disease) and chronic kidney failure presented with abdominal distension. As a result of neuromuscular malfunctions, she had received feeding jejunostomy 3 mo previously, as well as a permanent tracheostoma. The patient presented a backflow from the jejunostomy, and clinical signs of mechanical obstruction, ileus and fever. Initial laboratory findings showed elevated inflammatory parameters and serum lactate levels. When the abdominal symptoms progressed, contrast-enhanced CT revealed distinct pneumatosis within the jejunal wall and fulminant gas embolism in the portal vein system (Figures 1 and 2). An exploratory laparotomy was carried out due to suspected intestinal ischemia. No signs of mesenteric ischemia or a necrotic process were found, but only adhesions that underwent lysis (Figure 3). Although, the abdominal tenderness receded, the inflammatory laboratory findings were still elevated along with increased procalcitonin and positive blood cultures. The patient died on the 10th postoperative day from manifest disseminated intravascular coagulation and multiple organ failure (MOF) due to sepsis.

The second patient was an 80-year-old man suffering from chronic kidney failure, with a history of treated abdominal aorta aneurysm, who was in hospital because of acute abdominal pain, severe gas, feces retention, and bloating. The clinical symptoms and the laboratory and radiological findings (PVG and PI) (Figure 4) aroused suspicion of intestinal ischemia. An emergency laparotomy was carried out and 50 cm of ischemic terminal ileum were resected. The patient died on the 22nd postoperative day due to severe sepsis and MOF, and during the whole period, fever, elevated inflammatory markers, and positive blood cultures were present.

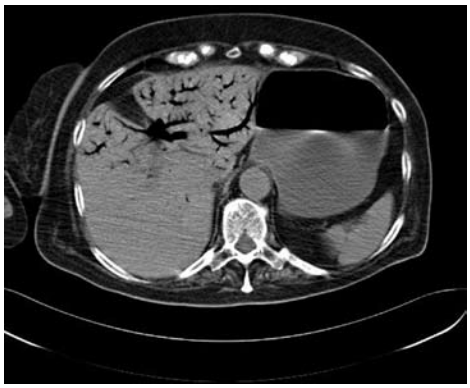

Figure 1 Fulminant presence of intrahepatic portal vein gas, especially in the left lobe of the liver.

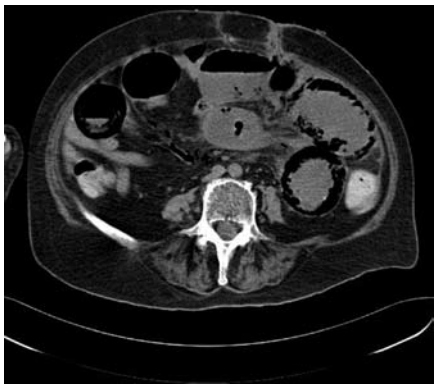

Figure 2 Presence of gas in the intestinal wall.

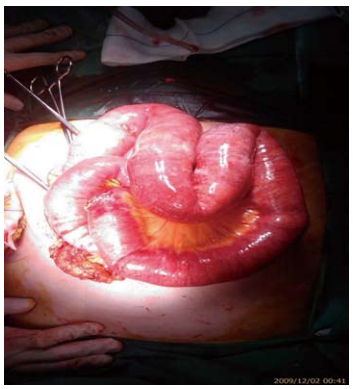

Figure 3 Perioperative image of the distended but not ischemic small bowel.

In both cases the radiological phenomenon showed a significant regression after surgical treatment of the primary underlying pathology, along with the patients' symptoms. However, the prognosis and outcome of the patients remained ominous. This raises the question: how seriously

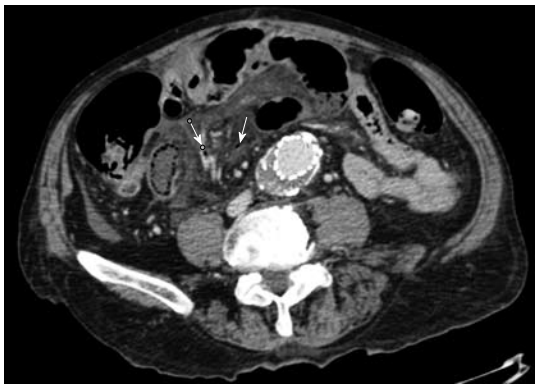

Figure 4 Gas in the intestinal wall and mesenteric veins (arrows).

should a surgeon take into consideration this unique radiological finding, along with the patient's condition during the diagnosis, treatment and prognosis of abdominal pathology?

DISCUSSION

Patients who present with PI/PVG fall into three general subgroups: mechanical, ischemic, and benign idiopathic, with a different range of age, clinical signs and laboratory findings, but with one common feature: an underlying abdominal disease and often previous abdominal surgery[9].

A radiological finding of PVG does not necessarily indicate severe underlying pathology. It can be seen in relatively benign situations such as after endoscopic procedures and gastric dilatation, which only necessitate conservative therapy[10]. Traditionally, PVG has been considered as an indicator of bad prognosis and associated with a particularly high mortality rate[11,12].

The dilemma is deciding how to manage the patient with newly diagnosed PI/PVG[13]. Surgical exploration is indicated in a large percentage of patients with mechanical and ischemic causes, as it was clearly demonstrated in the two present cases. Unfortunately, aggressive surgical tactics often fail. Extremes of age and comorbidity make many of these patients unsuitable for aggressive treatment such as revascularization or extended bowel resection. If expectant care is to be recommended, it is imperative for physicians to discriminate correctly between PI/PVG that has arisen from acute mesenteric ischemia from benign PI/PVG.

In particular, in critically ill patients with clear abdominal symptoms, radiographic control seems to be a waste of time. After the patient's resuscitation, salvage surgical intervention should be considered. When time is not an issue and CT can be performed that results in PI/PVG findings, the treatment goal is to deal with the underlying pathology in an appropriate manner, surgical or conservative, according to the three above mentioned causes (i.e. obstruction, ischemia, or iatrogenic intervention). When ischemia is suspected, the comorbidity factors that should be prioritized are the general vascular and heart condition of the patient, physical examination (abdominal pain, discomfort or tenderness, or bloody stools), and laboratory findings (serum lactate, or sepsis markers). If mesenteric ischemia is strongly suspected, an exploratory laparotomy is preferred if the general condition of the patient allows it; otherwise, conservative treatment is the only choice. However, when ischemia is a likely but not certain diagnosis, endoscopy or laparoscopy could offer the physician a less invasive method to access bowel viability and rule out mesenteric ischemia, while also offering the opportunity for easy conversion to open laparotomy if necessary. The advantages of these minimally invasive methods are known and particularly appreciated for this group of patients. Finally, when the differential diagnosis guides the physician to a benign situation, especially after a history of medical intervention over the previous days, observation could be the gold standard, along with medical conservative management. Additional imaging methods such as CT or magnetic resonance imaging mesenteric angiography could also count in the final diagnosis of this benign medical situation.

Concerning our patients, according to the above analysis, the first patient with bowel obstruction underwent radiological examination for being in a critical but stable situation. The signs of sepsis were ascribed to abdominal pathology as soon as other infection sources were excluded, and because of her neuromuscular disease, the patient did not demonstrate subjective symptoms. Surgical exploration, although therapeutic, did not improve the patient's outcome. For the second patient, surgical management of intestinal ischemia was absolutely indicated. However, the coexisting morbidity factors predicted a lethal outcome. The clinical findings of the patient were severe and suggested that the radiological examination had less value after all, in contrast to the first patient.

Nowadays, with the development of highly advanced imaging techniques, potentially severe pathology, such as bowel ischemia, is diagnosed at much earlier stages, which allows prompt treatment and significantly reduces mortality[14]. There is no definitive algorithm or accepted path of action in the surgical or medical community[15], and we are not sure if there should be one. PVG is not by itself a surgical indication and the treatment depends mainly on the underlying disease. The exact role of PVG as a diagnostic criterion probably emerges in patients with an inaccurate diagnosis, with a less or equal value to physical examination and apparently less value than other comorbidity factors. The prognosis is related to the pathology itself and is not influenced by the presence of PVG.

In conclusion, PVG seems to be a radiological parameter along with other diagnostic criteria, but it is certainly not proof of an ominous outcome in patients with underlying intra-abdominal pathology. Additionally, in benign or iatrogenic cases, this finding should provide a motive for further clinical and radiological evaluation.

REFERENCES

1 **Ho LM**, Paulson EK, Thompson WM. Pneumatosis intestinalis in the adult: benign to life-threatening causes. *AJR Am J Roentgenol* 2007; **188**: 1604-1613

2 **Ito M**, Horiguchi A, Miyakawa S. Pneumatosis intestinalis

and hepatic portal venous gas. *J Hepatobiliary Pancreat Surg* 2008; **15**: 334-337
3 **Schindera ST**, Triller J, Vock P, Hoppe H. Detection of hepatic portal venous gas: its clinical impact and outcome. *Emerg Radiol* 2006; **12**: 164-170
4 **Nelson AL**, Millington TM, Sahani D, Chung RT, Bauer C, Hertl M, Warshaw AL, Conrad C. Hepatic portal venous gas: the ABCs of management. *Arch Surg* 2009; **144**: 575-581; discussion 581
5 **Hou SK**, Chern CH, How CK, Chen JD, Wang LM, Lee CH. Hepatic portal venous gas: clinical significance of computed tomography findings. *Am J Emerg Med* 2004; **22**: 214-218
6 **Greenstein AJ**, Nguyen SQ, Berlin A, Corona J, Lee J, Wong E, Factor SH, Divino CM. Pneumatosis intestinalis in adults: management, surgical indications, and risk factors for mortality. *J Gastrointest Surg* 2007; **11**: 1268-1274
7 **Chan SC**, Wan YL, Cheung YC, Ng SH, Wong AM, Ng KK. Computed tomography findings in fatal cases of enormous hepatic portal venous gas. *World J Gastroenterol* 2005; **11**: 2953-2955
8 **St Peter SD**, Abbas MA, Kelly KA. The spectrum of pneumatosis intestinalis. *Arch Surg* 2003; **138**: 68-75
9 **Peloponissios N**, Halkic N, Pugnale M, Jornod P, Nordback P, Meyer A, Gillet M. Hepatic portal gas in adults: review of the literature and presentation of a consecutive series of 11 cases. *Arch Surg* 2003; **138**: 1367-1370
10 **Gorospe EC**. Benign hepatic portal venous gas in a critically ill patient. *Sci World J* 2008; **8**: 951-952
11 **Monneuse O**, Pilleul F, Barth X, Gruner L, Allaouchiche B, Valette PJ, Tissot E. Portal venous gas detected on computed tomography in emergency situations: surgery is still necessary. *World J Surg* 2007; **31**: 1065-1071
12 **Morris MS**, Gee AC, Cho SD, Limbaugh K, Underwood S, Ham B, Schreiber MA. Management and outcome of pneumatosis intestinalis. *Am J Surg* 2008; **195**: 679-682; discussion 682-683
13 **Hussain A**, Mahmood H, El-Hasani S. Portal vein gas in emergency surgery. *World J Emerg Surg* 2008; **3**: 21
14 **Alqahtani S**, Coffin CS, Burak K, Chen F, MacGregor J, Beck P. Hepatic portal venous gas: a report of two cases and a review of the epidemiology, pathogenesis, diagnosis and approach to management. *Can J Gastroenterol* 2007; **21**: 309-313
15 **Wayne E**, Ough M, Wu A, Liao J, Andresen KJ, Kuehn D, Wilkinson N. Management algorithm for pneumatosis intestinalis and portal venous gas: treatment and outcome of 88 consecutive cases. *J Gastrointest Surg* 2010; **14**: 437-448

S- Editor Cheng JX **L- Editor** Kerr C **E- Editor** Zheng XM

World Journal of Radiology

Online Submissions: http://www.wjgnet.com/1949-8470office
wjr@wjgnet.com
www.wjgnet.com

World J Radiol 2010 June 28; 2(6): I
ISSN 1949-8470 (online)

Acknowledgments to reviewers of *World Journal of Radiology*

Many reviewers have contributed their expertise and time to the peer review, a critical process to ensure the quality of *World Journal of Radiology*. The editors and authors of the articles submitted to the journal are grateful to the following reviewers for evaluating the articles (including those published in this issue and those rejected for this issue) during the last editing time period.

Ritesh Agarwal, MD, DM, MAMS, FCCP, Assistant Professor, Department of Pulmonary Medicine, Postgraduate Institute of Medical Education and Research, Sector-12, Chandigarh 160012, India

Panagiotis Antoniou, PhD, MSc, Medical Physics, Certified Medical Physicist, School of Medicine Democritus University of Thrace, 31 Irinis Str. Alexandroupolis 68100, Greece

Patrick K Ha, MD, Assistant Professor, Johns Hopkins Department of Otolaryngology, Johns Hopkins Head and Neck Surgery at GBMC, 1550 Orleans Street, David H Koch Cancer Research Building, Room 5M06, Baltimore, MD 21231, United States

Piyush Kumar, PhD, Associate Clinical Professor, Department of Oncology, University of Alberta, Cross Cancer Institute, 11560 University Avenue, Edmonton, Alberta, T6G 1Z2, Canada

Jai Soung Park, MD, PhD, Professor, Department of Radiology, Soonchunhyang University Buchen Hospital, 1174 jung-dong, Wonmi-gu, Bucheon, Gyeonggi-do 420-767, South Korea

Alexander D Rapidis, MD, DDS, PhD, FACS, Professor, Chairman, Department of Head and Neck/Maxillofacial Surgery, Greek Anticancer Institute, Saint Savvas Hospital, 171 Alexandras Avenue, 115 22 Athens, Greece

Volker Rudat, Professor, Department of Radiation Oncology, Saad Specialist Hospital, PO Box 30353, Al Khobar 31952, Saudi Arabia

Stéphane Supiot, Dr., MD, PhD, Department of Radiation Oncology, Centre René Gauducheau, St-Herblain, Nantes, 44800, France

Dinesh Vyas, Dr., Department of Minimally and Endosopic Surgery, St John Mercy Hospital, 851 E Fifth Street, Washington, DC 63090, United States

Juan Xu, PhD, University of Pittsburgh School of Medicine, UPMC Eye Center, 203 Lothrop St EEI- 835, Pittsburgh, PA 15213, United States

World Journal of Radiology

Online Submissions: http://www.wjgnet.com/1949-8470office
wjr@wjgnet.com
www.wjgnet.com

World J Radiol 2010 June 28; 2(6): I
ISSN 1949-8470 (online)

Meetings

Events Calendar 2010

January 4-8
Beaver Creek, Colorado, United States
18th Annual Winter Diagnostic Imaging Update

January 7-9
Leuven, Belgium
4th Leuven Course on Ear Imaging

January 16-17
Hollywood, Florida, United States
The Symposium on Clinical Interventional Oncology

January 17-21
Hollywood, Florida, United States
The International Symposium on Endovascular Therapy

January 21-22
Cairo, Egypt
BGICC Breast Gyne International Cancer Conference

January 21-24
Phoenix, AZ, United States
13th Society for Cardiovascular Magnetic Resonance (SCMR) Annual Scientific Sessions

January 23-23
Atlanta, GA, United States
Emory Winship Cancer Institute: Breast Cancer 2010: Advances in Science, Emerging Data, and Novel Therapeutics

January 25-29
Maui, HI, United States
Musculoskeletal & Neuroradiology MR Imaging Update in Maui

January 27-February 2
Albuquerque, NM, United States
2010 SNM Conjoint Mid-Winter Meetings

January 29-30
Barcelona, Spain
7th European Congress: Perspectives in Gynecologic Oncology

February 7-12
Vail, CO, United States
15th Annual Vail 2010: Multislice CT in Clinical Practice

February 11-13
Las Vegas, NV, United States
5th Annual Symposium on PET/CT and Molecular Imaging

February 16-19
Park City, UT, United States
6th Interventional/ Neurointerventional Conference

February 18-19
London, United Kingdom
Diagnostic and Interventional Radiology

February 18-21
Las Vegas, NV, United States
American Society of Spine Radiology Annual Symposium

February 20-20
Jacksonville, Florida, United States
Mayo Clinic Molecular Markers and Management of Breast Cancer

February 20-21
Bethesda, Maryland, United States
25th Anniversary Washington Neuroradiology Review

February 21-26
Orlando, FL, United States
The Abdominal Radiology Course

February 21-27
Snowmass, CO, United States
16th Annual Snowmass 2010: Clinical Ultrasound

February 22-26
Bethesda, MD, United States
48th Annual Dr. Kenneth M. Earle Memorial Neuropathology Review

February 24-27
Lake Buena Vista, FL, United States
ACRO 2010 American College of Radiation Oncology Symposium: Clinical Radiation Oncology Challenges

February 25-27
Chandler, AZ, United States
Multidisciplinary Head and Neck Cancer Symposium

February 26-27
Brussels, Belgium
10èmes Mises au Point en Imagerie Ostéo-Articulaire

February 27-March 1
Cairo, Egypt
7th Gastroenterology Hepatology & Endoscopy Symposium

February 28-March 4
Scottsdale, AZ, United States
International Congress XXIII on Endovascular Interventions

February 28-March 5
Breckenridge, CO, United States
5th Annual Breckenridge 2010: Musculoskeletal MRI

March 3-6
Las Vegas, Nevada, United States
11th Annual Advances in Breast Imaging and Interventions

March 4-8
Vienna, Austria
European Congress of Radiology (ECR 2010) Annual Meeting

March 5-7
Mt Tremblant, QC, Canada
Neuroimaging and Head & Neck Radiology Update in Mt Tremblant

March 7-11
San Diego, CA, United States
SCBT-MR Masters in Body Imaging: "What's New, What's Hot, What You May Not Have Known"

March 10-13
San Antonio, Texas, United States
Clinical Osteoporosis 2010: An ISCD-NOF Symposium

March 11-13
Barcelona, Spain
EORTC Group Meeting: EORTC Radiation Oncology Group

March 11-13
Hannover, Germany
40. Kongress der Deutschen Gesellschaft für Endoskopie und Bildgebende Verfahren e.V.

March 13-18
Tampa, FL, United states
Society of interventional radiology 35th Annual Scientific Meeting

March 14-17
Park City, UT, United States
14th Annual Park City 2010: MRI in Clinical Practice

March 22-26
Beaver Creek, CO, United States
NYU Radiology Spring Skiing Symposium in Beaver Creek

March 22-26
Maui, HI, United States
18th Annual Spring Diagnostic Imaging Update

March 24-27
San Diego, California, United States
2010 American institute of ultrasound in Medicine Annual Convention Preliminary Program

March 24-27
Barcelona, Spain
7th European Breast Cancer Conference

April 8-12
Shanghai, China
The 26th International Congress of Radiology

September 8-12
Guangzhou, China
Chinese Society of Interventional Radiology, 2010 CSIR

November 28-December 03
Chicago, United States
Radiological Society of North America: 2010 Annual Meeting

World Journal of Radiology

Online Submissions: http://www.wjgnet.com/1949-8470office
wjr@wjgnet.com
www.wjgnet.com

World J Radiol 2010 June 28; 2(6): I-V
ISSN 1949-8470 (online)

Instructions to authors

GENERAL INFORMATION

World Journal of Radiology (*World J Radiol*, *WJR*, online ISSN 1949-8470, DOI: 10.4329), is a monthly, open-access (OA), peer-reviewed journal supported by an editorial board of 318 experts in Radiology from 40 countries.

The biggest advantage of the OA model is that it provides free, full-text articles in PDF and other formats for experts and the public without registration, which eliminates the obstacle that traditional journals possess and usually delays the speed of the propagation and communication of scientific research results. The open access model has been proven to be a true approach that may achieve the ultimate goal of the journals, i.e. the maximization of the value to the readers, authors and society.

The role of academic journals is to exhibit the scientific levels of a country, a university, a center, a department, and even a scientist, and build an important bridge for communication between scientists and the public. As we all know, the significance of the publication of scientific articles lies not only in disseminating and communicating innovative scientific achievements and academic views, as well as promoting the application of scientific achievements, but also in formally recognizing the "priority" and "copyright" of innovative achievements published, as well as evaluating research performance and academic levels. So, to realize these desired attributes of *WJR* and create a well-recognized journal, the following four types of personal benefits should be maximized. The maximization of personal benefits refers to the pursuit of the maximum personal benefits in a well-considered optimal manner without violation of the laws, ethical rules and the benefits of others. (1) Maximization of the benefits of editorial board members: The primary task of editorial board members is to give a peer review of an unpublished scientific article *via* online office system to evaluate its innovativeness, scientific and practical values and determine whether it should be published or not. During peer review, editorial board members can also obtain cutting-edge information in that field at first hand. As leaders in their field, they have priority to be invited to write articles and publish commentary articles. We will put peer reviewers' names and affiliations along with the article they reviewed in the journal to acknowledge their contribution; (2) Maximization of the benefits of authors: Since *WJR* is an open-access journal, readers around the world can immediately download and read, free of charge, high-quality, peer-reviewed articles from *WJR* official website, thereby realizing the goals and significance of the communication between authors and peers as well as public reading; (3) Maximization of the benefits of readers: Readers can read or use, free of charge, high-quality peer-reviewed articles without any limits, and cite the arguments, viewpoints, concepts, theories, methods, results, conclusion or facts and data of pertinent literature so as to validate the innovativeness, scientific and practical values of their own research achievements, thus ensuring that their articles have novel arguments or viewpoints, solid evidence and correct conclusion; and (4) Maximization of the benefits of employees: It is an iron law that a first-class journal is unable to exist without first-class editors, and only first-class editors can create a first-class academic journal. We insist on strengthening our team cultivation and construction so that every employee, in an open, fair and transparent environment, could contribute their wisdom to edit and publish high-quality articles, thereby realizing the maximization of the personal benefits of editorial board members, authors and readers, and yielding the greatest social and economic benefits.

The major task of *WJR* is to rapidly report the most recent improvement in the research of medical imaging and radiation therapy by the radiologists. *WJR* accepts papers on the following aspects related to radiology: Abdominal radiology, women health radiology, cardiovascular radiology, chest radiology, genitourinary radiology, neuroradiology, head and neck radiology, interventional radiology, musculoskeletal radiology, molecular imaging, pediatric radiology, experimental radiology, radiological technology, nuclear medicine, PACS and radiology informatics, and ultrasound. We also encourage papers that cover all other areas of radiology as well as basic research.

The columns in the issues of *WJR* will include: (1) Editorial: To introduce and comment on major advances and developments in the field; (2) Frontier: To review representative achievements, comment on the state of current research, and propose directions for future research; (3) Topic Highlight: This column consists of three formats, including (A) 10 invited review articles on a hot topic, (B) a commentary on common issues of this hot topic, and (C) a commentary on the 10 individual articles; (4) Observation: To update the development of old and new questions, highlight unsolved problems, and provide strategies on how to solve the questions; (5) Guidelines for Basic Research: To provide guidelines for basic research; (6) Guidelines for Clinical Practice: To provide guidelines for clinical diagnosis and treatment; (7) Review: To review systemically progress and unresolved problems in the field, comment on the state of current research, and make suggestions for future work; (8) Original Articles: To report innovative and original findings in radiology; (9) Brief Articles: To briefly report the novel and innovative findings in radiology; (10) Case Report: To report a rare or typical case; (11) Letters to the Editor: To discuss and make reply to the contributions published in *WJR*, or to introduce and comment on a controversial issue of general interest; (12) Book Reviews: To introduce and comment on quality monographs of radiology; and (13) Guidelines: To introduce consensuses and guidelines reached by international and national academic authorities worldwide on the research in radiology.

CSSN
ISSN 1949-8470 (online)

Published by
Beijing Baishideng BioMed Scientific Co., Ltd.

SUBMISSION OF MANUSCRIPTS

Manuscripts should be typed in 1.5 line spacing and 12 pt. Book Antiqua with ample margins. Number all pages consecutively, and start each of the following sections on a new page: Title Page, Abstract, Introduction, Materials and Methods, Results, Discussion, Acknowledgements, References, Tables, Figures, and Figure Legends. Neither the editors nor the publisher are responsible for the opinions expressed by contributors. Manuscripts formally accepted for publication become the permanent property of Beijing Baishideng BioMed Scientifc Co., Ltd., and may not be reproduced by any means, in whole or in part, without the written permission of both the authors and the publisher. We reserve the right to copy-edit and put onto our website accepted manuscripts. Authors should follow the relevant guidelines for the care and use of laboratory animals of their institution or national animal welfare committee. For the sake of transparency in regard to the performance and reporting of clinical trials, we endorse the policy of the International Committee of Medical Journal Editors to refuse to publish papers on clinical trial results if the trial was not recorded in a publicly-accessible registry at its outset. The only register now available, to our knowledge, is http://www. clinicaltrials.gov sponsored by the United States National Library of Medicine and we encourage all potential contributors to register with it. However, in the case that other registers become available you will be duly notified. A letter of recommendation from each author's organization should be provided with the contributed article to ensure the privacy and secrecy of research is protected.

Authors should retain one copy of the text, tables, photographs and illustrations because rejected manuscripts will not be returned to the author(s) and the editors will not be responsible for loss or damage to photographs and illustrations sustained during mailing.

Online submissions

Manuscripts should be submitted through the Online Submission System at: http://www.wjgnet.com/1949-8470office. Authors are highly recommended to consult the ONLINE INSTRUCTIONS TO AUTHORS (http://www.wjgnet.com/1949-8470/g_info_20100316162358.htm) before attempting to submit online. For assistance, authors encountering problems with the Online Submission System may send an email describing the problem to wjr@wjgnet.com, or by telephone: +86-10-59080036. If you submit your manuscript online, do not make a postal contribution. Repeated online submission for the same manuscript is strictly prohibited.

MANUSCRIPT PREPARATION

All contributions should be written in English. All articles must be submitted using word-processing software. All submissions must be typed in 1.5 line spacing and 12 pt. Book Antiqua with ample margins. Style should conform to our house format. Required information for each of the manuscript sections is as follows:

Title page

Title: Title should be less than 12 words.

Running title: A short running title of less than 6 words should be provided.

Authorship: Authorship credit should be in accordance with the standard proposed by International Committee of Medical Journal Editors, based on (1) substantial contributions to conception and design, acquisition of data, or analysis and interpretation of data; (2) drafting the article or revising it critically for important intellectual content; and (3) final approval of the version to be published. Authors should meet conditions 1, 2, and 3.

Institution: Author names should be given first, then the complete name of institution, city, province and postcode. For example, Xu-Chen Zhang, Li-Xin Mei, Department of Pathology, Chengde Medical College, Chengde 067000, Hebei Province, China. One author may be represented from two institutions, for example, George Sgourakis, Department of General, Visceral, and Transplantation Surgery, Essen 45122, Germany; George Sgourakis, 2nd Surgical Department, Korgialenio-Benakio Red Cross Hospital, Athens 15451, Greece

Author contributions: The format of this section should be: Author contributions: Wang CL and Liang L contributed equally to this work; Wang CL, Liang L, Fu JF, Zou CC, Hong F and Wu XM designed the research; Wang CL, Zou CC, Hong F and Wu XM performed the research; Xue JZ and Lu JR contributed new reagents/analytic tools; Wang CL, Liang L and Fu JF analyzed the data; and Wang CL, Liang L and Fu JF wrote the paper.

Supportive foundations: The complete name and number of supportive foundations should be provided, e.g., Supported by National Natural Science Foundation of China, No. 30224801

Correspondence to: Only one corresponding address should be provided. Author names should be given first, then author title, affiliation, the complete name of institution, city, postcode, province, country, and email. All the letters in the email should be in lower case. A space interval should be inserted between country name and email address. For example, Montgomery Bissell, MD, Professor of Medicine, Chief, Liver Center, Gastroenterology Division, University of California, Box 0538, San Francisco, CA 94143, United States. montgomery.bissell@ucsf.edu

Telephone and fax: Telephone and fax should consist of +, country number, district number and telephone or fax number, e.g., Telephone: +86-10-59080039 Fax: +86-10-85381893

Peer reviewers: All articles received are subject to peer review. Normally, three experts are invited for each article. Decision for acceptance is made only when at least two experts recommend an article for publication. Reviewers for accepted manuscripts are acknowledged in each manuscript, and reviewers of articles which were not accepted will be acknowledged at the end of each issue. To ensure the quality of the articles published in *WJR*, reviewers of accepted manuscripts will be announced by publishing the name, title/position and institution of the reviewer in the footnote accompanying the printed article. For example, reviewers: Professor Jing-Yuan Fang, Shanghai Institute of Digestive Disease, Shanghai, Affiliated Renji Hospital, Medical Faculty, Shanghai Jiaotong University, Shanghai, China; Professor Xin-Wei Han, Department of Radiology, The First Affiliated Hospital, Zhengzhou University, Zhengzhou, Henan Province, China; and Professor Anren Kuang, Department of Nuclear Medicine, Huaxi Hospital, Sichuan University, Chengdu, Sichuan Province, China.

Abstract
There are unstructured abstracts (no more than 256 words) and structured abstracts (no more than 480). The specific requirements for structured abstracts are as follows:

An informative, structured abstracts of no more than 480 words should accompany each manuscript. Abstracts for original contributions should be structured into the following sections. AIM (no more than 20 words): Only the purpose should be included. Please write the aim as the form of "To investigate/study/…; MATERIALS AND METHODS (no more than 140 words); RESULTS (no more than 294 words): You should present *P* values where appropriate and must provide relevant data to illustrate how they were obtained, e.g. 6.92 ± 3.86 *vs* 3.61 ± 1.67, $P < 0.001$; CONCLUSION (no more than 26 words).

Key words
Please list 5-10 key words, selected mainly from *Index Medicus*, which reflect the content of the study.

Text
For articles of these sections, original articles, rapid communication and case reports, the main text should be structured into the following sections: INTRODUCTION, MATERIALS AND METHODS, RESULTS and DISCUSSION, and should include appropriate Figures and Tables. Data should be presented in the main text or in Figures and Tables, but not in both. The main text format of these sections, editorial, topic highlight, case report, letters to the editors, can be found at: http://www.wjgnet.com/1949-8470/g_info_20100313183720.htm.

Illustrations
Figures should be numbered as 1, 2, 3, *etc.*, and mentioned clearly in the main text. Provide a brief title for each figure on a separate page. Detailed legends should not be provided under the figures. This part should be added into the text where the figures are applicable. Figures should be either Photoshop or Illustrator files (in tiff, eps, jpeg formats) at high-resolution. Examples can be found at: http://www.wjgnet.com/1007-9327/13/4520.pdf; http://www.wjgnet.com/1007-9327/13/4554.pdf; http://www.wjgnet.com/1007-9327/13/4891.pdf; http://www.wjgnet.com/1007-9327/13/4986.pdf; http://www.wjgnet.com/1007-9327/13/4498.pdf. Keeping all elements compiled is necessary in line-art image. Scale bars should be used rather than magnification factors, with the length of the bar defined in the legend rather than on the bar itself. File names should identify the figure and panel. Avoid layering type directly over shaded or textured areas. Please use uniform legends for the same subjects. For example: Figure 1 Pathological changes in atrophic gastritis after treatment. A: ...; B: ...; C: ...; D: ...; E: ...; F: ...; G: …*etc.* It is our principle to publish high resolution-figures for the printed and E-versions.

Tables
Three-line tables should be numbered 1, 2, 3, *etc.*, and mentioned clearly in the main text. Provide a brief title for each table. Detailed legends should not be included under tables, but rather added into the text where applicable. The information should complement, but not duplicate the text. Use one horizontal line under the title, a second under column heads, and a third below the Table, above any footnotes. Vertical and italic lines should be omitted.

Notes in tables and illustrations
Data that are not statistically significant should not be noted. $^{a}P < 0.05$, $^{b}P < 0.01$ should be noted ($P > 0.05$ should not be noted). If there are other series of *P* values, $^{c}P < 0.05$ and $^{d}P < 0.01$ are used. A third series of *P* values can be expressed as $^{e}P < 0.05$ and $^{f}P < 0.01$. Other notes in tables or under illustrations should be expressed as ^{1}F, ^{2}F, ^{3}F; or sometimes as other symbols with a superscript (Arabic numerals) in the upper left corner. In a multi-curve illustration, each curve should be labeled with ●, ○, ■, □, ▲, △, *etc.*, in a certain sequence.

Acknowledgments
Brief acknowledgments of persons who have made genuine contributions to the manuscript and who endorse the data and conclusions should be included. Authors are responsible for obtaining written permission to use any copyrighted text and/or illustrations.

REFERENCES
Coding system
The author should number the references in Arabic numerals according to the citation order in the text. Put reference numbers in square brackets in superscript at the end of citation content or after the cited author's name. For citation content which is part of the narration, the coding number and square brackets should be typeset normally. For example, "Crohn's disease (CD) is associated with increased intestinal permeability[1,2]". If references are cited directly in the text, they should be put together within the text, for example, "From references[19,22-24], we know that..."

When the authors write the references, please ensure that the order in text is the same as in the references section, and also ensure the spelling accuracy of the first author's name. Do not list the same citation twice.

PMID and DOI
Pleased provide PubMed citation numbers to the reference list, e.g. PMID and DOI, which can be found at http://www.ncbi.nlm.nih.gov/sites/entrez?db=pubmed and http://www.crossref.org/SimpleTextQuery/, respectively. The numbers will be used in E-version of this journal.

Style for journal references
Authors: the name of the first author should be typed in boldfaced letters. The family name of all authors should be typed with the initial letter capitalized, followed by their abbreviated first and middle initials. (For example, Lian-Sheng Ma is abbreviated as Ma LS, Bo-Rong Pan as Pan BR). The title of the cited article and italicized journal title (journal title should be in its abbreviated form as shown in PubMed), publication date, volume number (in black), start page, and end page [PMID: 11819634 DOI: 10.3748/wjg.13.5396].

Style for book references
Authors: the name of the first author should be typed in boldfaced letters. The surname of all authors should be typed with the initial letter capitalized, followed by their abbreviated middle and first initials. (For example, Lian-Sheng Ma is abbreviated as Ma LS, Bo-Rong Pan as Pan BR) Book title. Publication number. Publication place: Publication press, Year: start page and end page.

Format

Journals

English journal article (list all authors and include the PMID where applicable)

1 **Jung EM**, Clevert DA, Schreyer AG, Schmitt S, Rennert J, Kubale R, Feuerbach S, Jung F. Evaluation of quantitative contrast harmonic imaging to assess malignancy of liver tumors: A prospective controlled two-center study. *World J Gastroenterol* 2007; **13**: 6356-6364 [PMID: 18081224 DOI: 10.3748/wjg.13.6356]

Chinese journal article (list all authors and include the PMID where applicable)

2 **Lin GZ**, Wang XZ, Wang P, Lin J, Yang FD. Immunologic effect of Jianpi Yishen decoction in treatment of Pixu-diarrhoea. *Shijie Huaren Xiaohua Zazhi* 1999; **7**: 285-287

In press

3 **Tian D**, Araki H, Stahl E, Bergelson J, Kreitman M. Signature of balancing selection in Arabidopsis. *Proc Natl Acad Sci USA* 2006; In press

Organization as author

4 **Diabetes Prevention Program Research Group**. Hypertension, insulin, and proinsulin in participants with impaired glucose tolerance. *Hypertension* 2002; **40**: 679-686 [PMID: 12411462 PMCID:2516377 DOI:10.1161/01.HYP.0000035706.28494.09]

Both personal authors and an organization as author

5 **Vallancien G**, Emberton M, Harving N, van Moorselaar RJ; Alf-One Study Group. Sexual dysfunction in 1, 274 European men suffering from lower urinary tract symptoms. *J Urol* 2003; **169**: 2257-2261 [PMID: 12771764 DOI:10.1097/01.ju.0000067940.76090.73]

No author given

6 21st century heart solution may have a sting in the tail. *BMJ* 2002; **325**: 184 [PMID: 12142303 DOI:10.1136/bmj.325.7357.184]

Volume with supplement

7 **Geraud G**, Spierings EL, Keywood C. Tolerability and safety of frovatriptan with short- and long-term use for treatment of migraine and in comparison with sumatriptan. *Headache* 2002; **42** Suppl 2: S93-99 [PMID: 12028325 DOI:10.1046/j.1526-4610.42.s2.7.x]

Issue with no volume

8 **Banit DM**, Kaufer H, Hartford JM. Intraoperative frozen section analysis in revision total joint arthroplasty. *Clin Orthop Relat Res* 2002; (**401**): 230-238 [PMID: 12151900 DOI:10.1097/00003086-200208000-00026]

No volume or issue

9 Outreach: Bringing HIV-positive individuals into care. *HRSA Careaction* 2002; 1-6 [PMID: 12154804]

Books

Personal author(s)

10 **Sherlock S**, Dooley J. Diseases of the liver and billiary system. 9th ed. Oxford: Blackwell Sci Pub, 1993: 258-296

Chapter in a book (list all authors)

11 **Lam SK**. Academic investigator's perspectives of medical treatment for peptic ulcer. In: Swabb EA, Azabo S. Ulcer disease: investigation and basis for therapy. New York: Marcel Dekker, 1991: 431-450

Author(s) and editor(s)

12 **Breedlove GK**, Schorfheide AM. Adolescent pregnancy. 2nd ed. Wieczorek RR, editor. White Plains (NY): March of Dimes Education Services, 2001: 20-34

Conference proceedings

13 **Harnden P**, Joffe JK, Jones WG, editors. Germ cell tumours V. Proceedings of the 5th Germ cell tumours Conference; 2001 Sep 13-15; Leeds, UK. New York: Springer, 2002: 30-56

Conference paper

14 **Christensen S**, Oppacher F. An analysis of Koza's computational effort statistic for genetic programming. In: Foster JA, Lutton E, Miller J, Ryan C, Tettamanzi AG, editors. Genetic programming. EuroGP 2002: Proceedings of the 5th European Conference on Genetic Programming; 2002 Apr 3-5; Kinsdale, Ireland. Berlin: Springer, 2002: 182-191

Electronic journal (list all authors)

15 Morse SS. Factors in the emergence of infectious diseases. Emerg Infect Dis serial online, 1995-01-03, cited 1996-06-05; 1(1): 24 screens. Available from: URL: http//www.cdc.gov/ncidod/EID/eid.htm

Patent (list all authors)

16 **Pagedas AC**, inventor; Ancel Surgical R&D Inc., assignee. Flexible endoscopic grasping and cutting device and positioning tool assembly. United States patent US 20020103498. 2002 Aug 1

Statistical data

Write as mean ± SD or mean ± SE.

Statistical expression

Express *t* test as *t* (in italics), *F* test as *F* (in italics), chi square test as χ^2 (in Greek), related coefficient as *r* (in italics), degree of freedom as υ (in Greek), sample number as *n* (in italics), and probability as *P* (in italics).

Units

Use SI units. For example: body mass, m (B) = 78 kg; blood pressure, p (B) = 16.2/12.3 kPa; incubation time, t (incubation) = 96 h, blood glucose concentration, c (glucose) 6.4 ± 2.1 mmol/L; blood CEA mass concentration, p (CEA) = 8.6 24.5 μg/L; CO_2 volume fraction, 50 mL/L CO_2, not 5% CO_2; likewise for 40 g/L formaldehyde, not 10% formalin; and mass fraction, 8 ng/g, *etc.* Arabic numerals such as 23, 243, 641 should be read 23 243 641.

The format for how to accurately write common units and quantums can be found at: http://www.wjgnet.com/1949-8470/g_info_20100313185816.htm.

Abbreviations

Standard abbreviations should be defined in the abstract and on first mention in the text. In general, terms should not be abbreviated unless they are used repeatedly and the abbreviation is helpful to the reader. Permissible abbreviations are listed in Units, Symbols and Abbreviations: A Guide for Biological and Medical Editors and Authors (Ed. Baron DN, 1988) published by The Royal Society of Medicine, London. Certain commonly used abbreviations, such as DNA, RNA, HIV, LD50, PCR, HBV, ECG, WBC, RBC, CT, ESR, CSF, IgG, ELISA, PBS, ATP, EDTA, mAb, can be used directly without further explanation.

Italics

Quantities: *t* time or temperature, *c* concentration, *A* area, *l* length, *m* mass, *V* volume.

Genotypes: *gyrA*, *arg* 1, *c myc*, *c fos*, *etc.*

Restriction enzymes: *Eco*RI, *Hin*dI, *Bam*HI, *Kbo* I, *Kpn* I, *etc.*
Biology: *H. pylori*, *E coli*, *etc.*

RE-SUBMISSION OF THE REVISED PAPER

Please revise your article according to the revision policies of *WJR*. The revised version including manuscript and high-resolution image figures (if any) should be re-submitted or uploaded online. The author should send copyright transfer letter, and responses to the reviewers and science news to us *via* email.

Editorial Office

World Journal of Radiology

Editorial Department: Room 903, Building D,
Ocean International Center,
No. 62 Dongsihuan Zhonglu,
Chaoyang District, Beijing 100025, China
E-mail: wjr@wjgnet.com
http://www.wjgnet.com
Telephone: +86-10-59080036
Fax: +86-10-85381893

Language evaluation

The language of a manuscript will be graded before it is sent for revision. (1) Grade A: priority publishing; (2) Grade B: minor language polishing; (3) Grade C: a great deal of language polishing needed; and (4) Grade D: rejected. Revised articles should reach Grade A or B.

Copyright assignment form

Please download a Copyright assignment form from http://www.wjgnet.com/1949-8470/g_info_20100313185522.htm.

Responses to reviewers

Please revise your article according to the comments/suggestions provided by the reviewers. The format for responses to the reviewers' comments can be found at: http://www.wjgnet.com/1949-8470/g_info_20100313185358.htm.

Proof of financial support

For paper supported by a foundation, authors should provide a copy of the document and serial number of the foundation.

Science news releases

Authors of accepted manuscripts are suggested to write a science news item to promote their articles. The news will be released rapidly at EurekAlert/AAAS (http://www.eurekalert.org). The title for news items should be less than 90 characters; the summary should be less than 75 words; and main body less than 500 words. Science news items should be lawful, ethical, and strictly based on your original content with an attractive title and interesting pictures.

Publication fee

Authors of accepted articles must pay a publication fee.
EDITORIAL, TOPIC HIGHLIGHTS, BOOK REVIEWS and LETTERS TO THE EDITOR are published free of charge.